The effect of lactose source on the stickiness of dairy powders

A thesis presented in partial fulfilment of the requirements for the degree of
Master of Engineering in Bioprocess Engineering
at Massey University, Palmerston North, New Zealand.

Rosalind A Murti
B. Tech (Hons)
2006

This thesis is dedicated to my late Grandfather Rev. Basil J. Hilder with much love.

"I see the solution to each problem as being detectable in the pattern and web of the whole. The connections between causes and effects are often much more subtle and complex than we with our rough and ready understanding of the physical world might naturally suppose" : *from "Dirk Gently's Holistic Detective Agency"*

ABSTRACT

The particle gun provides a valuable method to investigate powder stickiness properties. This method gives reproducible results when used under constant testing conditions and allows the isolation of factors influencing stickiness behaviour such as velocity and angle of impact. The $(T-Tg)_{critical}$ and rate of stickiness development obtained from the particle gun method were functions of the air velocity, angle of impact, powder a_w and ambient air conditions. Under constant testing conditions (feed rate of 0.3 $g.s^{-1}$, air velocity of 20 $m.s^{-1}$, ambient air at < 50 %RH, room temperature and constant powder a_w $(T-Tg)_{critical}$ was reproducible within ± 0.8°C while the rate of stickiness development was reproducible within ± 0.45 %deposition/°C.

The results obtained from the particle gun were consistently higher than the fluid bed results and can be explained by the different impact time and force experienced by the particles. Particle gun results can successfully be used to predict blockages in cyclones provided the appropriate correction is made for particle impact force and time. Blockage data from Te Rapa D5 indicates that the critical T–Tg where blockages occur in the cyclones is 27°C for SMP. Currently D5 is running satisfactorily for SMP at a T–Tg value of 28°C. Under these operation conditions the cyclone wall temperature results in a T–Tg value of 33°C, the same $(T-Tg)_{critical}$ value predicted by the particle gun for standardised SMP. This implies that the cyclone is operating correctly at the maximum T–Tg value before particles become sticky enough to cause blockage problems.

Protein standardisation of milk powder via the addition of milk permeate or lactose solution had no detectable effect on the stickiness characteristics of SMP or WMP as measured by the particle gun or the fluid bed rig. No difference was seen in either the bulk or surface composition of the milk powder. This provides evidence to dispel speculation by operators that permeate standardisation produces a more difficult to handle powder.

ACKNOWLEDGEMENTS

I would like to express my sincere gratitude to the various individuals and organisations for their contribution to this project. Thanks to Tech NZ for the funding that enabled this project to go ahead. I would like to thank my primary supervisor Dr. Tony Paterson for all his guidance, patience, and support throughout this project. Thanks to Dr. David Pearce my secondary supervisor for his invaluable assistance with the project and knowledge of milk powder and Fonterra. Many thanks to my third supervisor Dr. John Bronlund. You have been fantastic supervisors and I appreciate the time you have all set aside for all my questions and reading numerous drafts.

I would also like to thank the staff at Massey University ITE department, Ag Engineering, and Liz Nickless from the Confocal Microscope Unit for assistance with various aspects of this project. Thanks to Dr. Nigel Grieg for his statistical and error analysis advice.

Thanks to all the Fonterra staff who have provided assistance with this project. The FRC laboratory for sample analysis, FRC pilot plant crew for making and providing the SMP and WMP samples, and the staff at Fonterra Longburn where my experimental work was performed. Prof. Dong Chen of Auckland University (now MONASH) for the hours of ESCA analysis, Glen Hodges at Te Rapa for providing samples of SMP standardised by different methods, Roger Keedwell at Fonterra Longburn for helping me to re-program the fluid bed rig, and Frank Lin, Nigel Russell and Lisa Drysdale at Te Rapa for all the information they provided for this research.

I would also like to thank John Abrahamson from Canterbury University for his insightful and valuable information regarding gas cyclones and their operation.

I am grateful for the support of my friends and family throughout my Masters, Louis Buchanan (NZP), and especially my husband for his unconditional support.

TABLE OF CONTENTS

TABLE OF FIGURES

TABLE OF TABLES

CHAPTER 1 - PROJECT OVERVIEW

1.1 INTRODUCTION

Sticking and caking problems in the dairy industry currently cost thousands of dollars through down time and wasted product caused by a combination of blocked cyclones, fluid bed blocks and accumulated product on the ducting and spray drier walls. In addition, fires from powder accumulation also cost Fonterra hundreds of thousands of dollars. Over the last five years Massey University and Fonterra have been addressing this issue by researching into the fundamental causes of the problem and relating the identified mechanisms to what has been happening in the plant.

The main mechanisms have now been identified (Chatterjee 2004; Foster 2002; Zuo 2004) with the most recent project relating how such mechanisms can be used to predict when problems are likely to occur in the plant. Currently the work is having some success in stickiness prevention and in helping operators to decide how to alter the running of the plant when sticky conditions are encountered. The sticky curves developed in previous work reduce the amount of trial and error experimenting during processing to control stickiness problems.

1.2 RESEARCH PROBLEM

Recent industrial experience by operators suggests that protein standardisation through lactose addition to dairy powders from different sources show different tendencies to become sticky when being processed. It is thought that powder standardised by lactose from whey permeate is more difficult to process than powder standardised by straight addition of pure lactose. This work aims to confirm or reject this suggestion and to identify what causes the different lactose sources to behave differently when dried, if a difference is found.

1.3 PROJECT AIMS

The particle gun stickiness curves from previous work in this area (Chatterjee 2004; Zuo 2004) show a degree of scatter when used to replicate stickiness curves for the same powder. To be able to investigate the effects of different lactose sources for same specification powders it is necessary to further investigate the variation of stickiness measurements. In addition alternative methods for measuring stickiness curves give results offset to the particle gun technique.

This project will look at day-to-day variations of powder and ambient air conditions on sticky point measurements. Once the ambient air conditions are quantified the margin of error in the stickiness curve can be decreased. This will enable the detection of variations due to impact angle, velocity and material of construction with the aim of demonstrating whether or not stickiness is a function of the particle gun parameters. It is expected that the particle gun will be able to more accurately define $(T-Tg)_{critical}$ and the rate of stickiness development for powders, enabling operators to run industrial equipment as close to the critical value as possible and hence obtain maximum efficiency.

The project then aims to quantify the effects of different lactose sources on the stickiness measurements for skim milk powder. The refined apparatus will be used to demonstrate whether the lactose source has any real effect on stickiness characteristics of dairy powder.

1.4 PROJECT OBJECTIVES

1. Review literature and plant records with the aim of identifying any changes in the degree of caking problems with changes in the source of lactose, ambient air conditions, material and velocity or impact angle.
2. Quantify the effects of ambient air variations on the stickiness curve for skim milk powder.
3. Quantify the effects of velocity, impact angle and material of construction of the collection plate on the stickiness curve as measured by the particle gun.

4. Investigation of the stickiness variation caused by different lactose sources and draw conclusions as to whether or not different lactose sources affect the stickiness properties of a dairy powder.
5. Final recommendation regarding the best way to overcome stickiness problems in the area of spray drying dairy powders.

CHAPTER 2 - DAIRY POWDER STICKINESS: A REVIEW

"In milk, we have a unique raw material. We seek to lead the race to develop its nutritional potential by meeting the needs of an increasingly health-conscious world." www.fonterra.co.nz

2.1 INTRODUCTION

Milk powder is an important way of preserving milk and has been practiced since the 13th century, with industrial production since the 19th century (Fox and McSweeney 2003). Stickiness in dairy powders is a major problem in the dairy industry. It costs the industry hundreds of thousands of dollars causing widespread problems including deposits, quality degradation, decrease in product yields, plant shutdowns, cleaning and safety hazards (Adhikari et al. 2005; Hennigs et al. 2001; Papadakis and Bahu 1992). Spray dryers require frequent cleaning due to deposition of powder on the walls, associated ducting and cyclones. Deposits are undesirable for a number of reasons. Build up of powder can cause oxidation and browning problems degrading the final product. Milk powder deposits may cause combustion and explosion hazards, wall deposits give rise to lower product yields and increased downtime required to remove deposits (Chuy and Labuza 1994; Downton et al. 1982; Hennigs et al. 2001; Ozmen and Langrish 2002; Ozmen and Langrish 2003). Approaches to dealing with stickiness problems have been largely trial and error. Where the characterised sticky curve exists, approaches involve cooling the dryer walls, chamber design modifications and addition of drying aids such as maltodextrins (Papadakis and Bahu 1992).

This work is an extension of the investigation by Zuo (2004) and Chatterjee (2004) looking at the stickiness properties of dry particles. This approach is justified by the fact that particles are dried very rapidly during spray drying and exit dryers as dry solid particles. Other research (Adhikari et al. 2003a; Adhikari et al. 2003b) has investigated surface stickiness of milk powders as drying takes place. This project will look at milk powder stickiness problems encountered at the exit of the dryer, cyclone, ducting and drying chamber.

2.2 LACTOSE

Lactose is the major reducing carbohydrate (disaccharide sugar) found in the milk of most mammals. Lactose is a disaccharide condensation product of the type 1:4 from the hexose sugars glucose and galactose. The glycosidic OH group of the galactose on the carbon atom one reacts with the alcoholic OH group of the carbon atom four of the glucose (Foster, 2002).

Lactose has been used in many food industry applications. The primary reasons for the use of lactose are to reduce sweetness, aroma enhancement, improved colour binding, better mouth feel and increase storage life (Harper 1992). Lactose, used as an additive to milk powders to boost lactose levels and standardise protein content, comes from two sources: pure crystallised lactose from whey products or lactose added in the form of milk permeate (CODEX 1999).

2.2.1 Amorphous Lactose

Lactose can exist in several different forms, one of which is amorphous where the particles have no ordered crystalline structure. Lactose in the amorphous state exists in two forms – the glassy immobile form and the rubbery form where lactose can flow, leading to stickiness. Amorphous carbohydrates can undergo physical changes such as crystallisation, clumping, sticking and caking during storage, handling and processing (Harper 1992). When dealing with stickiness problems in amorphous lactose the most important physical properties are isotherms and the glass transition temperature profile. The glass to rubber transition takes place at a particular temperature, at a given moisture content/water activity (a_w) known as the glass transition temperature Tg, and is of interest to the dairy powder industry.

Amorphous lactose is formed when the solution is dried rapidly (such as spray drying) and the particles have no time to arrange themselves in an ordered fashion or when the molecular movement is stopped such as in freeze drying. Water is removed quickly and there is no time for crystallised lactose to form. In the amorphous state the α and β molecules of lactose are in a solid, metastable, non-crystalline matrix but are not at

equilibrium (Aguilera et al. 1995; Buma and van der Veen 1974; Jouppila and Roos 1994a). Amorphous lactose is highly hygroscopic; hence moisture content and product temperature are very important parameters for storing dairy powders. Water adsorption results in plasticization of amorphous lactose, which increases molecular mobility, allowing lactose to move into the more stable crystalline state.

During storage amorphous lactose re-crystallisation can occur with time if exposed to sufficient moisture and/or temperature (Jouppila and Roos 1994a). Amorphous lactose is relatively stable at less than 3% moisture and crystallisation is slow (Morr 1992). At moisture levels above 8% amorphous lactose begins to crystallise as α-lactose monohydrate. As amorphous lactose crystallises it releases moisture from the crystalline to the amorphous regions, reducing the local viscosity, which increases the rate of crystallisation of any amorphous carbohydrate present (Chuy and Labuza 1994; Foster 2002). The increase in available moisture contributes to caking, hence amorphous lactose present in powder should be stored with a water activity (a_w) below 0.25 (Foster 2002).

2.2.2 Water Sorption Isotherms

Water sorption isotherms illustrate the capacity of a powder for uptake or release of water when placed at different humidities at a specified temperature (Teunou and Fitzpatrick 1999). The amorphous lactose isotherm describes the equilibrium relationship between moisture content of the powder and relative humidity (RH) of the surrounding environment (Roos et al. 1996). Sorption isotherms plot the amount of water sorbed as a function of the a_w or RH of the vapour surrounding the material. RH corresponds to a_w multiplied by a factor of 100. At equilibrium

$$a_w = \frac{p}{p_o} = \frac{equilibriumRH}{100} \qquad (2\text{-}1)$$

It is useful to know or predict isotherms for dairy powders in order to determine the moisture content required for the stability of the final powder. This moisture content will depend on the powder composition and amount of amorphous sugar present (Foster 2002). Foster (2002) provides a method for predicting isotherms for dairy powders.

The Guggenheim-Anderson-de Boer (GAB) sorption model can be used to predict the adsorption data over a range of water activity values. This model is particularly useful for milk proteins and milk powders (Fox 1997). The GAB equation (Equation 1-2) is used as a model for the amorphous lactose moisture sorption isotherm (Adhikari et al. 2005; Foster 2002).

$$M_f = \frac{M_o f c a_w}{(1 - f a_w)(1 + (c-1) f a_w)} \qquad (2\text{-}2)$$
$$M = M_f + 1$$

2.2.3 Viscosity Phenomena

Sticking, caking and agglomeration tendencies of hygroscopic, amorphous powders are interpreted in terms of a mechanism of viscous flow driven by surface energy during particle contact (Downton et al. 1982; Peleg 1993). Viscosity is affected by both moisture content and temperature. At temperatures below the glass transition temperature (where the material exists in a glassy state) the viscosity is extremely high, greater than 10^{12} Pa.s, and no liquid flow can occur. Under the influence of water and/or temperature a glassy material transforms into a rubbery state at which the surface viscosity reduces to below 10^{8} Pa.s (Downton et al. 1982). In the rubbery state the surface material is readily sticky. This mechanism predicts that stickiness should occur for combinations of temperature and moisture content corresponding to viscosities within the range of 10^{6} to 10^{8} Pa.s. At viscosities less than 10^{6} the material remains in the amorphous form.

The temperature and viscosity relationship above the glass transition temperature is described by the William-Landel-Ferry (WLF) model. The WLF equation (Equation 1-3) describes the kinetics of mechanical properties of a material such as relaxation time and viscous properties above its transition temperature. This equation relates relaxation time to mechanical properties in amorphous materials to temperatures above the Tg point. When the property is viscosity Equation 1-3 is used (Bhandari and Howes 1999;

Downton et al. 1982). Increased fluidity due to a decrease in viscosity increases the powder cohesion which in turn increases the amount of adhesion.

$$\log_{10}\frac{\mu}{\mu_g}=\frac{-C}{B}\frac{(T-T_g)}{+(T-T_g)} \tag{2-3}$$

The Frenkel model (Equation 1-4) can be used to predict the critical viscosity for stickiness of powder particles (Boonyai et al. 2004).

$$\mu=\left(\frac{3}{2}\right)\left(\frac{a\sigma t}{x^2}\right) \tag{2-4}$$

The Frenkel equation shows that viscosity is time dependent (Peleg 1993), and since stickiness is limited by viscosity, stickiness must also be time dependent. Increased contact time and higher surface tension increases the bridge size; while greater viscosity or smaller particle size decreases the size of the liquid bridge build up in a given time (Paterson et al. 2005). Increased moisture lowers the glass transition temperature and therefore the temperature at which viscous flow occurs. If the rate of sticking is limited by viscosity as suggested by this equation, it follows that stickiness is only dependent on the temperature difference above the glass transition temperature (T–Tg) not the actual temperature and moisture conditions the powder experiences directly (Paterson et al. 2005).

2.2.4 Lactose Crystallisation

Lactose crystallisation is related to stickiness by two mechanisms. Firstly, with an increase in temperature or moisture water is released. The free water is absorbed by amorphous lactose lowering of the glass transition temperature (Tg), resulting in plasticization due to a decrease in viscosity enabling lactose to flow and bridges to form. The formation of solid bridges once Tg is sufficiently depressed leads to caking. Secondly, crystallisation of liquid bridges causes the formation of solid bridges of significant strength (Brooks 2000). α-lactose monohydrate is the most common lactose crystal form (Buma 1970). This structure is formed when lactose crystallisation occurs in the spray-dried product with sufficient water present. Bronlund (1997) has shown that an anhydrous product, thought to be β-lactose, is the product when amorphous lactose

crystallises at lower a_w (0.4 – 0.5), although the paper by Nezbed (1974) suggests a 50:50 β:α mixture crystal may exist.

Crystallisation of amorphous lactose can result in a loss of adsorbed water. The critical a_w where crystallisation starts for pure amorphous lactose was found to be 0.37 by Jouppila and Roos (1994a). The critical a_w and water content for crystallisation of amorphous lactose at 25°C was 0.33 and 7.2g H_2O/100g of total solids (TS) respectively (Jouppila and Roos 1994a).

The presence of crystalline lactose can be detected using a polarised light microscope as described by Zuo (2004). Crystalline lactose re-rotates polarised light, allowing observation under two opposing polarising lens. Amorphous lactose does not re-rotate light and thus no light is observed. Zuo (2004) observed the presence of crystalline lactose in some dairy powders containing amorphous lactose after storage for a long period of time.

2.3 Milk Standardisation

Currently, the situation in the dairy industry places emphasis on protein as opposed to fat as the most highly valued component in milk products. Payment schemes are based on protein and fat price determinates (Hardham 1998). Protein content in raw milk varies from 34% solids not fat (SNF) up to as high as 42% SNF and is calculated by multiplying Total Kjeldahl Nitrogen (TKN) by 6.38. CODEX (1999) regulations governing milk powder composition allow the reduction in protein levels from 42% to 34% (Protein:SNF). Milk permeate or pure lactose monohydrate solutions are combined with the milk stream to lower the protein content, while maintaining the natural casein/whey protein ratio of the original milk. Protein standardisation can be used to adjust the protein content up (up standardisation) or down (down standardisation) to overcome natural fluctuations and meet product specifications. Protein reduction is usually achieved by lactose addition resulting in an increase of lactose of 15% in WMP (54 to 39% lactose) and up to 20% in SMP (48 to 56% lactose) (D. L. Pearce, N. T. Russell and A. G. Foskett, 2004, personal communication). Up standardisation is achieved by removing a

portion of protein free ultrafiltration (UF) permeate. Down standardisation is achieved by mixing excess protein free UF milk permeate to skim milk. The end result of protein down standardisation is higher quantities of amorphous lactose present in the powder, making the powder more likely to stick during drying.

Fat and protein content in milk fluctuates widely depending on the breed of animal, feeding regime, geographical location and season. Protein content in New Zealand averages between 3.16 – 4.22 g/100 g (Roginski et al. (2003), data from 1996). Milk proteins are distributed in the milk serum in clusters of 2 – 8 molecules. The recombination of a milk stream such as permeate to milk should contain the same material as the primary milk. It should not significantly alter ratios of the individual water soluble molecules capable of penetrating the UF membrane and therefore should not effect the mineral composition of the final product, however this theoretical assumption does not always hold (Roginski et al. 2003). For protein adjustments in milk powder CODEX (1999) approves the addition of lactose as an alternative to UF permeate provided the casein/whey protein ratio of the original milk is unchanged.

2.3.1 Permeate Composition

Milk permeate contains mainly lactose, milk salts, minerals, non-protein nitrogen (NPN) and water. It is approximately 6% total solids of which more than 70% is lactose and around 0.7% is whey protein (Zall 1992). Normal milk has a pH of ~ 6.6. As with milk, the composition of permeate fluctuates with the season. Protein concentration in milk peaks in spring and autumn milk (370 – 470 g/kg protein in SMP), with a reduction in lactose concentration (to around 370 g/kg) during autumn (Newstead et al. 1977).

Hardham (1998) found that skim milk and sweet whey permeates increased the heat stability of milk, while acid whey decreased stability. This indicates that the salt concentration is important to the thermal stability of milk. The main salts in permeate are the unbound ions that are able to pass through the membrane separation stage. These include calcium, potassium, sodium, chloride, phosphate and citrate. With the addition of

permeate or lactose to down standardise the protein content in milk, the concentrations of these fractions (mmol/kg solids not fat) may be altered slightly.

2.3.2 Milk Salts

Salts present in milk are calcium, magnesium, sodium, potassium, phosphate, citrate and chloride. Soluble salts are present in various ionic forms and unionized complexes. Calcium and phosphate exist in excess in milk, such that the solubility of calcium phosphate is exceeded. An equilibrium exists in the distribution of calcium and phosphate between colloidal and soluble phases. At the normal pH of milk calcium phosphate is maintained in solution (Fox and McSweeney 1998). The insoluble colloidal form of calcium phosphate (CCP) is important for maintaining the integrity of the casein micelle (Fox 1997; Fox and McSweeney 2003). Addition of calcium to milk causes precipitation of soluble phosphate as CCP and a decrease in pH (Fox and McSweeney 1998). Lowering the pH dissolves colloidal calcium phosphate, as does reducing the temperature (Fox and McSweeney 1998). Addition of citrate reduces the concentrations of calcium ions and CCP, and increases soluble calcium, phosphate and pH.

2.4 GLASS TRANSITION TEMPERATURE

The concept of the glass transition point (Tg) was developed well prior to the 1990's in the area of plastics however it was not until the 1990's that Tg was used to explain the phenomenon of stickiness and state transformations in amorphous substances, particularly in relation to food stuffs. Peleg (1993) describes the concept of Tg as the progenitor of physical change in viscous behaviour of solid foods. The glass transition point is a second order transition between glass and rubber states. A glass is defined as an amorphous, non-crystalline solid which can be formed by rapid sub-cooling of the liquid or dehydration, to a viscosity as high as $10^{10} - 10^{14}$ Pa.s (Boonyai et al. 2004; Foster 2002). Below the Tg point solids exist as "glasses", above the Tg point they exist as "rubbers" due to decreased viscosity ($10^{6} - 10^{8}$) (Downton et al. 1982; Peleg 1993; Roos and Karel 1993). In amorphous systems the glass transition is temperature and composition dependent, and is characterised by a change in specific heat capacity. Typical physical changes governed by viscosity include crystallisation, stickiness and

collapse (Roos and Karel 1993). The sticky point temperature of sugar containing food has often been related to its Tg. Tg is becoming a fundamental parameter used to explain phenomenon such as stickiness, caking, agglomeration for amorphous and semi crystalline foods.

When the Tg is exceeded sufficiently, the viscosity at the surface of the particle decreases allowing the material to flow and liquid bridges to form between particles (Brooks 2000; Foster 2002; Zuo 2004). As food powders are not pure materials or completely homogenous, it is therefore not expected to observe a sharp Tg transition (Peleg 1993). This phase change is generally observed over a range of temperatures covering Tg onset and Tg end set of the transition, and the difference may be as high as 10°C (Roos and Karel 1993). However a single Tg value is often reported, usually the Tg onset or Tg mid point (Boonyai et al. 2004; Roos et al. 1996).

Roos and Karel (1991c) observed that the Tg decrease was most significant as moisture content increased from 0 to 5 g H_2O/100 g dry matter. Increased flow due to lower viscosity of the material in the rubber state allows stickiness, caking, collapse and crystallisation to occur (Foster 2002; Roos et al. 1996). Crystallisation forms solid bridges in the bulk sample resulting in caking. As crystallisation occurs moisture is released which is absorbed up by the remaining amorphous lactose initiating sticking in the rest of the powder (Foster 2002).

2.4.1 Determination of Tg

A glass can enter the rubbery state by either an increase in temperature at constant moisture or a_w or at a constant temperature and increase in moisture to reduce the Tg to below ambient temperature (Foster 2002).

Tg can be determined by a number of analytical methods. These methods detect a change in physical properties such as change in volume, enthalpy, mechanical and dielectric properties. The most common method is differential scanning calorimetry (DSC) as used by Foster (2002) that detects endothermal changes in apparent heat capacity during the

second order glass transition (Boonyai et al. 2004; D. L. Pearce, N. T. Russell and A. G. Foskett, 2004, personal communication; Roos et al. 1996). DSC measures temperature and heat flows associated with materials as a function of time and temperature. In DSC the scanning rate (heating rate) resulted in differences in the Tg determined (Aguilera et al. 1995). Caution must be taken in measurement and interpretation of Tg as it covers a broad temperature range and varies between instrumental differences.

There is an offset in the published data of Tg points for amorphous lactose. Brooks (2000) found this was due to residual moisture in amorphous lactose for samples equilibrated to a zero a_w, which can have a plasticising effect. Brooks (2000) found that the Tg of dry amorphous lactose was 115°C, but amorphous lactose with a a_w of zero still had approximately 1% moisture, resulting in a Tg of 101°C. This 101°C value is the commonly accepted literature value at a a_w of zero. For dairy powders Tg is more readily predicted from a_w measured using a RH probe, rather than moisture content, which includes moisture associated with proteins not involved in stickiness mechanisms.

Previous studies by Hennigs et al. (2001) found that the offset between the sticky point and Tg for skim milk was 14 – 22°C. Ozmen and Langrish (2002) suggest that the glass transition is about 10°C wide, and differences of 2 – 10°C were found between experimental and predicted glass transition temperatures, possibly due to fat and protein content in skim milk.

2.4.2 Predicting Tg

Tg can be predicted from the powder a_w and moisture content by various methods. The Gordon Taylor equation (Equation 1-5) predicts Tg from a_w or moisture content (Hennigs et al. 2001; Roos and Karel 1991b). Hennigs et al. (2001) used the equation to predict the Tg of skim milk for moisture contents from 0 – 10 g/100 g of dry powder.

$$T_g = \frac{w_L T_{gL} + k w_w T_{gw}}{w_L + k w_w} \qquad (2\text{-}5)$$

This is essentially a mass-proportional mixing rule with a 'contribution factor' (k) for the water component. Brooks (2000) used a value for T_{gL} of 115°C and k of 6.9, but found that a better prediction was obtained using the following third order equation (Equation 1-6) for amorphous lactose values $0 < a_w < 0.575$ (Paterson et al. 2005).

$$T_g = -530.66(a_w)^3 + 652.06(a_w)^2 - 366.33a_w + 99.458 \qquad (2\text{-}6)$$

Foster et al. (2005) provides Equation 1-7 for predicting Tg for multi-component powders where a_w is the water activity of the powder. This equation used the Tg of a multi component powder based on weighted addition and was found to give a good overall fit for dairy powders with amorphous sugars. a_w is an indirect measurement of the powder water content.

$$T_g = \sum_{i=1}^{n} x_i T_{gi}(a_w) \qquad (2\text{-}7)$$

2.4.3 Significance of Tg

The term stickiness is not well defined in the literature. Stickiness is the state where particles are able to stick to each other and/or to a surface, compared to caking where the particles have already stuck to each other and/or a surface and have formed a hard solid mass. Tg has been recognised as a parameter which helps to explain stickiness of amorphous and semi crystalline foods, particularly low weight carbohydrates (Bhandari and Howes 1999; Roos and Karel 1991b). At temperatures above Tg, the viscosity decreases allowing liquid bridging of amorphous carbohydrate to occur. The sticky point temperature (temperature above the Tg value where initiation of stickiness occurs) is a parameter of practical significance rather than the actual Tg. This temperature is described as the critical "x" factor in Zuo (2004) and is referred to as $(T-Tg)_{critical}$ in Paterson et al. (2006) and this work.

Exceeding the Tg of amorphous lactose leads to the structural change of sticking, caking, collapse and crystallisation of amorphous structure. Increasing the water content of the amorphous lactose lowers the Tg value. Tg also decreases with molecular weight. The

addition of high molecular weight maltodextrins increases the Tg of a material (Adhikari et al. 2004). Of the main carbohydrates glucose, fructose, lactose and sucrose, lactose has the highest Tg of 101°C at zero a_w (Roos and Karel 1993).

2.4.4 T–Tg

T–Tg is the temperature difference between the temperature of the powder (T) and the powder's glass transition temperature (Tg). The $(T-Tg)_{critical}$ temperature is the temperature change at which the initiation of stickiness occurs (called instantaneous stickiness in Zuo (2004) and Zuo et al. (2006)) as measured by the particle gun technique. Bhandari et al. (1997), Ozmen and Langrish (2003), Palzer (2005), Paterson et al. (2005), Roos and Karel (1991c) and Shuck et al. (2005) have also used the concept of viscosity of amorphous powders decreasing as the value of T–Tg increases to describe the sticking behaviour of amorphous powders.

Using the blow test method, Paterson et al. (2005) found that the development of stickiness with time was generally similar at the same T–Tg levels, regardless of what combination of temperature and RH was used. This indicates that the main factor in amorphous lactose stickiness is the temperature above Tg, $(T-Tg)_{critical}$. T–Tg can cause dramatic structural change leading to stickiness, caking, collapse, and crystallisation. T–Tg is the important parameter rather than the actual temperature the powder experiences (Brooks 2000; Chatterjee 2004; Paterson et al. 2005; Zuo 2004).

Ozmen and Langrish (2003) tested the hypothesis that the key parameter affecting wall deposition is the difference between the particle and sticky point temperature $(T-Tg)_{critical}$. They found that higher wall deposition was associated with increasing the particle temperature relative to the sticky point temperature, but there was no abrupt start/stop point at either side of the sticky point curve.

2.5 STICKINESS MECHANISMS

Stickiness is particularly a problem during drying and storage of sugar rich foods (Bhandari et al. 1997). Stickiness is a time, temperature and humidity dependent

phenomenon. There are two main factors that determine whether particles will deposit on the walls and associated surfaces. They are whether the particles approach the walls and whether or not they stick to the walls when they touch (Ozmen and Langrish 2003). Papadakis and Bahu (1992) report five major groups of mechanisms for particle attraction: intermolecular and electrostatic forces, mobile liquid bridges, immobile liquid bridges, solid bridges and mechanical interlocking. Cohesion refers to the particles sticking to the material of the dryer and associated equipment walls by the formation of bridges of material between the individual particles. Adhesion refers to the particles sticking to the surface of one another through the mechanisms described below. Cohesion is a measure of inter-particle forces thus reflecting the stickiness of the particle surfaces (Chen et al. 2004).

Stickiness is a material property, depending strongly on time, temperature, moisture content and humidity (Paterson et al. 2006; Zuo 2004; Zuo et al. 2006). Stickiness of amorphous food powders due to viscous flow mechanism is governed by temperature and water content (Downton et al. 1982). Stickiness occurs above certain values where the material behaves in a cohesive or adhesive fashion, due to the formation of liquid bridges between surface contact points. Stickiness of particles is a surface phenomenon affected by surface composition and characteristics of the particle (Adhikari et al. 2005; Chatterjee 2004; Foster 2002; Paterson et al. 2006; Peleg 1993; Zuo 2004). In powders, minor changes can result in changes to the particle surface properties, which result in major changes in the bulk behaviour as surface forces dominate (Peleg 1993).

Stickiness has been defined as the stage when liquid bridges between particles have formed and the sticky stage exists while the bridges are in a liquid state (Foster 2002). Caking refers to the solid mass that forms when the liquid bridges solidify. Stickiness refers to both particle-particle and particle-wall interactions as would occur in spray drying and storage. With time, these liquid bridges can crystallise resulting in irreversible consolidation of liquid bridges, caking (Aguilera et al. 1995).

The two main mechanisms of stickiness identified by Foster (2002) are:

1. Stickiness due to fat content. In powders containing greater than 42% total fat at temperatures exceeding 40°C molten fat liquid bridges form between adjacent particles
2. Stickiness due to amorphous lactose content. Amorphous lactose at temperatures above Tg behaves as a viscous liquid forming liquid bridges. Therefore it is important to be able to identify a critical temperature which exceeds Tg where sufficient liquid bridges form to cause initiation of stickiness.

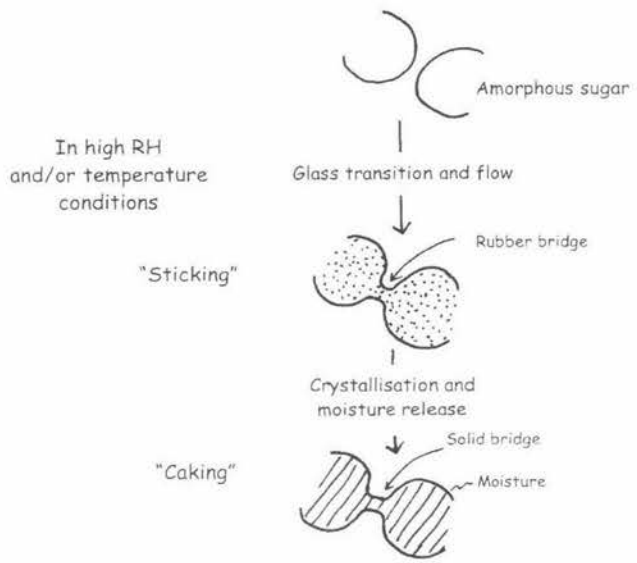

Figure 2-1. Diagram of amorphous lactose sticking and caking mechanism, Foster (2002).

As explained by Zuo (2004) and Ozmen and Langrish (2003) stickiness due to electrostatic forces and charge are insignificant compared to liquid bridging, a surface tension and viscosity related phenomenon. In SMP stickiness is due to amorphous lactose forming liquid bridges (Figure 2-1), the physical state is governed mostly by the state of the primary sugar, lactose (Jouppila and Roos 1994b; Zuo 2004). The caking temperature of the powder is different from the sticky temperature (Boonyai et al. 2004). Caking occurs over time while stickiness is virtually instantaneous. Proteins can also become sticky upon hydration (Chen et al. 2004). The extent that lactose, proteins and other components affect the overall stickiness of milk powder is not yet known quantitatively (Chen et al. 2004).

2.6 SURFACE COMPOSITION OF MILK POWDERS

Spray drying is the most important process for milk powder production. A powder's surface composition is important to its technical functionality (Zuo 2004). Surface composition is expected to influence functional properties such as wettability, dispersability, oxidative stability and flowability. Hennigs et al. (2001) state that little is known about the chemical surface composition of powders and the influence this has on powder properties.

Electro spectroscopy for chemical analysis (ESCA) has been used by various researchers to estimate the powder surface composition (Faldt and Bergenstahl 1996a; Kim et al. 2003). ESCA enables direct investigation of different components on the powders surface during drying and storage and is a reliable technique (Kim et al. 2005). It has been suggested that the composition of the air-water interface of the droplets formed during the spray drying process are reflected in the powder surface composition after drying (Kim et al. 2003). Since protein has a high surface activity it accumulates at the particle surface forming a film around the dried particle (Faldt and Bergenstahl 1996b). Using ESCA Faldt and Bergenstahl (1996b) found for a solution containing 1% whey protein on a dry weight basis, as much as 40% of the surface of the spray dried powder was covered with whey protein. The technique of scanning electron microscopy (SEM) also has been used to investigate surface composition. Contrasting results have been obtained when comparing SEM to ESCA with reference to fat released at the surface and protein encapsulation. This difference is likely to be due to the level of detection obtained by each method. ESCA is able to detect changes in fat release at the microscopic level, where this is below the detection level of SEM.

Faldt and Bergenstahl's (1996a; 1996b; 1996c) experiments using model emulsions indicate that fat (soybean oil) was encapsulated at the surface and interior of the particle by protein and to a certain extent amorphous lactose. A release of fat to the powder surface when stored under humid conditions was observed with the exception of powders containing a small amount of lactose. The release of fat for powders not containing

lactose must be at the microscopic level (below the detection of SEM). In contrast powders containing lactose where the fat is released to the surface by lactose re-crystallisation resulted in large changes in the particle structure. Models of whey protein, lactose and soybean oil used by Faldt and Bergenstahl (1996b) found that whey protein has a lower ability to encapsulate fat than sodium caseinate. The whey protein found on the surface of the particle increased when stored under humid conditions with amorphous lactose re-crystallisation again causing release of encapsulated material to the particle surface. The stability of the emulsion depends on the adsorbed layer of surface-active proteins and the ability of this layer to create repulsive interactions between the droplets (Faldt and Bergenstahl 1996c).

It has been shown that with increased lactose more fat is released to the particle surface during storage under humid conditions. After storage in humid conditions, the particle surface changed with increased indentations and particles agglomerated. Faldt and Bergenstahl (1996c) found that lactose at 5% dry weight prevented fat release under humid conditions. There were indications of an interaction of lactose with sodium caseinate, but any similar interaction with whey protein was too weak to observe. Faldt and Bergenstahl (1996c) did find an indication of interactions between whey protein and lactose, which keeps the emulsion droplets intact during drying and re-dispersion, but this interaction was not sufficient to keep the fat encapsulated.

Kim et al. (2003) investigated surface composition of milk powder compared to the bulk composition. Three difference scenarios on how the surface is formed in spray drying were presented: crust formation, solid/solute segregation and protein adsorption on air/liquid interface. This work provided an indication of a solid/solute segregation that must occur before a crust is formed in drying where the surface is expected to consist of the component with the smallest diffusion coefficient. It was also seen that protein, a surface-active component, dominated the surface composition, adsorbing preferentially to the air/liquid interface during atomisation in spray drying. The bulk composition was considerably different to the surface composition in both WMP and SMP (Table 2-2). Results are consistent with those of Faldt and Bergenstahl (1996b) where fat was over

represented at the particle surface compared to the bulk composition. Faldt and Sjoholm (1996) found similar results between model emulsion powders and industrial milk powder and between powders made industrially and those made using pilot/lab scale techniques indicating that the air-water interface is of importance rather than exact process parameters.

Table 2-1. Bulk composition compared to surface composition for spray dried milk powders.

Powder	Component	Bulk (%)	Surface (%)
WMP[1]	Lactose	40	2
	Protein	31	Negligible
	Fat	29	98
SMP[1]	Lactose	58	36
	Protein	41	46
	Fat	1	18
Emulsion powder[2]	Lactose	57	13
	Whey protein	38	50
	Soy bean oil	5	33

[1]Kim et al. (2003)

[2]Faldt and Bergenstahl (1996c)

2.7 MEASURING STICKINESS

Stickiness measurements have been developed over the last 50 years, however most techniques measure particles at slow moving or stationary phases. For a given moisture content, a distinct transition from the non-sticky to the sticky state has been observed when the temperature increases. This transition is called the sticky-point temperature. By varying the moisture content, different sticky-point temperatures can be found which form the sticky point curve when plotted against moisture content (Hennigs et al. 2001).

Stickiness data reported in the literature varies depending on the measurement test method used, the type of powder, and the temperature and humidity conditions. Test methods used vary from static particles to moving particles, long or short residence times, pre-conditioning of powders, velocities and particle contact points. Variations in the

sticky point measured by different methods exist and are most likely explained by particle residence time and velocity. D. L. Pearce, N. T. Russell and A. G. Foskett (2004, personal communication) have shown that the stickiness point is related to particle momentum.

2.7.1 Sticky Point Curves

The sticky point curve describes the safe and non-safe operating conditions to avoid powder stickiness (adhesion and cohesion). Sticky point temperature curves are used to develop an operational safety envelope to minimise stickiness during processing (Hennigs et al. 2001; Zuo 2004). Quantifying sticky curves assists plant operators in running their driers more efficiently (D. L. Pearce, N. T. Russell and A. G. Foskett, 2004, personal communication). Zuo (2004) described the construction and analysis of sticky point curves from temperature versus RH graphs. The curve for a particular powder is shown to follow the curve for the main amorphous sugar, in this case lactose, increased by a temperature increment T–Tg. Zuo (2004) describes graphical presentation of the data in the form of T-Tg as further representation of the sticky point (the x-intercept) with the slope representing the sensitivity of the powders tendency to stick with changes in temperature and humidity.

In convective drying, a lower temperature than the sticking point must be chosen for the gas exit temperature and product off take temperature (Lockemann 1999). The temperature at which thermal decomposition of a product commences gives an absolute upper limit for the safe operation of a drying unit. Lockemann (1999) suggests that for reliable operation of a contact dryer, the temperature of heated surfaces must remain below the sticking temperature.

2.7.2 Review of Stickiness Evaluation Techniques

Various techniques have been trialed to measure the stickiness and develop stickiness curves (Table 2-3). Hennigs et al. (2001) used a temperature range of 25 to 95°C for investigating the stickiness of skim milk powder using a rotational impeller in a bed of powder. They found that the stickiness was a function of bulk temperature and moisture

content and showed good agreement with the Tg of lactose and a sticky curve was obtained by adding 23.3°C to the predicted Tg. Chatterjee (2004) validated that a Tg + x line could be fitted to the stickiness curve for the particle gun method.

Stickiness and drying at the surface of a droplet has been investigated by Adhikari et al. (2005) and Adhikari et al. (2003b) with convective drying, observing the outer most layer and skin formation of an individual particle. In contrast to other results published, stickiness observed for the drop surface obtained a maximum peak of stickiness when the surface layer Tg reaches or just crosses the drop temperature (T_d). The drop surface becomes completely non-sticky when the surface layer Tg is higher than the drop temperature by 10°C. This means that a safe regime is defined where Tg of the surface layer is $\geq T_d + 10$°C (Adhikari et al. 2005). These results are contradictory to sticky point temperatures obtained by tests measuring cohesive properties. Adhikari et al. (2005) suggests that these differences are due to the stickiness relating to the adhesive force at the drop surface-equipment interface in their test method, and previous results using powders with moisture contents below 0.1 (dry basis kg H_2O/kg solid). Adhikari et al. (2005) suggest that sticky point tests reported in the literature are not applicable to drops or particles of low molecular weight sugars subject to convective drying. The drying behaviour and transport of agglomerates and bulk powders is different from that of a single spherical particle.

Table 2-2. Classification of the stickiness characterisation techniques for food powders, adapted from Boonyai et al. (2004).

Test Method	Particle velocity	Particle residence time
Direct Methods		
Pneumatic		
Particle gun	20 $m.s^{-1}$	< 1 second
Fluidised bed	0.22 - 0.44 $m.s^{-1}$	30 - 120 minutes
Blow test	0 $m.s^{-1}$	~ 30 minutes
Cyclone test	15 - 30 $m.s^{-1}$	1 - 3 minutes
Traditional		
Propeller driven	0 - 1 $m.s^{-1}$	
Ampoule	0 - 1 $m.s^{-1}$	
Optical probe[1]	0 - 1 $m.s^{-1}$	
Shear cell	0 - 1 $m.s^{-1}$	
In Situ stickiness tests		
Indirect Methods		
Glass transition temperature		
Thermal compression	0 $m.s^{-1}$	
Static mechanical test[2]	0 $m.s^{-1}$	3 -15 minutes
Stickiness and caking sensitivity index (DSC)[3]	0 $m.s^{-1}$	

[1] Lockemann (1999)

[2] Boonyai et al. (2005)

[3] Schuck et al. (2005)

2.7.2.1 Pneumatic Methods

Fluidisation, blow test, cyclone stickiness tests are the techniques which most closely simulate the stickiness behaviour of a material during dehydration, particularly spray and fluidised bed drying (Boonyai et al. 2004). The blow test is applicable to stickiness investigations during storage and transportation. It is important to measure stickiness in a dynamic condition since the dynamics within the dryer and surface property of the dryer wall can influence the stickiness of the drops/particles. The particle gun method has not been reviewed in the current literature as this technique is relatively new, but would fall into the above category for applicability of simulating spray drying (Table 2-2).

2.7.2.1.1 Particle Gun

The particle gun was designed to measure the point at which a powder becomes sticky. It is very useful in mimicking the industry conditions in spray drying. Zuo (2004) used a temperature range of 60 – 80°C which corresponds to spray drier outlet temperatures; and an air velocity of 20 $m.s^{-1}$. Air velocities found in industrial cyclones are 20 – 45 $m.s^{-1}$ and in ducts after the dryer 20 – 25ms^{-1} (Masters 1991). Masters (1991) states that pneumatic conveying velocities exceeding 20 $m.s^{-1}$ are recommended for most spray-dried products. Adhikari et al. (2005) report that common dryer outlet temperatures used when drying sticky materials are 65 – 90°C. The velocity 20 $m.s^{-1}$ was chosen in initial particle gun design work carried out by Massey University and Fonterra. A $(T-Tg)_{critical}$ of 24.7°C was obtained for amorphous lactose by Paterson et al. (2006). The amorphous lactose sticky point occurs in the range of 24 to 26°C above Tg, with 25°C also deduced by Brooks (2000) using the blow test method.

Paterson et al. (2006) assumed that insufficient drying was not a cause for stickiness in powders. This was based on the findings that stickiness was a surface phenomenon and the residence time of < 0.05 seconds in the particle gun was sufficient for physical changes to occur. This assumption is also supported by findings of Ozmen and Langrish (2003) that dry particles were observed non-deformed on impact with plates hung in various positions within a pilot spray dryer, indicating that the particle was dry almost instantaneously within the dryer.

The particle gun uses a powder delivery system where particles are fired through the gun at a stainless steel collection plate. The percent of powder deposited on the plate is measured for a constant temperature and varied RH. Creating a plot of %deposition versus RH the initial sticky point for a particular dry bulb temperature can be identified. The time of exposure of the particle is < 0.05 seconds, sufficient time for surface stickiness to manifest. Zuo (2004) and Chatterjee (2004) used the particle gun to determine stickiness curves for a wide range of dairy powders. These studies confirm that stickiness is indeed a surface phenomenon affected by the surface composition of the particles.

Unique to the particle gun technique is the fact that not only the initiation of stickiness at a particular temperature was observed, but the data can also be graphically displayed to give an indication of how quickly the powder becomes a problem as it enters the stickiness regime (Zuo et al. 2006). Graphing %deposition versus T–Tg results in a T–Tg plot. The advantage of using a T–Tg plot is that the distinctive stickiness point due to amorphous lactose is highlighted, with the slope describing the rate of stickiness development (Zuo et al. 2006). The $(T-Tg)_{critical}$ value can be used to construct the stickiness curve parallel to the Tg amorphous sugar curve.

The particle gun uses higher air velocities than the fluidised bed test. The results from the particle gun give higher temperature and a_w conditions for stickiness manifestation than the fluidised bed rig. This may be due to the particles at lower speeds having lower kinetic energies, requiring less force to hold them together on impact. At higher velocities particles may knock off other particles loosely adhering. Zuo (2004) suggests that stickiness is affected by such kinetic energy of the particles.

2.7.2.1.2 Fluidised Bed

Fluidisation allows close contact between individual particles in the air stream. Rapid mass and energy transfer is achieved (Boonyai et al. 2004). The air velocity varied between 0.22 $m.s^{-1}$ and 0.42 $m.s^{-1}$, and showed no effect on the end point (Chatterjee 2004). Chatterjee (2004) measured powder cohesive stickiness using the fluidised bed method. The observed end point was when complete seizure of the particle bed occurs.

Amorphous lactose powder had the lowest critical temperature difference above Tg and crystalline lactose was the least sticky (Chatterjee 2004). Stickiness depended on the amorphous lactose content and the particle size. Larger particle size affects the bed by particles having greater inertia, requiring a larger stickiness force to halt fluidisation. This method is limited in that it cannot be used for high fat powders which will not fluidise. The method primarily measures particle cohesion and does not consider factors such as trajectory, impact and material surface which are involved during spray drying.

Foster (2002) used the blow test to distinguish between fat caking and amorphous lactose caking in dairy powders.

2.7.2.1.3 Blow Test

The blow test was developed by Brooks (2000) and Paterson et al. (2005) who used the method to determine caking in dairy powders. The critical temperature of the initial sticky point was found to be 25°C above the glass transition point for amorphous lactose (Tg + 25°C) regardless of the combination of water activity and temperature used.

In this test the powder was pre-conditioned for different water activities and held in a bed. Air was passed through a tube at a fixed height and angle above the bed. The air velocity was increased until a channel was blown in the bed, with the flow rate measured as the stickiness or caking strength of the powder. This test allows readings to be taken over time and the ability to observe the time dependent sticking and caking phenomenon. This test is useful for the study of powder conditions for storage where the residence time is long enough for stickiness to develop, but is not suitable for measuring the conditions for initiation of stickiness of a particle impacting on the wall of a spray dryer.

2.7.2.1.4 Cyclone Stickiness Test

The cyclone test measures both cohesive and adhesive properties of powder particles. It simulates impaction on the chamber wall during spray drying. The system was preconditioned for the cyclone to equilibrate, after which one gram of powder was introduced. The air stream generates a rotary motion of powder particles. Stickiness was observed within 1 – 2 minutes (Boonyai et al. 2005). The test is fast and simple and appears to be practical for characterisation of material stickiness in spray drying, fluidised bed drying and pneumatic handling of dry powders (Boonyai et al. 2005).

The difference between the $(T-Tg)_{critical}$ observed between the cyclone test and the particle gun rig is probably due to the different air flows, particle trajectories and residence times between the two methods (Paterson et al. 2006). A constant temperature difference was observed between sticky curves for the cyclone test and the particle gun method (Paterson et al. 2006). In the cyclone test, particles travel for 1 – 2 minutes in the

humidified air, compared to a travelling time of 0.05 seconds in the particle gun. Particles in the cyclone test got sticky at lower temperatures than particles in the particle gun under the same RH air conditions. Longer residence times in the cyclone would allow moisture to diffuse from the outer layer (from the humidity of the air) to the inner core of the particles, hence perhaps the whole particle stickiness is observed rather than surface stickiness as with the particle gun method. With a long residence time, particles moving around in the cyclone have a higher probability of touching and adhering to the wall with multiple contacts.

Adhikari et al. (2005) found through *Biot* number investigations for mass transfer that moisture gradients exist in droplets of the size usually found in industrial spray dryers and should not be ignored. However temperature gradients can be safely ignored since the *Biot* number for heat transfer was found to be in the range of 0.06 to 0.1. Therefore it is the surface layer Tg value of the droplets that determines the particles surface stickiness.

It is unknown if the cyclone test or the particle gun test is a better measure of stickiness corresponding to industry experience. The cyclone method does include many parameters encountered industrially such as material of construction, angle of impact, velocity and involves the moisture of a whole particle as opposed to the surface measurement of the particle gun.

2.7.2.2 Traditional Methods

2.7.2.2.1 Propeller Driven Methods

This technique is the oldest of the stickiness measurement techniques. The sticky point tester consists of a tube containing a sample of known moisture content submerged in a heating medium. An impeller is turned manually (Chuy and Labuza 1994; Downton et al. 1982; Lazar et al. 1956) or mechanically (Hennigs et al. 2001; Ozkan et al. 2002). The sticky point is measured as a function of moisture content. The temperature is increased until the force to stir increases sharply as the particle surface becomes less

viscous. The sticky point curve generated can be used for selections of drying, handling and storage conditions for food powders. Sticky point methods such as various versions of propeller methods are predominantly influenced by the cohesion property of dry powders.

When comparing sticky point measuring devices for reliability and reproducibility results, Pasley et al. (1995) found the stirrer type propeller driven design to perform better than sheer cell methods.

2.7.2.2.2 Ampoule Method

The ampoule method is the simplest techniques for measuring stickiness. The powder cohesion is measured as influenced by increased temperature. The collapse or sticky point temperature is the temperature where the appearance of the samples surface changed from a porous solid to a viscous glassy matter. Chuy and Labuza (1994) used this method to measure surface caking temperature of infant dairy powders. Problems with this method arise if condensation forms within the ampoule.

2.7.2.2.3 Optical Probe Method

Developed by Lockemann (1999), this method is based on measuring changes on the reflectance property of a material at the sticky point. This technique is limited to only those materials that exhibit changes in the reflectance at the sticky point, that is not transparent materials (Boonyai et al. 2004).

2.7.2.2.4 Shear Cell

The shear cell method is commonly used for quantification of cohesion and adhesion of granular materials (Boonyai et al. 2004). In the shear cell method, powder is placed in a box and split in half horizontally or vertically. Various normal stresses and shear stress are applied to the top half of the cell while the lower half is held stationary. This method provides information on the cohesive force between particles, however it is not usually used to characterise the stickiness. It is useful for investigation of the flow behaviour of powders through chutes and hoppers.

A variation to the shear cell method, Chen et al. (2004) uses an unconfined yield stress, measuring powder cohesion over a range of temperatures and humidity. The test involves creating powder plugs and then shearing the plugs.

2.7.3 $(T-Tg)_{critical}$

The $(T-Tg)_{critical}$ value is of more practical significance than Tg for determining the onset of stickiness in dairy powders. The higher the $(T-Tg)_{critical}$ value, the more tolerant the powder is to higher humidity and/or temperature conditions with regard to instantaneous stickiness, as $(T-Tg)_{critical}$ is a function of a_w and/or moisture content of amorphous lactose Zuo (2004). The value of T–Tg that instantaneous stickiness occurs is an indication of where the powder would be expected to cause problems in transport lines (Paterson et al. 2006).

Foster (2002) suggests that Brooks (2000) is too conservative in his estimate of the $(T-Tg)_{critical}$. The stickiness point of amorphous lactose is reported as 10 – 20°C above Tg (Adhikari et al. 2005; Bhandari and Howes 1999) while 25°C was reported by Chatterjee (2004) and Brooks (2000) using the particle gun and fluid bed methods. Paterson et al. (2006) identified a $(T-Tg)_{critical}$ of 41.3°C for SMP using the particle gun rig. This value was higher than that of 21°C obtained by Chatterjee (2004) using the fluidised bed rig and 17.5°C for the stirrer test (Hennigs et al. 2001), all of which are above the Tg of amorphous lactose.

Zuo (2004) identified two ways to identify the $(T-Tg)_{critical}$ from raw data displayed as percent deposition versus relative humidity at constant temperature.

1. Identify the initial sticky point at a particular RH for each temperature tested. Fit a curve to data at temperatures above the Tg of amorphous lactose. Use the least squares method to identify $(T-Tg)_{critical}$, the difference between the powder Tg line and the sticky point line by best fit.
2. Plot percent deposition against T–Tg. $(T-Tg)_{critical}$ results as the x-intercept on the T–Tg axis when the data has been fitted with a linear regression. The slope of the line indicates the sensitivity of the powder to drying conditions.

The "x" value and the slope are unique to each powder. A stickiness curve is then created on a graph of temperature versus relative humidity.

2.7.4 Predicting $(T-Tg)_{critical}$

The original idea posed by Zuo (2004) was to generate stickiness curves for a range of powders and thus be able to predict the $(T-Tg)_{critical}$ value from a known composition. Correlations found between the $(T-Tg)_{critical}$ and the powder compositions were (a) between lactose content and $(T-Tg)_{critical}$ identified and (b) between the rate of stickiness development and lactose content. Correlations were stronger when lactose composition was expressed as %SNF (Zuo 2004). The following regression Equation 8 was obtained for powders with fat $\leq$ 42%TS (total solids).

$$(T - Tg)_{critical} = 53.91 + (-0.20337) \times \%TSFat + (-0.2648) \times \%TSLactose \qquad (1\text{-}8)$$

Zuo found this equation predicted a $(T-Tg)_{critical}$ within $\pm$ 10%. This error margin is rather large but the work by Zuo (2004) demonstrates the overall trend between the $(T-Tg)_{critical}$ and the percent amorphous lactose in the bulk powder. Since stickiness of the powder has been shown to be a surface phenomenon, further work is required in relation to surface composition and $(T-Tg)_{critical}$. This current work aims to reduce the error through further investigation and adjustment to the particle gun technique.

2.7.5 Particle Gun Result Repeatability

For spray drying processes precise temperature control is required. Only a few degree changes in temperature can cause instant stickiness. Tg and sticky temperatures vary depending on the technique used and the sample preparation method (Boonyai et al. 2004; Zuo 2004). For composite food powders having different species, the stickiness of the bulk powder is influenced by the components having the lowest Tg. Boonyai et al. (2004) state that Tg has been used as a stickiness indicator, but the accuracy, reliability, and applicability must be closely examined for each investigation. Further research will be required before an established empirical relationship can be applied between sticky and glass transition temperatures.

Replicate experiments completed by Zuo (2004) on SMP show considerable variation. $(T-Tg)_{critical}$ values obtained were 37.9 and 40.9°C, while the rate of stickiness development was 3.04 and 2.95 respectively. It was determined that crystallisation had begun in the oldest sample which could have contributed to the variation. Additional causes will be investigated in the current work, to identify whether the stickiness results are a function of the test method.

2.8 AMBIENT CONDITIONS EFFECT ON DAIRY POWDERS

The effect of ambient conditions on the dairy powder will be investigated with the aims of this work to obtain reproducible initial sticky point results with a reduced experimental error.

2.8.1 Water Activity & Relative Humidity

The temperature and RH inside the spray dryer will affect the temperature and moisture content of the skim milk particles and thus may affect the cohesiveness of the particles (Ozmen and Langrish 2003). Product quality is directly related to temperature and humidity experienced by the particles (Kieviet et al. 1997). The condition of the amorphous material depends on the temperature and moisture in the surrounding air (Zuo 2004). Fox (1997) states that to prevent lactose crystallisation in dairy powder storage, the moisture content should be below 6% corresponding to a water activity (a_w) of 0.4. Powders stored at < 0.01 and 0.12 a_w were still free flowing after one year of storage. The effect of exposing dairy powders to ambient air prior to testing is currently unknown.

Lactose crystallisation accelerates many deteriorative changes such as caking and oxidation, significantly decreasing storage stability. Jouppila and Roos (1994a) state that the amount of water sorbed by dehydrated skim milk was higher than that by lactose at RH < 40%. Crystallisation of pure lactose occurred at lower RHs (> 40%) than crystallisation of lactose in skim milk powder (> 50%) after one day at 24°C. Skim milk powder enzymatically hydrolysed lactose converted into galactose and glucose showed lower water sorption at RH < 40% than regular SMP. They found that the best model for predicting water sorption isotherms of dehydrated amorphous milk products was the

GAB model (Equation 1-2) which showed consistency at < 10% RH. Aguilera et al. (1995) found that amorphous lactose crystallised and released water at 42 – 52% RH at 25°C.

Differences in literature data for amounts of water sorbed by various milk products are possibly due to variations in material compositions, handling of materials and differences in methodology used. Jouppila and Roos (1994a) suggest that even short exposures of samples to high RH may change the physical state of the material, cause crystallisation, and decrease the amount of water sorbed, especially at low RH. Their results support time-dependent crystallisation and implicate water plasticization and the delay of crystallisation caused by other components in the milk powder.

The sorption moisture in milk products is mainly due to carbohydrate and protein components in the SNF fraction (Fox 1997). The water sorption by milk and whey proteins is sensitive to the chemical environment such as NaCl content.

2.8.1.1 Whey Powder

Teunou and Fitzpatrick (1999) and Teunou et al. (1999) investigated powder flowability in a range of food powders including skim milk and whey permeate. Flowability (measured using an annular shear cell) decreased with increasing RH (36% to 66%RH) and increasing temperature, however the effect observed also depends on the time the powder was exposed to the conditions. Whey permeate powder (d_{50} = 98 μm) is less coarse than SMP (d_{50} = 197 μm) suggesting susceptibility to cohesion and less free flowing. Teunou et al. (1999) found that whey permeate powder at 3.8% water content has a higher Tg (112°C) compared to skim milk powder at 4.6% water content (60°C) measured using DSC with heating rate of 10°C/minute. The Tg of whey powder (which contains a high amount of lactose) appears to be high compared to the amorphous lactose Tg of 101°C at zero a_w (Brooks 2000). Drying of whey protein solutions with low lactose concentrations result in powders with a porous microstructure and large vacuoles (Fox and McSweeney 2003).

In whey permeate powders lactic acid and salts contribute to stickiness in addition to the amorphous lactose present (Early 1998) resulting in wall deposits and blocked cyclones. It was also found that lactic acid content increased as the sticking point temperature decreased in whey. However Early did not check for the presence of glucose or galactose, the products of lactose hydrolysis by lactic acid bacteria. Fox (1997) suggests that there is a link between lactic acid content and hygroscopic properties in whey powders, which is consistent with claims by Early (1998).

2.8.2 Storage, Crystallisation & Relaxation

Relaxation time refers to the rate of structural change in amorphous material. The change in mechanical properties is related to the Tg. In the glassy state this can take a very long time (Roos et al. 1996). Since the amorphous material exists in a non-equilibrium state, time dependent changes occur as the matter approaches equilibrium. The WLF equation (Equation 1-3) describes temperature dependence of mechanical properties above Tg.

Hancock and Dalton (1999) investigated the effect of temperature and RH on the water vapour sorption of pharmaceutical sugars over several months of storage. Water vapour was determined gravimetrically and at all conditions 5 – 50°C and 0 – 90% RH water was sorbed. At increasing RH, spontaneous crystallisation occurred. At each humidity tested, increasing the storage temperature was found to decrease the water sorbed indicating an exothermic process. Crystallisation occurred as humidity increased from 20 – 60% for amorphous lactose, transforming to the most stable state. It was deduced that when water vapour interacts with amorphous sugars it either:

a) acts as a catalyst for crystallisation (confirmed in sucrose), lowering the energetic barrier for crystallisation and/or altering the interfacial energy for nuclei formation; or

b) acts as a reaction substrate (confirmed in lactose).

Initiation of crystallisation was detected before a change in the isotherm. Therefore it is not recommended to estimate the crystallisation point from isotherms (Hancock and Dalton 1999).

Chuy and Labuza (1994) carried out similar experiments on the caking and stickiness of powders based on Tg. Results obtained were similar to Hancock and Dalton (1999). At the slowest heating rate trialed, the caking and surface caking temperatures were lower when compared to results from fast heating rates. Prior storage temperature for infant formula powders was found to have a random effect on the caking temperatures observed. At higher storage temperatures some of the amorphous sugar may have crystallised and reacted with protein as browning was observed. These changes result in less amorphous lactose being available for collapse and thus a higher caking temperature.

2.9 OTHER POSSIBLE FACTORS EFFECTING STICKY POINT

It has been identified in previous work that the stickiness measurement and its repeatability may be affected by various aspects of the technique. Velocity, angle of impact, surface composition and pre-conditioning of powder may affect the stickiness result obtained. This work aims to adjust such factors to mimic industrial spray dryers investigate the effect on the initiation of stickiness and reduce the experimental error.

2.9.1 Angle of Impact

Particle trajectory, temperature and humidity are dependent on airflow patterns in the drying chamber. In sticking and caking the conditions under which particles come in contact with drying surfaces is of interest.

In NIRO compact type driers air enters with tangential velocity component referred to as the swirl. In most other dryer designs air enters as plug flow. The degree of swirl is termed the swirl angle, which is the angle between axial and tangential velocity components of the drying air at the inlet (Kieviet et al. 1997). The swirl angle influences the airflow pattern in the dryer. Kieviet et al. (1997) investigated modelling of the air flow patterns and temperatures in a pilot spray dryer. Small angles resulted in a fast flowing core, with slow circulation around the core. Increasing the swirl angle to a critical value resulted in vortex breakdown.

Ozmen and Langrish (2003) investigated the wall deposition of milk powder in a pilot spray dryer. They used a co-current spray drier to investigate the effect of varying the swirl vane angle for inlet air, inlet air temperature and liquid flow rate on wall deposition flux of skim milk powder. Inlet air swirl was found to significantly influence the wall deposition flux, with the highest angle of 30° giving rise to the largest wall deposition flux. Of the sticky tests found in the literature, only the cyclone test includes an effect of angle of impact encountered by the moving particles.

2.9.2 Material of Construction

Ozmen and Langrish (2004) observed the highest wall deposition flux when the particle temperature was closest to, or above the sticky point temperature. The sticky point temperature was determined using a stirred impeller as described by Lazar (1956) as the temperature that the required force to turn the impeller suddenly increased under constant humidity conditions. Changing the wall material did not have any significant effect on the observed wall deposition flux between using a non-stick material (nylon), adhesive tape or stainless steel inside a pilot scale spray dryer. Condensation present on the plate surface resulted in higher wall deposition fluxes because the particles impacting on the surface fell into a liquid film. Ozmen and Langrish (2003) suggest that it is likely that cohesion between particles occurs at a similar rate to adhesion in wall deposition of milk powder, with the observed plates covered in a fine layer of particles after 30 minutes. Ozmen and Langrish (2003) also found the temperature difference between the particle and the sticky point temperature of the skim milk powder to influence the wall deposition flux ($g.m^{-3}.hr^{-1}$).

When dry particles are being transported (cyclone, ducting, drying chambers) they may become electro-statically charged, particularly the insulator lactose. Grounding the dryer to reduce adhesion by electrostatic force did not show a significant effect on the wall deposition flux (Ozmen and Langrish 2003). Chen et al. (2004) also found that earthing dryers had little effect on particle adhesion/cohesion observed.

Michalski et al. (1997) provides a review on the mechanisms of adhesion. Food adhesion is governed by interlocking, wetting, electrostatic and chemical forces. Mechanical interlocking is governed by the surface topography at the angstrom level which is affected by the surface roughness. Leclercq-Perlat and Lalande (1994) found the greater the degree of surface irregularity the greater the chance of soil remaining during cleaning. Leclercq-Perlat and Lalande (1994) investigated the cleanability and surface characteristics of various materials used in the food and dairy industry using topography techniques and a yoghurt-culture mixture. When the material topography was reasonably smooth at a microscopic scale, clean ability differences were due to the chemical composition of the surface. The main fouling components were proteins for stainless steel and fat for plastics. A variety of stainless steel 304L were investigated with 2B glazed steel finished after mechanical rolling with a 220 grit sandpaper finish of 304L (G2BL) and bright annealing finish of 304L (RB08) being the best in terms of cleanability. The two most common in the dairy industry were 304L and glazed steel finished 304L (G2B) which were the most difficult to clean. 316 2B stainless steel is used in the dryer and cyclones used for SMP manufacture at Fonterra Te Rapa.

2.9.3 Effect of Velocity

The fluidised bed method used by Chatterjee (2004) results in a $(T-Tg)_{critical}$ value of 21°C, compared to the 17.5°C of the stirrer test and the 41.3°C of the particle gun for SMP reported by Paterson et al. (2006) and Zuo (2004). The increase in $(T-Tg)_{critical}$ measurements indicates that the stickiness of the powder is probably a function of the particle velocity. Zuo (2004) suggests that such differences are due to the differences in the technique used, indicating that stickiness is a function of the dynamics of the particle impact, as well as the air conditions. To further investigate this hypothesis this work will (a) examine industrial data to work towards deciding which method is most appropriate to obtain stickiness curves for industry, (b) examine the effect of velocity on $(T-Tg)_{critical}$ of a powder using the particle gun.

2.10 CONCLUSIONS

The particle gun simulates conditions found in industrial chambers, cyclones and ducting surfaces after driers. The gun is useful in mimicking the actual spray drier operating conditions by controlling air velocity, temperature and RH. This method was developed to measure the initiation of stickiness with particles travelling and hitting walls at velocities, temperatures and RH similar to those encountered industrially.

Outlet temperatures for spray drying heat sensitive products are usually around 60°C (Bhandari et al. 1997). Inlet temperatures used are in the range of 160 – 220°C, and outlet temperature usually 70 – 90°C. Droplets in spray drying typically never reach a temperature greater than 70°C (Fox 1997). In the initial stages of drying the particle temperature is close to the wet bulb temperature of the drying air, at the end of the drying operation the particles reach a temperature close to the outlet air temperature. The temperature range tested by Zuo (2004) was between 60 – 80°C. The RH range tested was 10 – 50 %RH (also reported as a_w equivalent).

Due to the significant negative economic consequences to the industrial processing and handling of sticky products, investigations to find an accurate, simpler and cheaper technique to characterise the stickiness behaviour of these types of products are still in demand (Boonyai et al. 2004).

CHAPTER 3 - MATERIALS & METHODS

3.1 INTRODUCTION

O'Donnell et al. (2002) described a method for a constant humidity air supply system which formed the basis for the particle gun rig. Chatterjee (2004) used the particle gun rig to determine stickiness for a range of dairy powders at temperatures of 28 to 52°C. Chatterjee (2004) discovered significant discrepancies between the temperature and humidity readings of the air leaving the air heater and at the air exiting the tip of the gun. These differences were found to be due to heat loss in the lines hence the low temperature range of the work. Zuo (2004) further modified the particle gun rig to minimise heat loss and measured the air temperature and RH at the gun outlet to define the final conditions. Zuo (2004) used a range of temperatures (60 – 80°C) and relative humilities similar to those experienced in industrial spray dryers. An air velocity of 20 $m.s^{-1}$ has been used by Zuo (2004) and Chatterjee (2004) based on industrial velocities experienced, 20 – 45 $m.s^{-1}$ (Masters 1991) and Crofskey (2000) initial recommendations. Typical air velocities are > 20 $m.s^{-1}$ for powder conveying and 10 – 25 $m.s^{-1}$ in ducts (Masters 1991).

A bench-top scale fluid-bed bed measurement method was investigated as a comparison to the particle gun method. The fluid bed apparatus has been used by T. Llewellyn (2005, personal communication), Chatterjee (2004), and D. L. Pearce, N. T. Russell and A. G. Foskett (2004, personal communication) to investigate powder stickiness related to industrial fluidised beds. The fluid bed rig results were compared to the particle gun results to detect stickiness variations due to lactose sources and test method.

3.2 MATERIALS

Amorphous lactose and fat are the primary components that cause stickiness in dairy powder (Chatterjee 2004; Foster 2002; Zuo 2004). The source of lactose (either from milk permeate or pure lactose solutions used in down standardisation of protein in SMP) was investigated to identify if this factor is indeed influencing the stickiness behaviour of such skim milk powders. The use of SMP eliminates additional stickiness complications

involving fat stickiness mechanisms. The effect was also investigated in WMP following the findings from the SMP samples.

SMP and WMP were made using the Fonterra Research Centre pilot plant modified Anhydro spray drier. Skim milk was concentrated to around 50% solids, and then spray-dried at an exhaust air temperature of 92°C (refer to Bloore (1981) for further details). Powders used in this work include skim milk powder (SMP) and whole milk powder (WMP) down standardised to 34% protein using either milk permeate or lactose solution. Six powders were produced under the same conditions: unstandardised, standardised with lactose solution and standardised with permeate for both skim and whole milk (Appendix 2). Composition was determined on a total solids basis. Additional SMP samples were also obtained for testing (Appendix 3).

3.3 METHODS

Two methods were used to investigate milk powder stickiness. The particle gun rig was used to investigate the effects of the ambient conditions and test parameters on the stickiness results. The particle gun method was used to detect the influence of lactose source on powder stickiness once the effect of the operating parameters was known. The fluid-bed apparatus was also used to investigate differences in stickiness due to lactose source for SMP and WMP.

The effect of particle size distribution was neglected in prior work using the particle gun rig. A riffler was used to sub-sample the powder ensuring a representative particle size distribution was obtained. Sealed sub-samples containing enough powder for one day's experiments ensured minimal sample exposure.

3.3.1 Particle Gun Rig Construction

Massey University in conjunction with Fonterra Research Centre developed the particle gun, which has been used successfully in previous work by Zuo (2004) and Chatterjee (2004). The initial sticky point was measured for particles travelling and impacting walls at velocities, temperatures and RH conditions similar to those encountered in the ducting

and cyclones of industrial-scale plants. The particle gun rig is constructed of two parts: a constant temperature and RH air supply and a particle feeding system that enabled the particle to be "fired" at a collection plate at the desired velocity (Figure 3-1). A venturi effect was used to create suction through the glass funnel fitted in a hole in the centre of the vortex chamber through which the powder was fed.

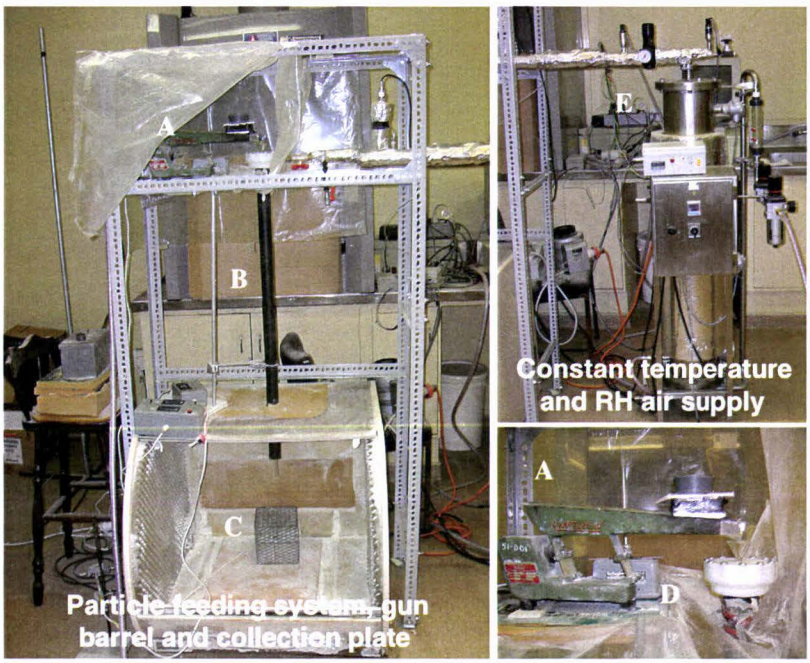

Figure 3-1. The modified particle gun rig. A vibratory feeder, B gun barrel, C collection plate, D vortex chamber with glass funnel, E water bubble column.

The temperature range of interest was 60 – 80°C, with most industrial drying operations running close to or above 80°C. A tip temperature of 78°C was achieved by setting the air heater to 88°C and the water heater to 70°C. Air velocities used for the particle gun were 20 $m.s^{-1}$, followed by subsequent investigation into the effect of air velocity over the range of 10 – 30 $m.s^{-1}$. Air temperature and velocity were measured with a hand held anemometer (Testovent 4000).

3.3.1.1 Particle Gun Set Up

The system used for this current work was similar to Zuo (2004) including minor adjustments based on her recommendations. Figure 3-2 shows the schematic set up of the improved particle gun rig. Alterations to the particle gun included:

1) Valve W3 was replaced by a pressure regulator valve, with an internal spring sized to handle 1 – 50 psig. This ensured that the air velocity did not have to be re-adjusted after every RH adjustment.

2) A mechanical vibratory feeder was added to feed the particles into the funnel. This reduced variation in the results due to inconsistent feed rates.

3) The plastic encasement around the feeder set up minimised fluctuations in the RH and temperature of the surrounding air. Zuo (2004) assumed the particle surface gained equilibrium with the air in the particle gun upon entry. Zuo's work limited the time the powder was exposed to the ambient air conditions prior to and during testing, however the effects of this exposure were unknown. In this work the room ambient air conditions were held constant by the use of an air-conditioning unit, with the air directly above the feeder controlled by an additional air stream (compressed air or a mix of compressed air and humidified air) flowing into the enclosed feeder.

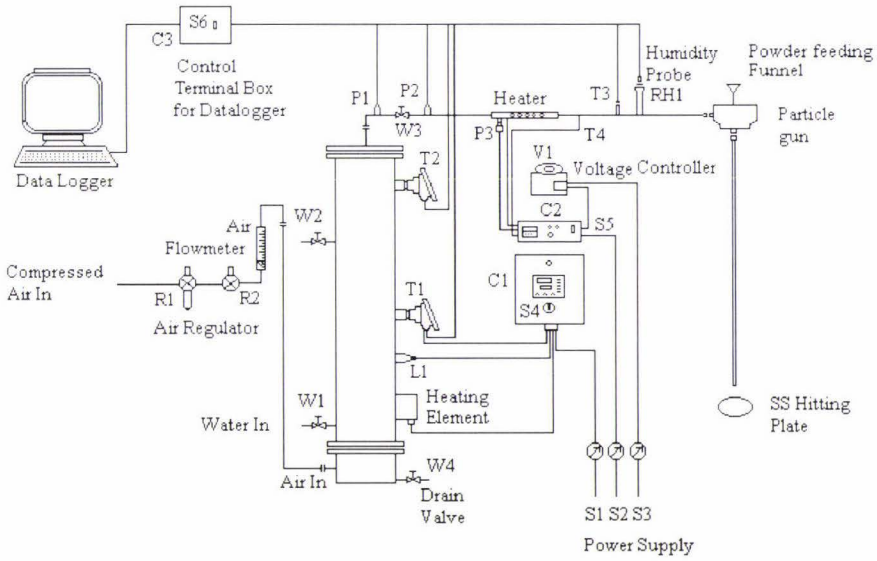

Figure 3-2. Particle gun rig schematic diagram, Zuo (2004).

A constant air temperature and velocity was used to fire the dairy powder particles at a collection plate down a 105 cm long, 8 mm internal diameter Perspex tube. The RH of

the air was gradually increased and the percent of powder adhered to the collection plate recorded at each setting. Using an air velocity of 20 $m.s^{-1}$ to fire the particles onto the collection plate gave the powder particles a residence time of 0.053 seconds, which was sufficient time for the observed surface stickiness to manifest. A constant air supply was ensured by passing compressed air through two pressure regulators R1 and R2 (Figure 3-2). R1 eliminates any pressure fluctuation from the compressor, while R2 controls the pressure of the bubble column. The air passes though a flow meter before entering the steel bubble column used to saturate the air under high pressure. The column temperature was kept constant though a heating element in the bottom (GCS-300 Shinko water temperature controller). The air stream passes though the bubble column at a pressure of up to 8 bar, then through an expansion valve (W3) to lower the pressure. The RH of the air stream is determined by the ratio of high (P1) and low (P2) pressures. The inline heater (CAL 3200 air temperature controller) enables the desired air outlet temperature to be achieved. The RH was increased by reducing the differential pressure between P1 and P2 by altering R2. Alternatively, increasing the water temperature in the column, allowing more water vapour in the air to be carried through the bubble column will increase RH, while increasing the inline heater will decrease RH. All temperature, pressures and air humidity were tracked on the computer (PC Direct 580Ax, Windows '95) using an Opto 22 logger.

The powder feeding system involved a glass funnel fitted into the top of the vortex chamber (designed by Massey University and Fonterra using Bernoulli's equation and a CFD program) which creates a venturi effect. This draws the powder down the funnel and into the firing tube where the air stream enters the vortex chamber tangentially.

3.3.1.2 Particle Gun Experimental Protocol

The operation procedure of the particle gun rig is detailed in Chatterjee (2004). Collection plates were placed 16 cm directly below the 105 cm long, 8 mm internal diameter Perspex tube. Chatterjee (2004) states that the time for the plate to be placed under the gun air stream to avoid possible heating and condensation was less than a minute. To avoid condensation forming on the collection plates, the plates were pre-

warmed on top of the bubble column. Round 316 2B stainless steel collection plates of 75 mm diameter were weighted before and after each powder sample to determine the %deposition of powder adhered. Equation 3-1 was used to calculate the percentage of powder mass collected at various particle gun tip temperature and RH conditions.

$$\%deposition = \frac{powder.mass.adhering.to.collection.plate}{initial.powder.mass} \times 100 \qquad (3\text{-}1)$$

To limit the time the powder was exposed to the ambient air, the sample was weighed out immediately prior to feeding into the particle gun. The dry bulb temperature of the air in the particle gun was held constant at 78°C, while the RH of the air was increased for each sample of powder fired through the gun to obtain a data set at a particular air velocity and dry bulb temperature. All RH and temperature readings were taken at the gun tip. The particle feed rate of 0.3 $g.s^{-1}$ was chosen because this gave the lowest standard deviation for the %deposition data at various tip RH conditions for the range 0.3 – 0.6 $g.s^{-1}$ investigated (Appendix 4B). For full operational details, refer to Chatterjee (2004) and Zuo (2004).

Various air velocities were obtained by altering the amount of air flowing out of the humidifying section of the rig by adjusting the pressure regulator W3. Stands were used to alter the angle of the collection plate, resulting in impact angles of 29, 45, 61 and 90° to the vertical.

The ambient and outlet temperature and humidity conditions were recorded and system adjustments made to obtain the desired conditions. Other system readings were logged on the computer enabling easy monitoring and quick changes. Once the system had reached a steady state (~ 85 minutes) the experimental work was performed. It took around 10 – 20 minutes for the tip RH to stabilise after each adjustment. After each experimental run the funnel and chute were cleaned with hot water and dried. One set of data points at a single temperature could be obtained in one day.

3.3.1.3 Graphical Analysis

The particle gun results were graphed as %deposition versus T–Tg at a particular outlet temperature, referred to as the T–Tg plot. The x-intercept was obtained by simple linear regression of data points showing significant deposition (> 0.2 %deposition) and was defined as the point of initial stickiness, $(T-Tg)_{critical}$, as developed in previous work by Paterson et al. (2006) and Zuo (2004). The slope of this regression line is an indication of the rate at which stickiness develops, with a steeper slope representing a stickier, more difficult to handle powder. The Tg of SMP was calculated using the third-order cubic equation (Equation 3-2) developed by Paterson et al. (2005) for $0 < a_w < 0.575$ for the Tg of amorphous lactose. The powder a_w was assumed equivalent to the %RH measured at the gun tip divided by 100.

$$T_g = -530.66(a_w)^3 + 652.06(a_w)^2 - 366.33a_w + 99.458 \qquad (3\text{-}2)$$

Linear regression residuals provided evidence of data curvature. This suggested that perhaps fitting an exponential curve or transforming the data would provide a better model fit. Various data transformations and an exponential model were investigated without satisfactory results. The simple linear regression approach was adopted because the point of interest is the x intercept, easily estimated using the linear approach. The presence of curvature may have been exaggerated by the size of the data set collected. One air outlet temperature was investigated in this work, compared to a range analysed by Zuo (2004) .

3.3.2 Bench-top Fluidised Bed Stickiness Rig

To measure particle stickiness behaviour in a dynamic environment, comparable to the commercial spray dryer, a bench-top scale fluidised bed set-up was developed by Fonterra prior to the work done by Chatterjee (2004). T. Llewellyn (2005, personal communication) modified the fluid bed rig to allow powders to be tested in conditions above 80°C. The fluidised bed rig measures powder particles cohesive stickiness behaviour with changing temperature and humidity conditions in a powder bed. The particle gun method, in contrast, measures powder stickiness of adhesion to a hard surface upon direct impact.

The fluidised bed rig allows observation of the powder particles responding to changing humidity conditions at a constant dry bulb temperature. Under certain conditions the particles loose flowability and become sticky, clumping together and inhibiting fluidisation. The RH and temperature at the time of fluidisation breakdown are recorded as the powder sticky point and is plotted as RH versus temperature to create a stickiness curve, offset from the amorphous lactose curve by T–Tg.

3.3.2.1 Fluidised Bed Rig Set Up

The bench top fluidised bed environment mimics the inside of a spray dryer fluidised bed and is used to obtain an estimate of the conditions which cause the particle surface to become sufficiently sticky to result in operational problems. Air is humidified using a water bath and a small humidification column. The humid air from the water column is then heated using two inline heating elements (ECM880 Kiln Controller). The temperature is measured just before the air enters the fluidisation column through a sintered disk below the powder bed (Figures 3-3 and 3-4). It took anywhere from half to 2 hours for the fluidising particle bed to collapse/seize depending on the powder, temperature and RH. Three to four points on the sticky curve could be obtained in one day.

An Opto 22 analogue data logger 4 – 20 mA, version 3 connected to a PC was used to log the parameters for each test. A MS-DOS program data logger configuration file was created and calibrated for the probes used. Calibration involved calculation of P_0 and P_1 values for offset and slope respectively. The RH probe (Rotronic Hygromer Serie 1200) was calibrated externally using salt solutions, with nominal calibration values of P_0 and P_1 used in logger software configuration file. An external correction factor was calculated and then applied to the probe RH reading (probe calibration curves shown in Appendix 1).

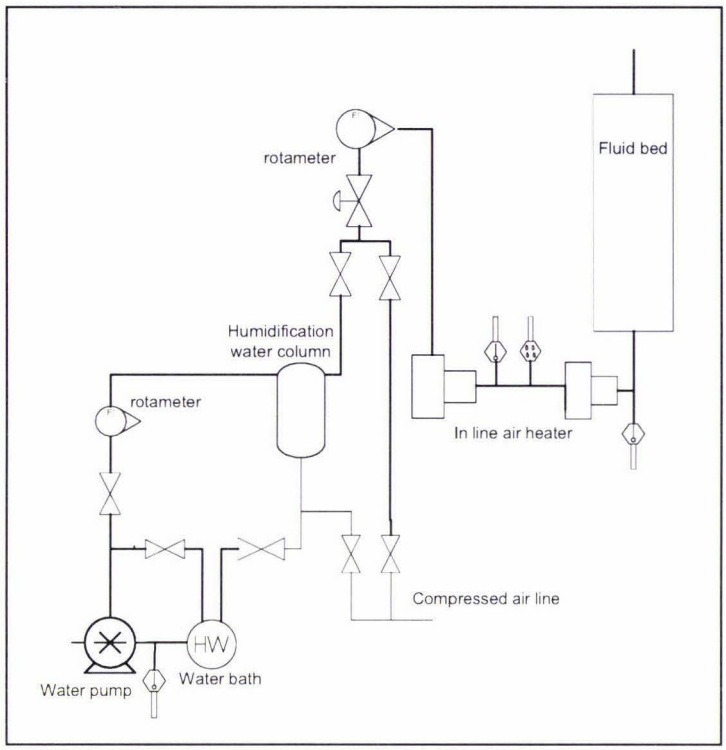

Figure 3-3. Schematic diagram of fluidised bed rig.

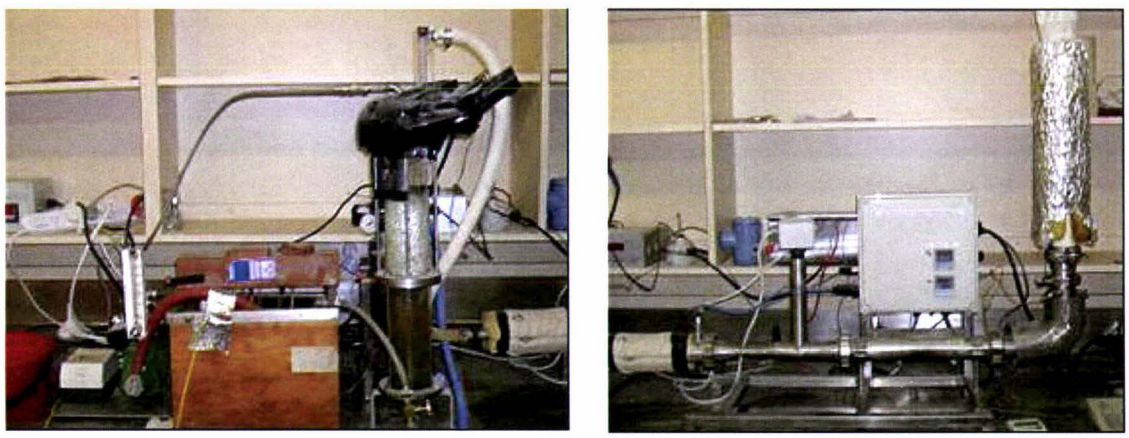

Figure 3-4. Bench top scale fluidised bed rig, left hand side shows air humidification column, right hand side shows air heater with insulated fluid bed column.

3.3.2.2 Bench-top Fluidised Bed Rig Experimental Protocol

The operating procedure for the fluidised bed rig is clearly outlined in Appendix 1 of T. Llewellyn (2005, personal communication). During an experiment the dry bulb temperature was kept constant while the wet bulb temperature was slowly increased,

resulting in an increase in RH. The end point was determined by visual observation of the bed collapse. This was defined as the point where the fluidising particle bed began to collapse and the adhered particle mass could be revitalised temporarily for a short period by vibration but would collapse soon afterwards.

The rate of wet bulb temperature increase is important. T. Llewellyn (2005, personal communication) found that rates higher than $0.2^{\circ}C.min^{-1}$ shifted the sticky curve to the right, suggesting that the moisture transport to the particle surface is the rate-limiting step in this technique. 20 g of powder was satisfactory for detecting the bed collapse without significant loss of fines out the top of the fluidising column. Air velocities used in the fluidisation bed range from 0.22 – 0.42 $m.s^{-1}$, corresponding to airflow rates of 26 – 50 $L.min^{-1}$. Chatterjee (2004) states that varying the air velocity within this range showed no effect on the stickiness endpoint obtained. Airflow rates of approximately 35 $L.min^{-1}$ (0.23 $m.s^{-1}$) were used for SMP based on the 44 $L.min^{-1}$ recommended for SMP by T. Llewellyn (2005, personal communication). WMP samples were more difficult to fluidise than SMP samples, requiring higher airflow rates of 0.33 – 0.47 $m.s^{-1}$. For WMP the sticky point was harder to identify, and was deemed the point at which fluidisation stopped for 1 – 2 seconds after a solid tap on the fluidised bed base. Balling and size segregation similar to that described by Xu and Zhu (2005) was observed at airflow rates above 0.42 $m.s^{-1}$, making it extremely hard to accurately determine the fluidisation end point, as a result 0.36 – 0.42 $m.s^{-1}$ was used for WMP samples.

3.3.3 Relative Humidity Probe Calibrations

RH probes were calibrated against saturated salt solutions using two or three points to create a standard curve. A line of best fit was then applied to the graph to find the appropriate correction factors for each probe. LiCl (11.3%RH) and NaCl (75.4%RH) saturated salt solutions and Rotronic Ag calibration chemical standards 10%, 35%, 65% and 80% solutions were used for probe calibration. Calibration curves are shown in Appendix 1.

3.3.4 Water Activity Measurement

The water activity of the powder was measured prior to testing. Bronlund (1997) describes a_w measurements as being much more sensitive than moisture content measurements, and the preferred method for identifying the state of moisture relations. a_w is equivalent to the %RH/100 of the air in both thermal and moisture equilibrium with the product of which the a_w is being measured. An electronic Aqua Lab 3TE a_w meter was used to determine the powder a_w when available. A Rotronic HygroPalm portable RH probe inserted into the powder bag was used when the meter was not available. The probe was allowed to equilibrate for at least 20 minutes before the reading was taken. Electronic a_w meter equilibration times of five minutes have been reported, therefore leaving the RH probe in the powder and at the particle gun tip for 10 – 15 minutes was appropriate.

3.3.5 Error Analysis

Standard errors (S.E.) were calculated using the Equation 3-3 with n-1 degrees of freedom and t_{n-1} obtained from student t-distribution tables at a 95% level of significance where $\alpha/2$ is 0.025 for a 2-tailed t-distribution and n is the number of replicates performed (Engineering Statistics Handbook 2005).

$$S.E. = \frac{Std.deviation}{\sqrt{n}} \times t_{n-1} \qquad (3\text{-}3)$$

Applying MINITAB[14] fitted line command to the %deposition versus T–Tg data created a 95% confidence interval for $(T-Tg)_{critical}$. The standard error in the slope (rate of stickiness development) was obtained from the regression analysis table.

3.4 CONCLUSIONS

The particle gun and the fluid bed stickiness tests are both valid techniques for determining dairy powder stickiness. The fluid bed technique is restricted to less cohesive powders, with high fat powders unable to be fluidised. The results for the particle gun characterisation and reproducibility are presented in Chapter 4. The particle gun results on the effect of angle of impact and air velocity are presented in Chapter 5.

The comparison between the fluid bed and the particle gun results are also examined in Chapter 5. Fluid bed and particle gun results are presented in Chapter 6 for comparison between the different lactose sources used in standardisation.

RH probe measurements were within ±2 %RH. Air velocity measurements were within ± 0.5 $m.s^{-1}$. Thermometer readings were accurate to within ± 0.5°C.

CHAPTER 4 - EFFECT OF AMBIENT CONDITIONS ON THE STICKINSS CURVE

4.1 INTRODUCTION

Previous work on identifying sticky points using the fluidised bed rig and the particle gun was carried out by Chatterjee (2004) and Zuo (2004). $(T-Tg)_{critical}$ values have been obtained for a large variety of dairy powders with varying compositions in an effort to relate stickiness to composition and lactose content. No attempts were made to include significant replication in determining the reproducibility and accuracy of these measurements. The lack of significant replicates of particle gun results has been due to the focus and time constraints of previous work. Zuo (2004) has completed one replicate of the complete curve for a particular SMP after a period of three months storage, but has not looked at the reproducibility of any particular point required for the creation of the sticky point curve.

Results for the $(T-Tg)_{critical}$ value obtained by Zuo (2004) show a variation of 7.6% using the T–Tg plot approach. Using the fitted stickiness curve approach the $(T-Tg)_{critical}$ obtained varied by 11% between the two replicates. This is considerable variation when determining differences between similar powders. The T–Tg plot approach combines the effects of temperature and RH effects, which reduces the variation obtained by graphical analysis. Several variables have been proposed as the cause for such day-to-day variation including ambient temperature and humidity, initial powder a_w and powder feed rate. It is likely that under a controlled environment replication of the particle gun rig is better than that observed by Zuo (2004).

Both Chatterjee and Zuo's work assume that the powder surface reaches equilibrium with the particle gun conditions virtually instantaneously. Previous work was based on the assumption that dairy powders did not require any pre-conditioning prior to testing. Zuo (2004) claimed that powder feed rate had little effect on the observed deposition.

4.1.1 Developments in Ambient Condition Effects on Powders

Powder property measurement is important because these properties intrinsically affect powder behaviour during storage, handling and processing (Fitzpatrick et al. 2004). The RH of ambient air is usually much higher than the water activity of most food powders following processing and therefore many powders readily adsorb moisture during handling. Temperature and moisture content have been shown to effect powder cohesion. Buma (1971) and Rennie et al. (1999) concluded that moisture content plays an important part in SMP and WMP cohesion, particularly over 6%wt (corresponding to 50 – 70 %RH, 0.33 a_w[1]). Storage temperature and air exposure was found to affect flour, tea, whey permeate and skim milk powder flowability (Fitzpatrick et al. 2004; Teunou and Fitzpatrick 1999). A major increase in cohesion of SMP was observed at 46%RH at 20°C but was not seen in WMP (Fitzpatrick et al. 2004). It was shown that small changes in moisture content, particle size, storage time and temperature have a large influence on flowability. Teunou and Fitzpatrick (1999) found that critical relative humidity (CRH) for powder caking increases with increasing temperatures in the range of 5 – 20°C, which can be explained by the increase in plasticity of the lactose component. Flowability (measured by annular shear cell) of whey permeate powder was significantly reduced with increasing RH (20 – 44%), with 33%CRH at 20°C. The temperature range investigated was 5 – 40°C and the humidity range 20 – 76%RH.

The changes in flowability are likely to be due to changing interactions between particles as the powder components adsorb moisture. With smaller particle sizes larger surface area per unit volume is exposed for water sorption. Cohesiveness increases are likely to be due to increased thermo plasticity of components present in the powder, especially lactose and fat resulting in greater contact area and surface stickiness (Buma 1971; Fitzpatrick et al. 2004; Rennie et al. 1999). An alternative explanation by Rennie et al. (1999) suggests the cohesion increase is a result of liquid bridging and capillary forces as moisture condenses between the particles forming strong cohesive bonds.

[1] Calculated for lactose standardised SMP using the prediction model developed by Foster (2002) for 6%wt moisture.

Chen et al. (2004) found that above 50%RH at room temperatures (~ 20°C) cohesion in WMP increased dramatically with increasing air RH. Below 50%RH powder cohesion measured as unconfined yield stress did not change much at all. 50%RH represents a a_w of 0.5 (moisture content of 8.8%wt[2]) which is above the Tg of most dairy powders at room temperature, hence the viscosity of amorphous sugars decreases enabling the formation of liquid bridging. Cohesion is a measure of inter-particle force thus reflecting the stickiness of the powder surface (Chen et al. 2004).

Fat, lactose, particle size and moisture all contribute to cohesion. Various authors (Buma 1971; Chen et al. 2004; Fitzpatrick et al. 2004; Rennie et al. 1999; Teunou and Fitzpatrick 1999) have found that ambient air conditions affect dairy powder characteristics. This chapter identifies the ways the point of stickiness initiation and the rate of stickiness development as measured by the particle gun were affected by ambient air humidity, temperature, and powder initial water activity. The variation in $(T-Tg)_{critical}$ and the rate of stickiness development (slope of T–Tg plot) obtained due to variations in ambient air humidity, ambient temperature, and powder a_w between different days were then evaluated. The effects of such variables were quantified in order to reduce the error margin for the stickiness curve. From these experiments the inherent error of the particle gun technique was determined.

4.2 EXPERIMENTAL METHOD

Initial trials were performed on the particle gun to refine aspects of the method that were significantly influenced by variations in the operator's technique. The parameters for the operator to take particular care over include the tip RH measurement, central placement of the collection plate under the gun tip, brief powder exposure to the ambient air and pre-warming of collection plates. Condensation on the collection plate placed under the particle gun tip significantly increased the powder collected because particles stick to the resulting film of water. This implies that if the target surface is sufficiently moist, the powder particles will stick.

[2] Calculated for lactose standardised SMP using the prediction model developed by Foster (2002).

Unstandardised SMP was sub-sampled to obtain replicate tests under different ambient air conditions (RH and temperature), powder a_w and feed rates while holding all other particle gun conditions constant. A 2^4 factorial design was chosen for the initial investigation into these variables, with the slope and x-intercept for the T–Tg plot obtained for each of the 16 trials using an abbreviated curve. All experiments were performed at tip conditions of 20 $m.s^{-1}$ and 78°C, using unstandardised SMP at room temperature (20 ± 5°C) unless stated otherwise. The factorial design included four factors each at two levels (ambient temperature, ambient RH, powder a_w and feed rate) with the aim of investigating each factor's influence on the slope and $(T-Tg)_{critical}$ of the T–Tg plot. The two levels investigated were ambient RH of 56 and 72%, dry bulb ambient air temperature of 24 and 27°C, feed rate of 0.3 and 0.4 $g.s^{-1}$, and SMP at 0.13 and 0.23 a_w. Using the adjacent fluid bed rig the air entering the enclosed feeding chamber was altered. The feed rate was adjusted by altering the height of the hopper positioned on the vibrating feeder. The curve generated was for three tip %RH conditions with two to three replicates at each condition. When looking at the graph of %deposition versus T–Tg values, it should be noted that the Tg equation developed in (Foster 2002) has an error of ± 5% in the models investigated.

Equation 4.1 (Perry and Green 1997) using D equal to 2.33×10^{-14} (diffusivity for amorphous lactose given by Bronlund (1997)) and R equal to 41.4 μm estimates that over the 0.05 seconds the particle travels down the particle gun barrel only the outer 0.02 μm of the particle experiences moisture diffusion. This corresponds to 0.28% of the particle's total volume being affected in the gun chute (Table 4-1).

$$F_A = \frac{6}{R}\sqrt{\frac{Dt}{\pi}} \tag{4.1}$$

4.2.1 Powder Pre-conditioning

Powders can be pre-conditioned to achieve specified water activities prior to testing by several methods. Chen at al. (2004) and Rennie et al. (1999) describe a method for pre-conditioning a powder surface using a fluidised bed. The process of humidification and heating must be rapid to prevent secondary effects to the powder. For the conditioning of

powder particle as a whole rather than just the surface layer longer fluidisation times are required. Alternatively powders can be placed over saturated salt solutions to achieve the desired powder a_w. There are limited salt solutions available for low range RH conditions. To achieve the desired a_w through the whole particle over salt solutions thin layers must be used and left to equilibrate for at least three weeks.

Calculations by Bronlund (1997) show that over five hours is required for a 3 mm layer of amorphous lactose powder to reach equilibrium after a step change in RH. Foster (2002) has described powder conditioning using a fluid bed for approximately 15 hours indicating that between 5 to 15 hours is an appropriate timeframe. Using Equations 4-2 to 4-9 for a sphere of diameter $2R$ with a first kind of boundary condition, the average fraction of moisture conversion was estimated for the centre position of the particle. Calculations for the time required for a particle to reach an average 98% fraction of moisture conversion show that the time required will be approximately eight hours (Figure 4-1) for a particle of 41.4 μm in radius and an assumed D of 2.33×10^{-14} (Bronlund 1997).

$$C\frac{\partial\theta}{\partial t} = \lambda\frac{\partial^2\theta}{\partial r^2} + \frac{2\lambda}{r}\frac{\partial\theta}{\partial r} \qquad \text{for } t > 0 \qquad \text{at } 0 < r < R \qquad (4\text{-}2)$$

$$\theta = \theta_a \qquad \text{for } t > 0 \qquad \text{at } r = R \qquad (4\text{-}3)$$

$$\frac{\partial\theta}{\partial r} = 0 \qquad \text{for } t > 0 \qquad \text{at } r = 0 \qquad (4\text{-}4)$$

$$\theta = \theta_i \qquad \text{for } t = 0 \qquad \text{at } 0 < r < R \qquad (4\text{-}5)$$

$$Y = \sum_{m=1}^{\infty}\frac{2}{\pi}\frac{R}{r}\frac{(-1)^{m-1}}{m}\sin\left(m\pi\frac{r}{R}\right)\exp\left[-m^2\pi^2 Fo\right] \qquad (4\text{-}6)$$

$$Y_{av} = \sum_{m=1}^{\infty}\frac{6}{\pi^2}\frac{1}{m^2}\exp\left[-m^2\pi^2 Fo\right] \qquad (4\text{-}7)$$

where $$Fo = \frac{Dt}{R^2} = \frac{\lambda t}{\rho c R^2} = \frac{\lambda t}{C_p R^2} \qquad (4\text{-}8)$$

and $$Y_{av} = \frac{(M_{av} - M_a)}{(M_i - M_a)} \qquad (4\text{-}9)$$

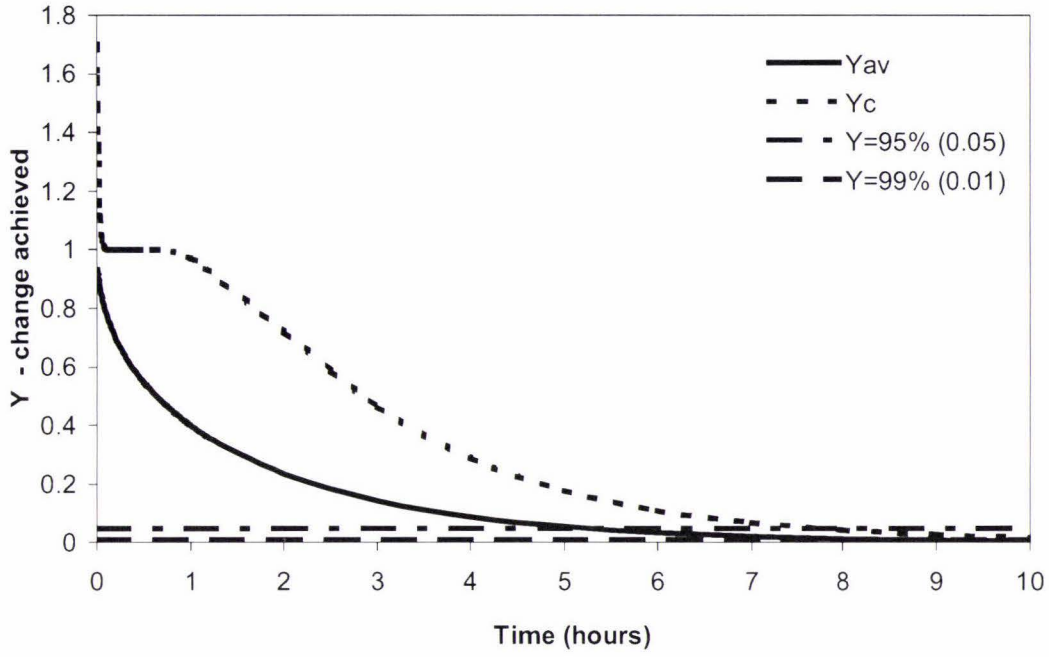

Figure 4-1. Moisture content change achieved (Y) with time for SMP. Y_c represents change achieved in particle centre, Y_{av} represents average change achieved across the particle.

Powders for this work were pre-conditioned using the fluid bed rig. Dry powder was placed in the bed and air at 18 – 23°C and the desired RH passed through for approximately 7 to 8 hours to achieve approximately 98% average fraction of conversion. During conditioning care was taken to ensure that the powder was kept well below the Tg of the powder to ensure that crystallisation did not occur during subsequent handling and storage. Conditioned powder was packaged into airtight foil lined sample bags and stored in a cool place. It is possible that pre-conditioning of the powder may influence the particle structure and/or surface and hence affecting how a particle reacts on impact with the collection plate. Changes in the amorphous lactose during conditioning should not present any problems since the powder was kept below the Tg (0.37 a_w at 25°C). (Fox 1997) reports that at 24°C the time for lactose crystallisation to develop in dairy powders is five years at 0.37 a_w, three months at 0.44 a_w and 20 hours at 0.48 a_w.

In prior work a simplistic view of the sticking mechanism was taken, suggesting that it was only the particle surface involved in the sticking behaviour observed. If the particle surface alone is responsible for the observed stickiness characteristics and reaches equilibrium with the conditions of the particle gun air, then variation of the initial powder a_w should have little effect on the %deposition obtained.

4.2.2 Ambient Air Conditions

The effect of ambient air conditions (temperature and RH) on stickiness characteristics involves time dependent moisture sorption at the particle surface, altering the surface properties. Additionally a small fraction of air relative to the air flowing through the particle gun chute is drawn into the gun at the venturi created at the powder feed point. Ambient air drawn into the particle gun mixes with the humidified air combined with heat loss over the length of the gun barrel and results in the tip conditions. These tip conditions are the critical conditions when measuring the stickiness of the powder. Under the conditions of outlet air velocity of 21 $m.s^{-1}$ (V_3), gun outlet air RH of 17%, ambient air RH of 44%, ambient air dry bulb temperature of 25°C (θ_2) and particle gun inlet air dry bulb temperature of 88°C (θ_1), 0.3% extra mass flow of ambient air entered the particle gun barrel, calculated by Equations 4-10 and 4-11 (Appendix 5A). This corresponds to a 1 ms^{-1} increase in air velocity exiting the particle gun and a 0.5% change in the RH of the air exiting the particle gun barrel.

$$m_1 + m_2 = m_3 \tag{4-10}$$

$$Cp_1\theta_1 m_1 + Cp_2\theta_2 m_2 = Cp_3\theta_3 m_3 + heatlosses \tag{4-11}$$

4.3 FACTORIAL EXPERIMENT RESULTS

Over the range of testing conditions the $(T-Tg)_{critical}$ and slope varied extensively. $(T-Tg)_{critical}$ varied between 23 – 45°C while the slope of the curve varied from 0.6 – 4.2 %deposition/°C. The Factorial results were then analysed using MINITAB[14] to determine the significant factors affecting the $(T-Tg)_{critical}$ and slope values. Factor A refers to initial powder a_w, B to ambient temperature, C to ambient air RH and D to powder feed rate. See Appendix 4A for further results.

4.3.1 Factors Affecting $(T-Tg)_{critical}$

The main factors affecting $(T-Tg)_{critical}$ at a 95% level of confidence were powder a_w, ambient RH and the interaction between ambient temperature and RH. This interaction was expected because air RH is dependent on temperature, with air being able to hold more moisture at higher temperatures. Temperature was not a main factor influencing the stickiness result. This was not surprising because the temperature range achieved was smaller than that desired. Teunou and Fitzpatrick (1999) found that storage temperature alone has no major impact on flowability provided that no component exceeds the relevant glass transition temperature. Varying temperature from above freezing to 30 – 40°C does not usually have a major impact on powder flowability, however at temperatures above 25°C a small increase in SMP cohesiveness was observed (Teunou and Fitzpatrick 1999).

Powder a_w had the largest affect on the x intercept, with a lower intercept obtained at a higher a_w. Increasing the ambient RH also decreased $(T-Tg)_{critical}$ making the powder appear stickier at high humidity and higher moisture content compared to a less humid atmosphere and a drier powder.

Errors in $(T-Tg)_{critical}$ were significantly effected by the ambient RH, ambient temperature and the interactions of factors ABC, CD, AB, ABCD respectively in order of magnitude. Higher errors in $(T-Tg)_{critical}$ were observed at a higher ambient temperature and lower ambient RH.

4.3.2 Factors Affecting the Slope of T–Tg Curve

The main factor affecting the slope at a 95% level of confidence was powder a_w. Increasing the powder a_w increased the slope, indicating that the powder becomes stickier faster at 0.23 a_w than at 0.13 a_w. Slope variations were larger at higher ambient temperature and lower ambient RH conditions, however the effect of either factor was not statistically significant at a 95% level of confidence.

The influence of the powder a_w on the stickiness result obtained from the factorial design experiment indicates that stickiness may not be as simply explained as previously thought. It is possible that the rate of stickiness development is not only influenced by the surface of the particle but also by the particles softening as a whole.

4.4 EFFECT OF WATER ACTIVITY & AMBIENT CONDITIONS

The effect of a_w and ambient air RH were investigated in greater depth following the factorial experiment. The main effects from the factorial experiment were investigated in greater depth because the factorial experiment involved only a few tip RH combinations. The selection of tip RH conditions obtained from the experiments was found to give additional variation in $(T-Tg)_{critical}$ when expressed as %deposition versus T–Tg. It was therefore decided that more points spread along the T–Tg curve would provide a better estimate of $(T-Tg)_{critical}$ and the rate of stickiness development.

4.4.1 Effect of Powder Feed Rate on the Particle Gun Technique

The effect of powder feed rate was investigated while holding all other conditions constant (15 g unstandardised SMP at 0.13 a_w, outlet air temperature 77°C, air velocity of 20 $m.s^{-1}$, ambient RH of 44%RH and ambient temperature of 22°C). Three feed rates were investigated (0.3, 0.4 and 0.55 $g.s^{-1}$) obtained by using a funnel set at increasing distances above the vibratory feeder. Five replicates were obtained at five different tip %RH conditions for each of the feed rates of interest. The $(T-Tg)_{critical}$ values obtained were 35.2 ± 1.5, 34.9 ± 2 and 38 ± 1.7°C respectively for increasing feed rates (95% confidence interval, CI, Appendix 4B). The slopes obtained were 1.6, 1.4 and 1.7 %deposition/°C respectively. Standard errors (S.E.) in the slope were 0.11, 0.11 and 0.13 respectively. There was no statistically significant difference between the $(T-Tg)_{critical}$ values obtained for the powder feed rates 0.3 to 0.55 $g.s^{-1}$ investigated. A feed rate of 0.3 $g.s^{-1}$ was chosen for future work as it had the overall lowest S.E and CI.

4.4.2 Effect of Ambient Air RH on Powder Stickiness

The ambient RH was increased from 40 to 70%RH. Increasing the ambient RH at a room temperature decreased $(T-Tg)_{critical}$ making the powder appear stickier: 17.7 ± 0.5°C at

70%RH, 22.2 ± 1.8°C at 60%RH and 32.5 ± 1.9°C at 40 – 50%RH (S.E. $\alpha = 0.5$, $n = 6$, 12 and 11 respectively), Figure 4-2; see also Appendix 4D. The ambient air RH had no substantial effect on the rate of stickiness development as determined by the slopes of the graph.

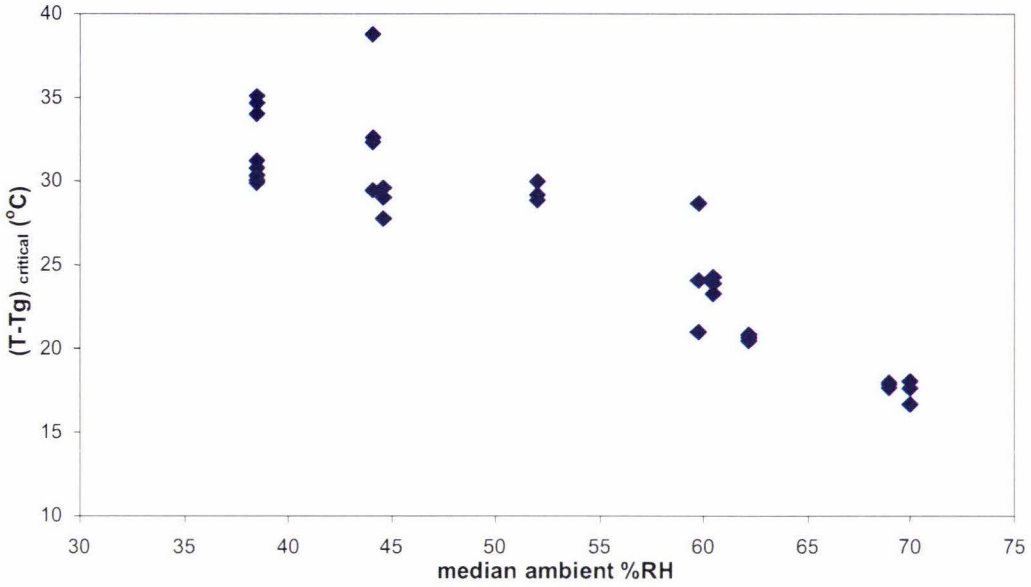

Figure 4-2. Effect of ambient air RH on $(T-Tg)_{critical}$ at 20 ± 5°C. Replications at various ambient RH conditions included.

The results suggest that the particle and its surface did not completely reach equilibrium with the particle gun air because the ambient air conditions influenced the result obtained. This was expected given that the particle residence time in the particle gun chute at an air velocity of 20 $m.s^{-1}$ is 0.05 s. The moment the powder particles are exposed to the ambient atmosphere the surface begins to adsorb moisture due to the hygroscopic nature of amorphous material. Sorption/desorption must be occurring at the particle surface once the particles enter the gun barrel due to the difference between the ambient and gun air conditions. Calculations performed to quantify the moisture absorbed by the particle travelling down the gun barrel indicated that this did not cause any significant drop in the measured tip RH. The particles moving down the gun barrel reduced a tip RH of 30%RH to 29.9 for SMP particles fed at a rate of 0.3 $g.s^{-1}$ (Appendix 5B).

In addition the length of time the powder spends in the feed system before entering the particle gun will have an influence on the stickiness result. In this work the length of time the powder was exposed was held as constant as possible, however larger masses of powder would have experienced longer exposure times in the feeder system, and further work is needed to quantify any effect.

Using Equation 4-1 the distance moisture diffuses into a SMP particle with varying amounts of amorphous lactose covering the particle surface was estimated (Table 4-4). The diffusivity of the particle surface was estimated as a fraction of that for 100% amorphous lactose, 2.33 $x10^{-14}$ $m.s^{-1}$ (Bronlund 1997). This indicates that approximately 0.17 – 0.28% of the particle volume is influenced by the conditions experienced in the particle gun chute, depending on the surface coverage of amorphous lactose. In the time taken to introduce the powder sample into the particle gun chute (1 – 3 minutes) moisture diffuses into approximately 5.80 – 16.75% of the particle volume.

Table 4-4. Diffusion through SMP particles with varying surface lactose coverage (R = 41.4 μm).

Diffusion distance into particle (μm)	Particle volume effected (%)	Time particle exposed (s)	Diffusivity, D (x 10^{-14} $m.s^{-1}$)	Amorphous lactose (%)
0.04	0.28	0.05	2.33	100
0.03	0.20	0.05	1.20	51.5[a]
0.03	0.21	0.05	1.35	58[b]
0.02	0.17	0.05	0.84	36[c]
1.38	9.67	60	2.33	100
0.98	6.94	60	1.20	51.5[a]
1.04	7.36	60	1.35	58[b]
0.82	5.80	60	0.84	36[c]
2.45	16.75	180	2.33	100
1.73	12.02	180	1.20	51.5[a]
1.84	12.75	180	1.35	58[b]
1.44	10.05	180	0.84	36[c]

[a] bulk lactose composition for unstandardised SMP

[b] bulk lactose composition for standardised SMP, Kim et al. (2003)

[c] surface (10 nm) lactose composition for standardised SMP, Kim et al. (2003)

At increased ambient RH, the particles will have a softer surface layer due to additional adsorbed moisture prior to entering the particle gun. Increased surface plasticity will cause greater deformation upon impact with the collection plate explaining why $(T-Tg)_{critical}$ is decreased. It is therefore necessary to maintain standard testing conditions to ensure that the results obtained for different powders tested on different days are consistent.

4.4.3 Effect of Powder Initial water activity on Stickiness

Looking at an extended range of initial SMP a_w due to the factorial experiment shows that increasing a_w from 0.1 to 0.39 had no distinct effect on the point of stickiness initiation, $(T-Tg)_{critical}$ (Figure 4-3), but significantly increased the slope of the T–Tg curve (Figure 4-4). Figure 4-3 shows that at each ambient RH condition $(T-Tg)_{critical}$ remains constant with increasing initial powder a_w. Increasing initial powder a_w has little effect on $(T-Tg)_{critical}$. Figure 4-3 also shows that as ambient RH is increased $(T-Tg)_{critical}$ is decreased. This evidence may explain why similar SMPs tested by (Zuo 2004) were found to have similar $(T-Tg)_{critical}$ values but widely varying slopes.

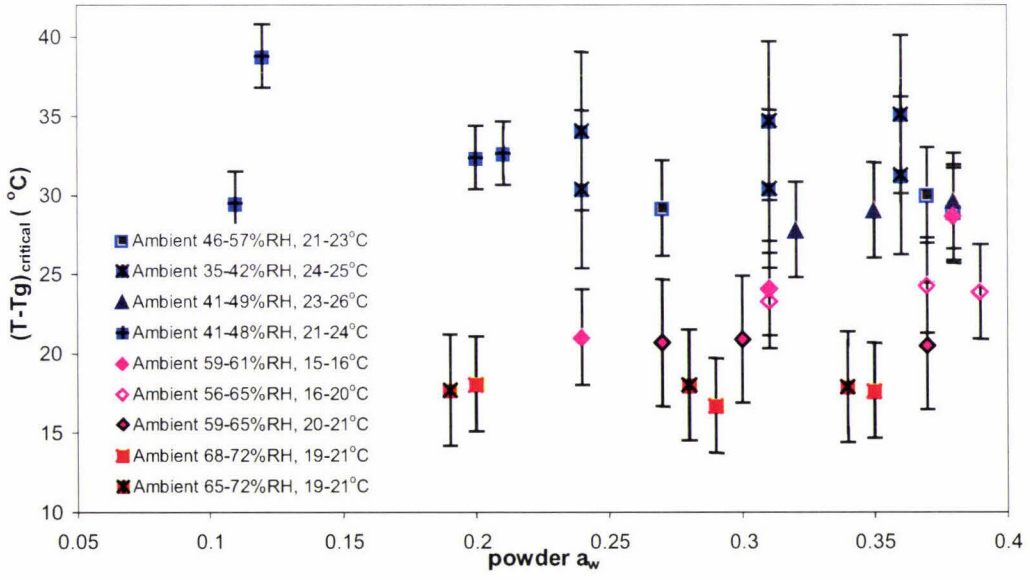

Figure 4-3. Effect of powder a_w on $(T-Tg)_{critical}$ under different ambient RH conditions at room temperature. Obtained using SMP. The error bars represent the 95% CI for each $(T-Tg)_{critical}$.

Particles become sticky at similar critical conditions regardless of their initial a_w confirming the initiation of stickiness is indeed a surface phenomenon; however the moister the particle the greater the rate of stickiness development (Figure 4-4). The initiation of stickiness is due to the surface conditions of the particle reaching a critical viscosity for sufficient liquid bridging to develop, adhering the particle to the collection plate. The increased rate of stickiness development can be explained by deformation mechanics. Moister particles are more plastic in nature resulting in greater deformation due to decreased internal strength and consequently greater surface area available for adhesion upon impact. Fewer elastic deformations occur and hence fewer particles will rebound off the collection plate resulting in the increased rate of stickiness development observed. Ozmen and Langrish (2003) also found that the wall deposition flux for SMP in a pilot-scale co-current spray drier was greater at a higher product moisture content.

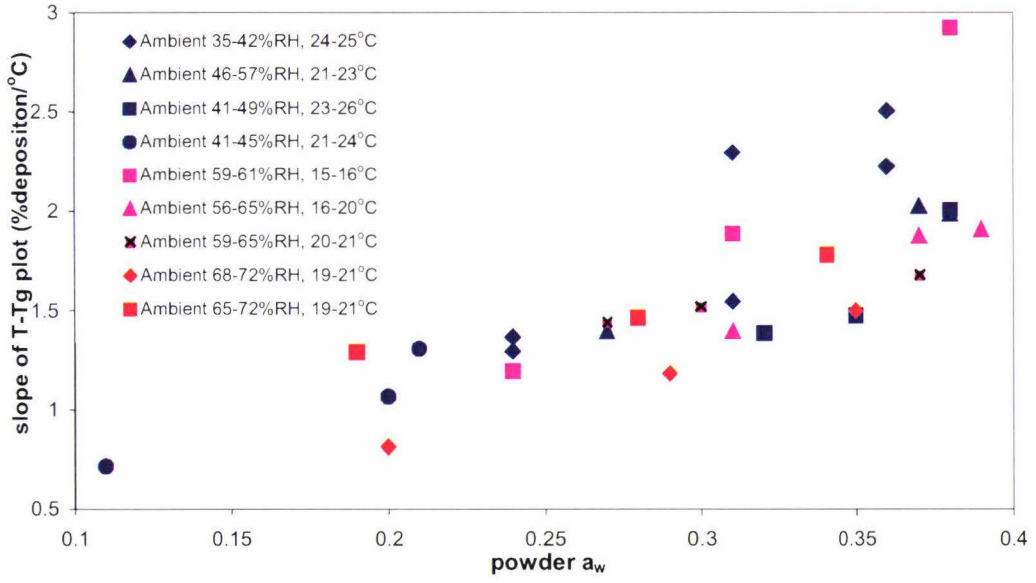

Figure 4-4. Effect of powder a_w on the rate of stickiness development under different ambient RH conditions at room temperature. Obtained using SMP.

4.4.4 Time Dependent Plasticization

Stickiness measurements with SMP (0.23 a_w) samples exposed to ambient air at 45 ± 4 %RH at 26°C for zero, 10 and 20 minutes prior to testing were trialed. It was thought that longer exposure times would result in the powder absorbing more moisture and

hence greater plastic deformation should be observed. An increase in cohesion and texture was observed in the thin layer of particles exposed to the ambient air. This means that upon exposure the powder surface changes instantly. A complete set of data points at a particle gun outlet air temperature of 78°C was not obtained because the exposed powder stuck at the point of entry at gun tip conditions above 24.5 %RH. It is likely that the exposure time plasticised the particle surface but did not cause crystallisation, as lactose crystallisation at the particle surface would have made the powder less sticky. Faldt and Bergenstahl (1996a) state that at 75 %RH at room temperature the time for lactose crystallisation is 100 s. From the limited data available it appears that the initiation of stickiness is approximately the same for the three powder treatments. This confirms that the increase in powder plasticity has a greater effect on the rate of stickiness development than stickiness initiation. It also indicates that exposure to ambient air above 50%RH has a greater influence on the initiation of stickiness than the time the powder is exposed.

4.5 Inherent Errors and Repeatability of the Particle Gun

It is important to identify the reproducibility of the particle gun technique in order to understand the limitations of this test method. Evaluation of the errors inherent in the particle gun technique allows different powders to be tested against each other to confirm whether or not they are significantly different at a 95% level of confidence. It provides an important benchmark for the test sensitivity and the limits of detection of the particle gun technique. Once the effects of the various conditions were identified, four replicate tests were performed under standard operating conditions (room temperature, < 50% ambient RH, air velocity 20 $m.s^{-1}$, 0.24 a_w SMP, 0.3 $g.s^{-1}$) to evaluate the inherent error in the technique.

4.5.1 Reproducibility of %Deposition Values

In order for the particle gun technique to provide reproducible results each point used in the analysis must be reproducible. Various quantities of powder were fired down the particle gun apparatus onto collection plates under constant conditions. It was confirmed that the amount of powder used in the test is not critical since deposition is worked out as

a percentage of powder used. Errors associated with the %deposition values increased as the tip RH and the amount of powder adhering to the collection plate increased (Figure 4-5). The repeatability of a single point at a particular particle gun tip condition gave standard deviations of between 0.1 – 5.5% deposition. The increase in variability at higher tip RH can be explained by the changing surface of the collection plate as more powder is adhering to powder already stuck to the plate. Under the air stream some particle agglomerations were observed to roll down the deposited powder surface and off the collection plate. To limit the increasing variation at higher %deposition levels the amount of powder analysed should be adjusted to avoid overloading the collection plate[3]. At higher RH powder particles also start to adhere to the inside of the particle gun barrel, introducing additional variation due to an unknown quantity of powder loss.

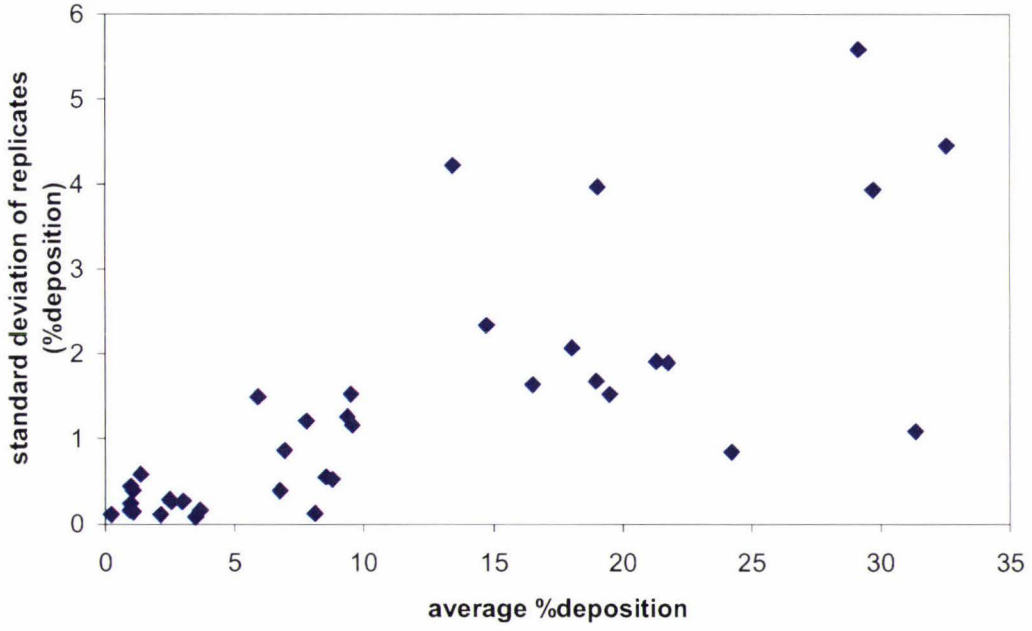

Figure 4-5. Standard deviation of replicates at various deposition levels.

4.5.2 Reproducibility of $(T-Tg)_{critical}$

Zuo (2004) obtained $(T-Tg)_{critical}$ values of 37.9 and 40.9°C from two replicate runs of the same SMP, a difference of 3°C. Reproducible results of $(T-Tg)_{critical}$ equal to 33.6°C

[3] ~ 2 g of powder deposition on the collection plate resulted in ~ 1.7 standard deviations at deposition levels above 20%

were obtained for unstandardised SMP (Figure 4-6) under standard testing conditions (room temperature, < 50% ambient RH, air velocity 20 $m.s^{-1}$, SMP 0.24 a_w, 0.3 $g.s^{-1}$). The standard error in $(T-Tg)_{critical}$ was calculated as ± 0.8°C. This error is reasonable considering the error in measuring %RH using a humidity probe is given as ± 2%RH (D. L. Pearce, N. T. Russell and A. G. Foskett, 2004, personal communication) and shows a considerable improvement over the results obtained by Zuo (2004). Hennigs (2001) reports a similar error level for sticky point measurements on SMP using a modified stirrer test based on the method of Lazar (1956). Hennigs (2001) reported results to ± 1°C, which is of similar reproducibility to the particle gun, however the particle gun technique is a dynamic test method and provides information on both the initiation of stickiness and the rate of stickiness development.

4.5.3 Reproducibility of the Rate of Stickiness Development

Zuo (2004) obtained values of 3.04 and 2.95 %deposition/°C for the slope of the T–Tg plot from two replicate runs of the same SMP, a difference of 0.09 %deposition/°C. In this work, the rate of stickiness development under the same standard operating conditions was 3.1 %deposition/°C (Figure 4-6), reproducible with a standard error of ± 0.45 %deposition/°C. There has been a reduction in the amount of scatter in the data collected at any temperature. The differences in the results obtained by (Zuo 2004) are explained by the age of the sample, uncontrolled ambient air conditions, and an increase in powder a_w to 0.4 a_w after 3 months storage prior to the replicate test.

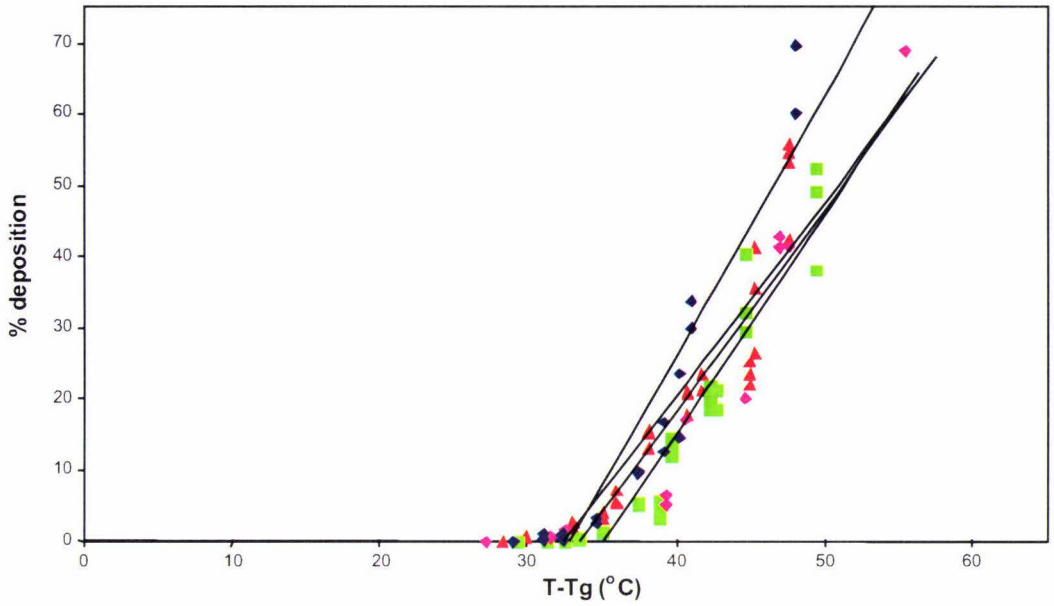

Figure 4-6. T–Tg plot showing the reproducibility of the results under constant testing conditions for unstandardised SMP.

4.6 CONCLUSIONS

Ambient conditions affect the surface of the milk powder from the moment it is exposed. Even though this time was reduced as much as possible (to ~ 1 – 3 minutes), an effect was still observed. The $(T-Tg)_{critical}$ and the rate of stickiness development obtained for SMP were functions of the ambient air RH and initial powder a_w respectively. Increasing the ambient air humidity from 40 to 70%RH decreased $(T-Tg)_{critical}$ by 44%. This indicates that the surface of the particle is indeed the main parameter involved in the initiation of stickiness.

Powder a_w does not seem to have any significant effect on the $(T-Tg)_{critical}$ value obtained. This confirms the hypothesis that the initiation of stickiness measured by the particle gun is indeed a surface phenomenon. The rate of stickiness development increased with increasing powder a_w (0.11 – 0.39). This is likely to be due to moister particles becoming stickier faster due to increased plastic deformation. Particles with a higher moisture content are more likely to deform and adhere under impact.

For unstandardised SMP $(T-Tg)_{critical}$ was determined as 33.6 ± 0.8°C with a rate of stickiness development of 3.1 ± 0.45 %deposition/°C under standard testing conditions. It is necessary to maintain standard testing conditions so as not to influence the results obtained for different powders tested on different days. Powder exposure and the ambient air temperature and RH should be kept as low as practically possible to ensure minimal influence on the particle surface. It is important to place the pre-warmed collection plate centrally under the particle gun barrel and to avoid plate overloading.

CHAPTER 5 - ADDITIONAL FACTORS INFLUENCING STICKINESS AS MEASURED BY THE PARTICLE GUN

5.1 INTRODUCTION

Collection plate material, velocity of particles and the angle of impact onto the collection plate are thought to affect the stickiness measurement obtained for a particular powder. Previous authors (Palzer 2005; D. L. Pearce, N. T. Russell and A. G. Foskett, 2004, personal communication; Zuo 2004) have identified that particle velocity and momentum play a significant role in the rate at which solid deposition occurs in spray drying. It has been proposed in previous literature (Palzer 2005; Zuo 2004) that particle velocity/momentum is the most likely reason for the difference in the sticky point found between different test methods. Increased velocity leads to an increase in impact force as the energy contained by the particle is increased. It has been shown that when the fluid bed apparatus (air velocity of 0.22 – 0.44 $m.s^{-1}$) and the particle gun (20 $m.s^{-1}$) are compared for similar powders, the particle gun gives a $(T-T_g)_{critical}$ value typically 6 – 10°C higher than the fluid bed. The objectives of this section are to identify the effect of velocity, angle of impact and collection plate material have on the sticky curve obtained using the particle gun.

D. L. Pearce, N. T. Russell and A. G. Foskett's (2004, personal communication) work on the fluid bed apparatus found air velocity, particle size and rate of moisture diffusion to be the key factors influencing the sticky point. Larger particles required higher air flows to maintain momentum and consequently larger adhesion forces and liquid bridging to halt their increased momentum. This chapter aims to identify the effect air velocity has on the stickiness characteristics of SMP measured by the particle gun. It also compares results obtained between the particle gun and the fluid bed apparatus.

5.2 EXPERIMENTAL PROCEDURE

A series of experiments was designed and executed to obtain $(T-Tg)_{critical}$ values and corresponding rates of stickiness development for air velocities of 10 – 30 ms^{-1} and

angles of impact (29 – 90°). Permeate standardised SMP was used under standard test conditions as described in Chapter 3 and 4. Angled stands were used to obtain various angles of impact between the particle stream and the collection plate. All plates were placed with the centre of the plate 16 cm below the particle gun tip to be consistent with previous work.

5.3 EFFECT OF AIR VELOCITY ON THE PARTICLE GUN STICKY POINT

With sticking processes the mechanical properties of the particles and particle surface are influential for the resulting adhesion. For amorphous material moisture content, temperature, particle impact force and the duration of the force all influence the mechanical properties. At moderate moisture and pressure conditions the contact time for significant adhesion is long. If the viscosity of the material is decreased either by changes in temperature or moisture to a level enabling viscous bridges to form by viscous flow the process is referred to as sintering (Palzer 2005). Sintering is likely to occur in the case of a fluid bed. In the particle gun where particles are fired at a plate, viscous flow (sintering) and viscoelastic deformation are the most likely mechanisms for adhesion. Viscoelastic deformation becomes more important for developing adhesion forces between particles with shorter contact times and higher applied pressure.

Collision work by Kantak and Davis (2005) demonstrated inelastic losses increases with an increase in impact velocity accompanied by a decrease in the restitution coefficient. Shalaby et al. (2005) investigated variations in the coefficient of restitution from elastic to completely inelastic bouncing behaviour using a particle-wall model for a gas cyclone. The coefficient of restitution indicated only minor influence on the predicted efficiency grade of the cyclone. Milk powder particles are likely to undergo inelastic collisions because of their porous, compressible nature, which would suggest particle aggregation near the walls.

Viscoelastic solids react to stress partly by elastically like a solid, and partly by plastically deforming like a viscous fluid (Johnson 1985). Viscoelasticity depends on the

strain rate, temperature and moisture content of the product. Palzer (2005) has shown that stickiness expressed in the form of T–Tg is dependent on the type of sticking mechanics experienced and the impact force experienced by the particle, with T–Tg increasing with decreased particle contact time. Palzer (2005) combined WLF, Navier-Stokes and viscoelastic knowledge to develop Equation 5-1 to predict the T–Tg value depending on the time of contact between particles. Using Equation 5-1 Palzer (2005) was able to successfully predict parameters for the blockage of a fluidised bed.

$$t = \left(\frac{5a^2\pi}{4\gamma a\pi + 2F_t}\right)\eta_g\left(\frac{X}{a}\right)^2 10^{[C(T-T_g)]/[B+(T-T_g)]} \qquad (5\text{-}1)$$

where $\left(\frac{X}{a}\right) = 0.1$

5.3.1 Effect of Air Velocity on $(T-Tg)_{critical}$

It was expected that increasing the particle gun air velocity would increase the $(T-Tg)_{critical}$ value obtained. This was indeed found to be the case as shown in Figure 5-1. This is explained by greater particle deformation under an increased force, resulting in fewer particles responding elastically. At a 90° angle of impact, increasing air velocity from 10 $m.s^{-1}$ to 30 $m.s^{-1}$ increased $(T-Tg)_{critical}$ from 32 to 38°C, an increase of $0.3°C.m^{-1}.s$. Increasing the impact force decreases the time required for viscous flow and sticking to develop, while increasing the air velocity decreases the impact time. According to Palzer (2005) this increases the T–Tg value obtained, which is consistent with the results shown in Figure 5-1.

At a 90° angle of impact (collection plate perpendicular to the particle gun barrel) decreasing the distance between the gun tip and the plate resulted in less deposition due to higher air velocity at the point of contact. With the plate at an angle less than 90° decreasing the distance to the plate resulted in greater deposition (Appendix 4C). Therefore a constant distance between the collection plate centre and the particle gun tip of 16 cm was set. During the experimental work it was observed that at air velocities of 10 $m.s^{-1}$ particles were agglomerating in the particle gun barrel and hitting the collection

plate as larger agglomerates than those observed at 20 $m.s^{-1}$. At increased velocity greater scouring/indents in the particles adhering to the collection plate were observed directly under the air stream exiting the particle gun. Scouring is also observed in ducting bends of spray dryers where particles impact on ducting and bends.

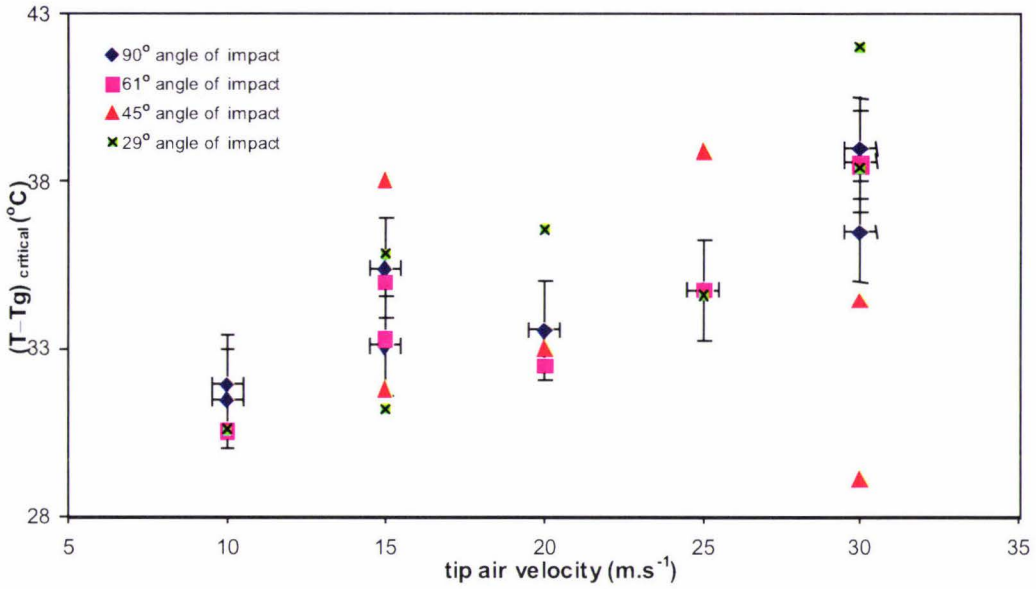

Figure 5-1. Effect of air velocity and angle of impact on $(T-Tg)_{critical}$ obtained under standard ambient conditions, SMP 0.24 a_w. The error bars represent the S.E. found for $(T-Tg)_{critical}$ and the error in velocity.

5.3.2 Effect of Air Velocity on the Rate of Stickiness Development

At a 90° angle of impact, the rate of stickiness development (slope of T–Tg plot) showed an overall slightly decreasing trend with increasing velocity (Figure 5-2). This indicates that the SMP became stickier faster at 10 $m.s^{-1}$ than at 30 $m.s^{-1}$, which is likely to be due to the increased residence time of the particle travelling down the particle gun barrel (0.105 and 0.035 s respectively). This increased residence time will enable moisture to penetrate a thicker outer layer of the particle, 0.07 μm compared with 0.04 μm, resulting in a greater proportion of the particle undergoing plastic deformation. At 0.035 s enough of the particle surface is affected to alter the viscosity and enable liquid bridging, resulting in instantaneous stickiness. The effect of velocity on the slope of the T–Tg plot was insignificant at any particular angle of impact (Figure 5-2).

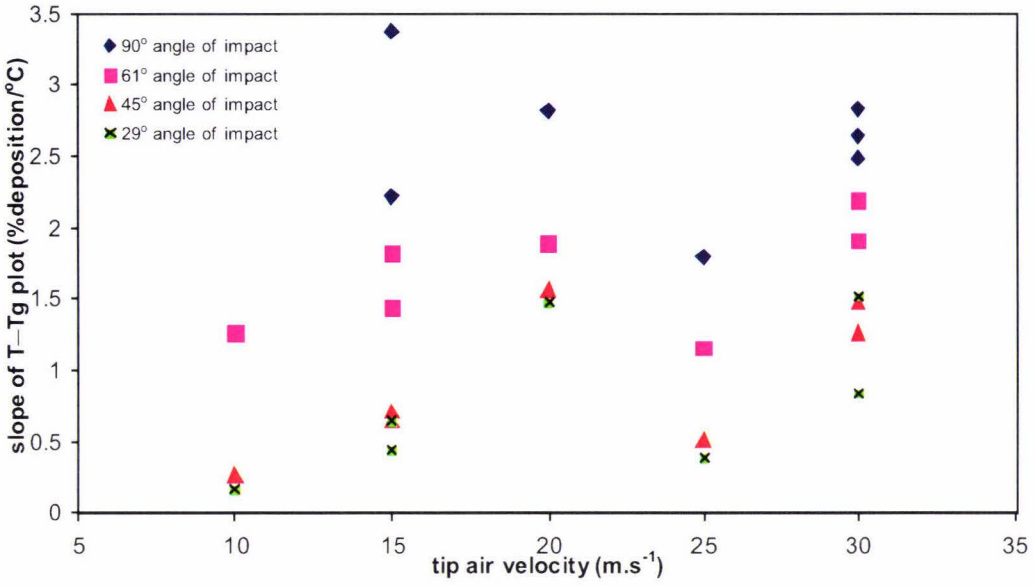

Figure 5-2. Effect of air velocity and angle of impact on the rate of stickiness development obtained under standard ambient conditions, SMP 0.24 a_w.

5.4 COMPARISON OF FLUID BED & PARTICLE GUN

Previous work by Zuo et al. (2006) has shown that the fluid bed method gives lower T–Tg values than that obtained by the particle gun, with a general offset of 6 – 10°C. This difference is thought to be due in part to velocity as well as the technique and particle residence time differences. Both methods involve sintering though the particle residence time and velocity are considerably different, < 0.05 seconds at 20 $m.s^{-1}$ in the particle gun barrel and ½ – 1½ hour at 0.23 $m.s^{-1}$ in the fluid bed. Table 5-1 shows the results obtained for the two methods using identical powder samples. The results for the particle gun are in general higher than that for the fluid bed. Refer to Tables 6-5 and 6-6 (Chapter 6) for comparisons between all powders tested in this work.

Equation 5-1 explains potential factors contributing to the difference in sticky point between alternative testing methods due to differences in impact force and impact time between particles. It provides a useful insight into theoretical adjustments to $(T–Tg)_{critical}$ in order to relate the instantaneous sticky point obtained to various regions in drying equipment and transport systems for dairy powders.

Table 5-1. $(T-Tg)_{critical}$ comparisons between Particle gun and Fluid bed methods.

Powder	Particle gun (°C) (± 0.8)	Fluid bed (°C) (± 2)
SMP lactose standardised (34% SNF)	32.3	23
SMP permeate standardised (34% SNF)	31.5	19
SMP unstandardised (45% SNF)	33.6	35
Various SMP previously tested	37.9 – 42 (Zuo 2004)	14 & 33 [4]
WMP lactose standardised (34% SNF)	34.6	17
WMP permeate standardised (34% SNF)	34.5	22
WMP unstandardised (45% SNF)	33.6	20
Various WMP previously tested	33.7 – 40 (Zuo 2004)	29, 30 & 37 [4]
Predicted by Hertzian equations[1, a]	69	31
Predicted by Jet impact equations[2, a]	86	-
Predicted by collision energy equations[3]	-	31

[1] Hoppmann (1995)

[2] Perry and Green (1997)

[3] Xu and Zhu (2005)

[4] T. Llewellyn, 2005, personal communication

[a] Predictions are from Palzer (2005) Equation (5-1) using either Hertzian, Jet impact equations or Collision theory equations given by Xu and Zhu (2005) to predict the impact time of the collision.

5.4.1 Effect of Powder a_w on Fluid Bed Results

With the fluid bed residence times of ½ to 2 hours are observed before bed collapse/seizure. There is quite a variation between the replicate tests using unstandardised SMP conditioned to various a_w's (Table 5-2). The effect of powder a_w appears to be minimal given the difficulty in determination of the end point using the fluid bed. More data needs to be obtained in order to confirm the presence of any trend. It is expected that the residence time in the fluid bed is sufficient for the surface of the particles to obtain equilibrium with the fluidising air, eliminating the need to pre-condition test powders.

Table 5-2. Fluid bed results for unstandardised SMP with various initial powder a_w values.

SMP initial a_w	T–Tg (± 2 °C)	Replicates (n)	95% CI (± S.E.x t_n)
0.23	30	3	1.3
0.26	27	3	1.3
0.29	34	3	2.4
0.34	25	3	2.5

Chen et al. (2004) used a fluid bed to achieve surface moisture content change in dairy powders. Fluidisation times of 5 – 30 minutes were used, typically 15 minutes. The particle surface RH reduced very slowly after some 5 minutes of settling time after fluidisation. This means the RH of the air is representative of the value next to the particle approximately 5 minutes after humidification. It is highly probable that the particle surface in the fluid bed rig achieves equilibrium with the fluidising air during the time taken to reach bed collapse conditions. Starting conditions, water bath heating rate and air velocity should still be held constant between powders tested to ensure comparable results.

The particle gun results are in general higher than those obtained by the fluid bed method. The differences observed between the particle gun and fluid bed results are consistent with work done by Palzer (2005) and Zuo (2005).

5.5 RELATIONSHIP BETWEEN VELOCITY, CONTACT TIME, FORCE & T–TG

Fluid bed and particle gun experimental results were compared to the theoretical T–Tg value obtained by rearranging Equation 5-1 for T–Tg. The following equations were used to estimate a time of contact upon impact (t) for each test method. Three approaches were used to investigate the relationship between velocity and $(T–Tg)_{critical}$. Three approaches were used to estimate t in order to determine T–Tg using Equation 5-1: Hertzian theory for impact forces (Equations 5-2 to 5-5, Hoppmann (1995)), the momentum balance for jet impact on a plate combined with Hertzian equations

(Equations 5-2, 5-3 & 5-6, Perry and Green (1997)), and collision energy equations given by Xu and Zhu (2005) combined with Hertzian equations. Hertzian theory although formulated for elastic impacts can still be used to obtain useful engineering results even though plastic deformation occurs locally (Hoppmann 1995).

$$\alpha = \left(\frac{15}{16} v_1^{\,2} \left(\frac{1 - v_1^{\,2}}{E_1} + \frac{1 - v_2^{\,2}}{E_2} \right) m_p \right)^{\frac{2}{5}} R^{-\frac{1}{5}} \qquad (5\text{-}2)^{4}$$

$$t = \frac{\alpha}{V} \qquad (5\text{-}3)^{5}$$

$$J = m_p V (1 + e) \quad \text{and} \quad F = \frac{J}{t} \qquad (5\text{-}4)^{6}$$

$$F = \frac{m_p V^2}{\alpha} \qquad (5\text{-}5)^{7}$$

$$F = pqV / g_c \sin \vartheta \qquad (5\text{-}6)^{8}$$

Hertzian equations used to obtain t for substitution into Equation 5-1 predicted a time of impact of 1.2×10^{-7} s resulting in a T–Tg value of 69°C for the particle gun, and an impact time of 0.1 s for the fluid bed giving a T–Tg value of 31°C (Appendix 5F). Using collision energy equations presented by Xu and Zhu (2005) a time of impact of 0.1 s was substituted into Equation 5-1, resulting a in a T–Tg value of 31°C for the fluid bed (Appendix 5F). Using the jet impact relationship for the particle gun (Equation 5-6) an impact time of 9.5×10^{-8} s was obtained resulting in a much higher prediction of T–Tg of 86°C. This theory indicates that the particle gun method results should be significantly higher than the fluid bed results. The calculated values overestimate the experimental T–Tg results obtained, however they are within the same order of magnitude. The overestimation of the predicted T–Tg values may be due to assumptions made in

[4] Hertzian theory for the collision of two spheres, Hoppmann (1995).
[5] Time of impact from Hertzian theory for the collision of two spheres, Hoppmann (1995).
[6] Equations for momentum used to calculate t, time of impact taken from Hertizan theory for the collision of two spheres, Hoppmann (1995).
[7] Hertzian theory for the collision of two spheres equation for Force of impact used to calculate t, Hoppmann (1995).
[8] Equation for force of impact for jet impact relationship used in conjunction with Hertzian equations to calculate t, Perry and Green (1997).

calculating F_t and the choice of equations used for this. The discrepancy noted in the fluid bed results is within reasonable margins considering the Hertzian approximation and experimental error.

Algebraic manipulation of Equations 5-1 to 5-3 (Appendix 5G) using either selected F equation for F_t, assuming that the bridge diameter/particle diameter (X/a) ratio required for adhesion remains constant, indicates that a quadratic equation develops with a local maxima experienced under certain combinations of F_t and t. Altering the air velocity suggests that this maxima may be around 23 $m.s^{-1}$ (possibly demonstrated by the 45° angle of impact results, Figure 5-1). The effect of increasing velocity may increase or decrease the powder sticky point with varying combinations of particle properties.

5.6 EFFECT OF ANGLE OF IMPACT ON T–TG PLOT

The cyclone test is the only published method for evaluating stickiness in a dynamic way which takes into account the particle impacting at an angle. However it does not allow isolation of the effect impact angle has on the sticky point of a powder. Most common dryers have a cone angle of 60 – 40° with the powder discharged at the exit by gravity with a dwell time of around 15 s (Fox and McSweeney 2003).

The particle gun work to date has used an angle of impact at 90°, perpendicular to the collection plate. However 90° angels are rarely encountered in industrial dryer equipment. The particle gun technique allows easy manipulation of the position of the collection plate. Impact angles 90, 61, 45 and 29° were investigated in this work. When particles collide with a target, not all the force is directed in the normal direction. A percentage of the momentum is directed parallel to the collection plate surface, resulting in particles rebounding with a significant horizontal component. Particles were observed to be glancing off the angled plates resulting in adhered particles.

5.6.1 Angle of Impact & $(T–Tg)_{critical}$

The initiation of stickiness where the particles start to adhere to the plate remains unchanged for various angles (Figure 5-3). Once critical surface conditions required for

liquid bridging and adhesion to occur are obtained by the particles, the particles stick to the collection plate regardless of the angle, resulting in $(T-Tg)_{critical}$ remaining constant for a given velocity.

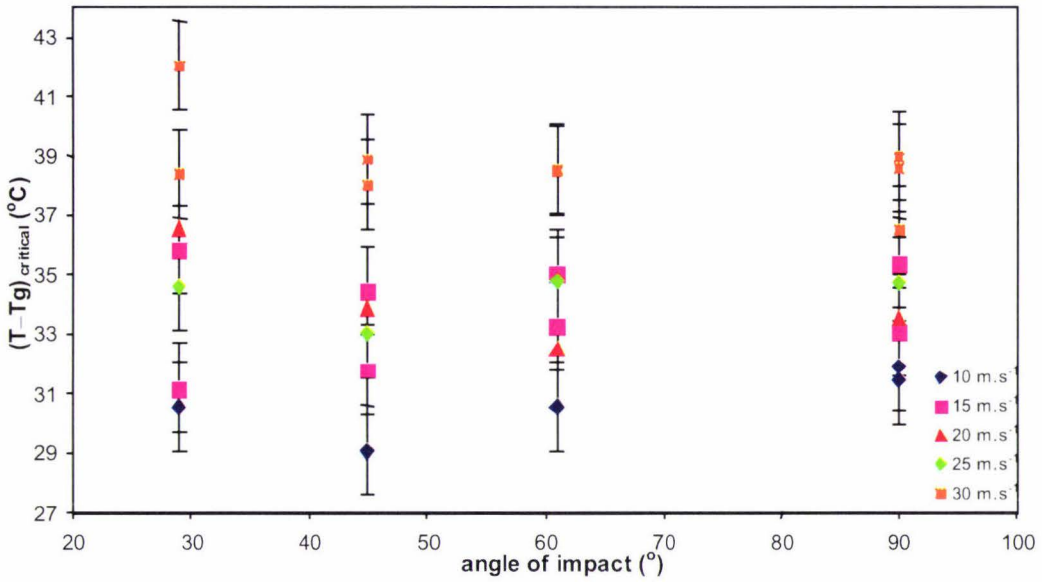

Figure 5-3. Effect of angle of impact and velocity on $(T-Tg)_{critical}$ obtained under standard operating conditions, SMP 0.24 a_w. The error bars represent the S.E. found for $(T-Tg)_{critical}$.

5.6.2 Angle of Impact & Rate of Stickiness Development

As the angle of impact was decreased, the weight of the powder deposit collected decreased. As a result the slope of the T–Tg plot (the rate of stickiness development) decreased with decreasing angle of impact (Figure 5-4). The rate of stickiness development was the greatest when particles had the least chance of rebounding off the collection surface (i.e. 90°). Once a particle surface became sticky, increasing the angle of impact increased the rate of deposition and therefore 90° impact angles should be avoided. Even though $(T-Tg)_{critical}$ remains unchanged with angle of impact, the rate at which powder begins to build up was significantly influenced by angle.

Further investigation is required to understand whether there is any industrial significance of the point at which the trend lines for various air velocities in Figure 5-4 cross, 70 – 80° angle of impact.

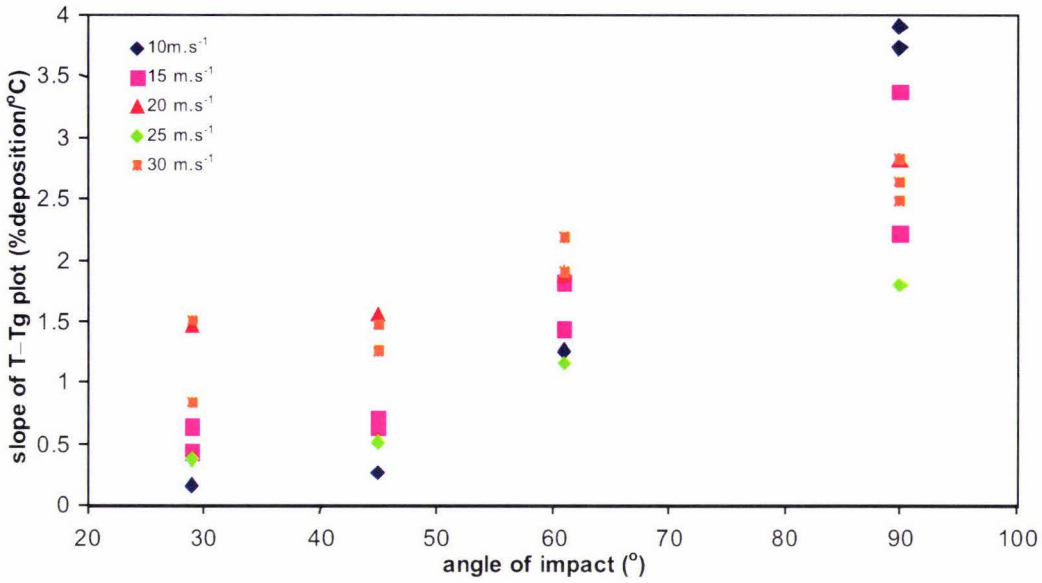

Figure 5-4. Effect of angle of impact and velocity on the rate of stickiness development obtained under standard operating conditions, SMP 0.24 a_w.

5.6.3 Effect of Force on $(T-Tg)_{critical}$ & Rate of Stickiness Development

The velocity impact on the collection plate was converted to the normal force for each angle of impact. Figure 5-5 shows that $(T-T)_{critical}$ is independent to the normal force experienced. Figure 5-6 shows that the rate of stickiness development also appears to be independent to the normal force (see also Appendix 4C).

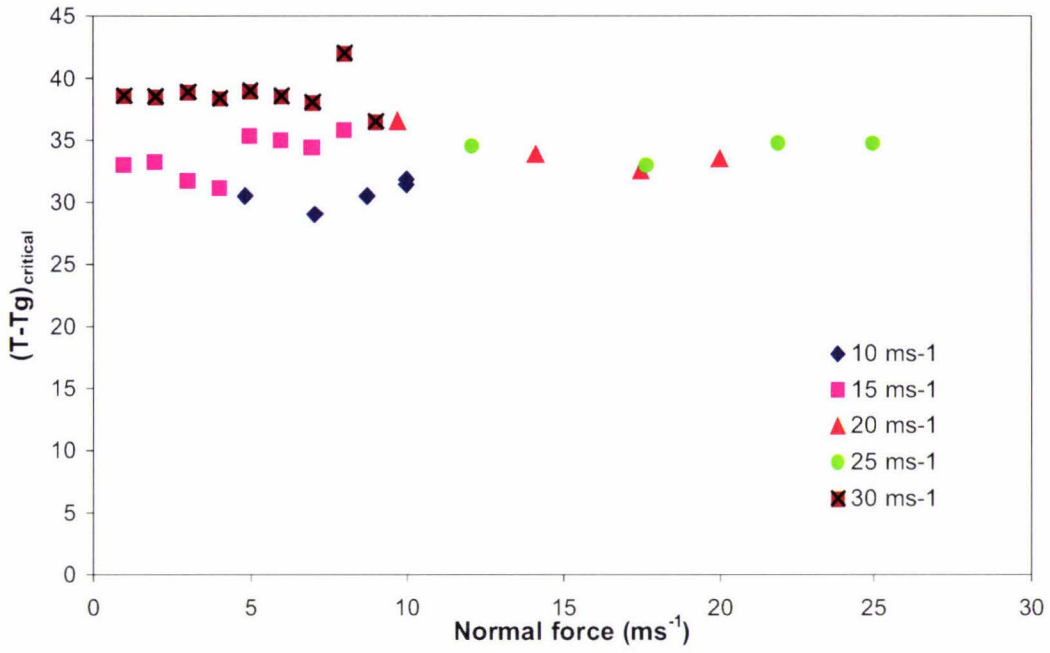

Figure 5-5. Effect of force on $(T-Tg)_{critical}$ for SMP 0.24 a_w under standard operating conditions. Angle of impact converted to normal force velocity.

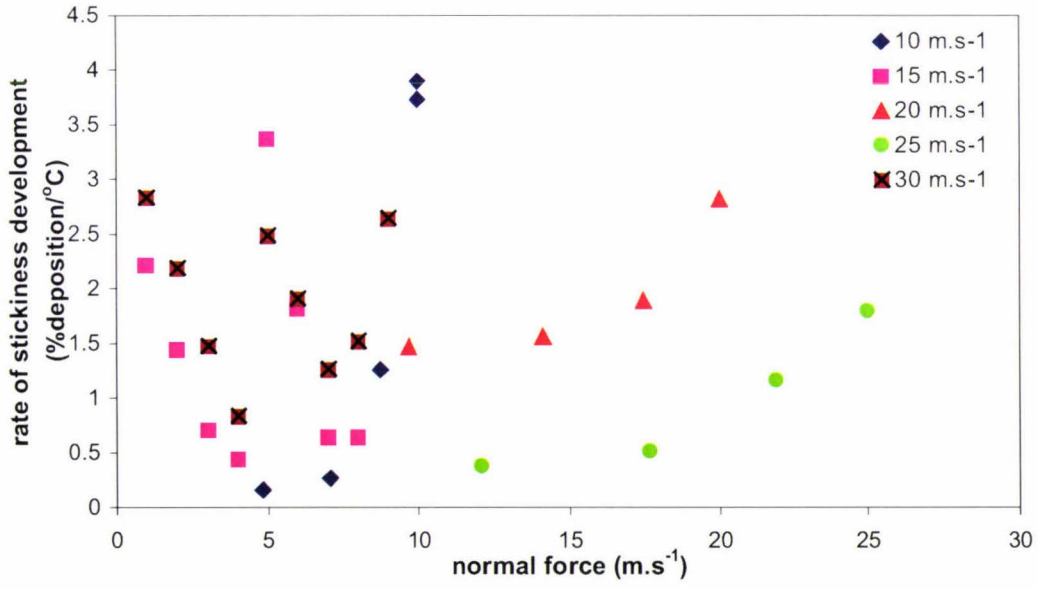

Figure 5-6. Effect of force on the rate of stickiness development for SMP 0.24 a_w under standard operating conditions. Angle of impact converted to normal force velocity.

5.7 EFFECT OF COLLECTION PLATE MATERIAL ON SMP STICKINESS

Many techniques have been developed to test the stickiness of food powders (Bhandari and Howes 2005; Chuy and Labuza 1994; Downton et al. 1982; Hennigs et al. 2001; Lazar et al. 1956; Lockemann 1999; Paterson et al. 2001). Most of these tests did not consider the importance of surface energy of particle-particle or particle-substrate interfaces. Of the papers published relating stickiness difficulties to drying equipment and design, inadequate focus has been given to both the interfacial (adhesive) and interphase (cohesive) surface energies that contribute to stickiness. Knowledge of surface energy of various materials can help in material design and material selection in a given situation.

In spray drying, powder stickiness is not purely by adhesion onto the dryer wall. At the accumulation stage, the cohesive force between the particles can play a role since the wall can be completely covered with the material. It is important to avoid the early stage of adhesion which can act as a seed for further accumulation of under-dried or sticky particles (Bhandari and Howes 2005). To reduce the contact area of the particle with the wall, it is important that the wall material has a low surface energy. In many drying situations stainless steel is used as the wall material because of its durability, ease of cleaning and for reasons of hygiene, but stainless steel metal has a high surface energy (71 $mN.m^{-1}$) (Bhandari and Howes 2005). Teflon has been found to be very useful in the handling and processing of food materials due to its extremely low surface energy (18 $mN.m^{-1}$), relative inertness, high tensile strength, and thermal stability (Bhandari and Howes 2005). Stainless steel is the most commonly used material in the dairy industry; typically either 304 or 316 grade stainless steel is used and may have different surfaces or coatings.

The relationship between surface energy and stiffness is expressed by the Young's modulus (Pocius 2002). This relationship shows that increasing stiffness results in an increase in surface energy and describes how a material reacts to a given tensile force.

Surface energy has a crucial role in the understanding of adhesion phenomena (Pocius 2002).

Some drying operations have reported using low energy contact surfaces in drying equipment to avoid the problems caused by stickiness. Bhandari and Howes (2005) provide a good review of relating the stickiness property of foods undergoing drying and dried products to their surface energetics. The stickiness property is directly related to the interfacial surface energy of contacting materials (Bhandari and Howes 2005). Normally inorganic materials have higher surface energy than organic material therefore organic materials have fewer tendencies to cause material sticking. Metals have high a surface energy therefore materials tend to stick more on a metal surface. Polymers have a low surface energy, and therefore are difficult to wet (Bhandari and Howes 2005).

Michalski et al. (1997) demonstrated that the solid surface energy of various packaging materials influenced the adhesion of food emulsions differently. Papadakis and Bahu (1992) report the use of Teflon coatings, paints and such hydrophobic material to reduce adhesion of sticky components for soil handling procedures. Bhandari and Howes (2005) state that liquid flow is dictated by the surface tension/surface energy of the system, however there is no evidence to suggest that the material surface plays a significant role in the mechanism of instantaneous stickiness.

5.7.1 Collection Plate vs. $(T-Tg)_{critical}$

There appears to be no definite trend for the $(T-Tg)_{critical}$ values obtained for different collection plate materials (Table 5-3) given the 95% confidence intervals obtained by simple linear regression (MINITAB[14]). Particles were observed to repel further to the edges of the Teflon plate. Double-sided Sellotape on stainless steel was used to imitate a powder-coated surface, a method used by Ozmen and Langrish (2003). For the sticky tape surface, a constant powder coating of ~ 0.3 %deposition prior to the increase in deposition due to increasing RH was obtained.

Polyethylene foam with a ridged surface was used. As a comparison, the polyethylene foam had a Shaw hardness of 61, silicone rubber had a hardness of 97, while metals have a Shaw hardness of over 100. It was thought that a more elastic surface such as rubber may increase $(T-Tg)_{critical}$ because of less particle deformation due to a softer impacts, analogous to work on impacting of lactose crystals causing a cake build up by McLeod (2002). However, the modulus of elasticity (Young's modulus) did not influence $(T-Tg)_{critical}$ (Table 5-3).

Table 5-3. Effect of collection plate material on $(T-Tg)_{critical}$ using the particle gun with permeate standardised SMP under standard operating conditions.

Collection plate material	$(T-Tg)_{critical}$ (°C)	Surface energy ($mN.m^{-1}$)	Modulus of elasticity (GPa)	Poisson ratio	Plate thickness (mm)
Teflon	30.4	18[1]	0.5[1]	0.46[5]	2
Silicone rubber	30	22-56[3]	0.01-0.1[2]*	0.49[4]*	3.9
Polyethylene foam	31.6	39-46[1]			5
Centurion Gasket	30				1.5
Stainless steel + sticky tape	28.6				1
316 2B Stainless steel	31.5		207[1]	0.28[2]	1
Copper	29.2	71[1]	124[2]	0.34[2]	0.9
Mild steel	30.8		212[3]	0.25[4]	2

[1] Pocius (2002)

[2] Winter (2005)

[3] Siegel (2006)

[4] Matweb Team (2006)

[5] Kantak and Davis (2005)

*estimate from rubber and silicon

5.7.2 Collection Plate vs. Rate of Stickiness Development

There does not appear to be any significant trend in the rate of stickiness development between the various collection plate materials (Table 5-4). This supports the findings of Ozmen and Langrish (2003) who confirmed that adhesion and cohesion occur at similar rates for different surfaces placed inside a spray dryer.

Table 5-4. Effect of collection plate material on the rate of SMP stickiness development using the particle gun with permeate standardised SMP under standard operating conditions.

Collection plate material	Slope of T–Tg plot (%deposition/°C)	Modulus of elasticity (GPa)	Poisson ratio	Plate thickness (mm)
Teflon	3.61	0.5[1]	0.38	2
Silicone rubber	4.89	0.01-0.1[2]*	0.49	3.9
Polyethylene foam	5.03			5
Centurion Gasket	4.28			1.5
Stainless steel + sticky tape	3.42			1
316 2B Stainless steel	3.29	207[1]	0.283[2]	1
Copper	3.71	124[2]	0.345[2]	0.9
Mild steel	4.80	212[3]	0.25[4]	2

[1] Ramakrishna (2006)

[2] Department of Material Science and Engineering Cornell University (2006)

[3] Wikipedia (2006)

[4] Matweb Team (2006)

* rubber

5.8 CONCLUSIONS

Increasing air velocity increases the point of initiation of stickiness measured by the particle gun. Particle gun results are in general higher than those obtained by the fluid bed. The particle gun measures the point of initiation of stickiness where particles begin to adhere to the collection plate, as opposed to particles developing adhesion forces between them in the fluid bed causing bed seizure. The momentum, impact force and impact time associated with the particle influences the difference seen in the T–Tg results. The differences seen between the particle gun and the fluid bed method are consistent with work by Palzer (2005).

Decreasing angle of impact had no significant effect on $(T-Tg)_{critical}$. However with impact angles less than 90°, the rate of stickiness development was reduced. 90° angles are rarely found in industrial situations therefore this implies that the point above $(T-Tg)_{critical}$ where powder build-up becomes a problem industrially may be higher than that predicted by the particle gun with the collection plate at 90°.

A range of collection plate materials showed that the collection plate material used had no influence on the sticking behaviour of SMP. This is in contrast to studies that have suggested that a non-stick surface can assist in reducing product adhesion and that cohesion is strongly influenced by surface energetics. It is however consistent with the findings that cohesion and adhesion occur at similar rates. The mechanism of the initiation of stickiness due to liquid bridging and viscoelastic deformation as measured by the particle gun was independent of the material properties for the various collection plates investigated.

An extension of this work would be to investigate particle gun air velocities lower than 10 $m.s^{-1}$. Firing particles down the gun barrel at a stationary plate also means the particles are hitting a changing, uneven surface of agglomerated particles. It would be interesting to investigate the results of particles fired at a moving collection plate to eliminate the effect of particle build up with time. An opportunity for high-speed camera work looking at the mechanics involved with particle collision may exist.

CHAPTER 6 - EFFECT OF LACTOSE SOURCE ON MILK POWDER STICKINESS

6.1 INTRODUCTION

Recent industrial experience has operators believing that lactose additions to dairy powders from different sources show different tendencies to become sticky when being processed, with lactose from whey permeate being a more difficult source than straight addition of pure lactose. The aim of this section is to identify if there is any significant and measurable difference in the stickiness properties between powders standardised with pure lactose solution or milk permeate.

CODEX (1999) allows the addition of milk permeate to raw milk in order to standardise protein levels. Milk protein levels vary and peak around 42% SNF (Roginski et al. 2003), and CODEX regulations allow this level to be manipulated to 34% SNF by the addition of pure lactose solution (α monohydrate lactose crystals made into solution) or alternatively milk permeate (~ 5% lactose). The only difference between standardisation via permeate or lactose solution is that milk permeate contains additional milk salts and whey proteins whereas pure lactose solution does not.

6.1.1 Milk Proteins

Milk is a complex biological fluid containing many proteins and enzymes. With heating, enzymes and protein molecules are inactivated or denatured. Milk protein is largely made up of casein (~ 80%), in the form of α_{s1}, α_{s2}, β and κ types. Heating and cooling causes the calcium phosphate equilibrium to shift. Heating induces the precipitation of calcium phosphate; with prolonged heating denaturing whey proteins, while cooling dissolves colloidal calcium phosphate. The greater the heat treatment the faster the rate of change (Fox 2003).

D. L. Pearce, N. T. Russell and A. G. Foskett (2004, personal communication) found a strong relationship between protein (and hence) lactose in powders and the position of the

sticky curve using the fluidised bed apparatus. Dairy powders with low protein contents were found to be stickier than similar powders with high protein contents when tested above 60°C. Decreasing protein content in dairy powder via the addition of lactose increases stickiness due to increased amorphous lactose.

6.1.2 Milk Salts

Minerals and milk salts are typically grouped together under the same general group. Milk concentration is accompanied by a pH change as the salt equilibria are altered (Fox 1995). Whey typically contains 8 – 10% minerals on a dry weight basis (Roginski et al. 2003). At high temperatures (such as prior to spray drying) calcium phosphate precipitates, with evaporation increasing the concentration of lactose and salts (Fox and McSweeney 2003). This increase results in the transfer of soluble calcium phosphate to colloidal form inducing a pH drop. Salts interact with the casein micelle structure, particularly calcium and phosphate, influencing the stability by maintaining or destroying the micelle structure. Salts are usually present in milk at 5 – 40 mM concentration (Fox 1995). The caking problems of whey powders are mainly attributed to amorphous lactose, but whey protein and whey minerals are reported to also contribute to the powder hygroscopicity (Sienkiewicz and Riedel 1990). Therefore milk salt concentration and pH are also of importance for problematic powders.

In a supersaturated lactose solution, non-lactose constituents (mineral salts, proteins and lactic acids) can exert an influence on the crystallisation rate and on product properties of the subsequent powder. Mineral salts and lactic acid influence mutarotation, while salts and whey proteins have a negative influence on hygroscopicity (Sienkiewicz and Riedel 1990). Preheating the solution to 86 – 88°C denatures whey proteins, with acid whey proteins being more stable than rennet whey proteins.

6.2 POWDERS INVESTIGATED

Powders standardised with different lactose sources were obtained from Fonterra's Te Rapa and Waitoa sites in addition to six powders made at the Fonterra Research Centre pilot plant as described in Appendix 2.

6.2.1 Bulk Composition

Tables 6-1 and 6-2 show the composition data for the six powders and milk solutions made in the pilot plant – skim and whole milk standardised with lactose solution or milk permeate and unstandardised. In all samples the presence of minerals (Na, Ca, Cl, S and K) was observed with a total elemental concentration of less than 1%. Skim milk standardised with milk permeate had higher levels of ash, calcium, chloride, potassium, magnesium, sodium and phosphorous. There was no significant compositional difference between lactose and permeate standardisation methods when expressed as relative bulk composition (%wt), Appendix 2. As expected, the bulk composition differs when the protein level is down standardised. This trend is also seen in the surface composition results (Tables 6-3 and 6-4).

Table 6-1. Powder properties and milk composition for SMP samples.

SMP		*Standardisation method*		
		Unstandardised	Lactose	Permeate
d(0.5)	μm	82.84	74.81	78.02
PD	g/cm^3	1.14	1.09	1.09
BD (100 taps)	g/cm^3	0.66	0.57	0.60
Moisture		3.38	3.91	4.26
Flow (NIRO)	s	25.26	80.13	78.91
Ash	%w/w	0.79	0.75	0.89
Calcium	mg/kg	1360	1260	1360
Chloride	mmol/kg	28.9	26.2	38.0
Fat	%w/w	0.05	0.05	0.05
Potassium	mg/kg	1460	1360	1850
Lactose monohydrate	%w/w	4.92	6.40	6.18
Magnesium	mg/kg	123	114	141
Sodium	mg/kg	413	387	543
Protein	%w/w	4.26	3.98	3.91
Inorganic P	mmol/kg	17.5	16.6	18.1
Total solids	%w/w	9.56	10.87	10.52

Table 6-2. Powder properties and milk composition for WMP samples.

WMP		*Standardisation method*		
		Unstandardised	Lactose	Permeate
d(0.5)	μm	83.24	-	79.20
PD	g/cm^3	1.06	1.05	1.06
BD (100 taps)	g/cm^3	0.56	0.57	0.57
Moisture		2.15	2.44	2.38
Flow (NIRO)	s	78.18	50.64	76.06
Ash	%w/w	0.76	0.71	0.84
Calcium	mg/kg	1280	1220	1260
Chloride	mmol/kg	27.1	25.8	36.1
Fat	%w/w	3.10	3.59	3.44
Potassium	mg/kg	1410	1340	1760
Lactose monohydrate	%w/w	4.70	6.19	5.82
Magnesium	mg/kg	116	109	130
Sodium	mg/kg	394	374	512
Protein	%w/w	3.10	3.71	4.45
Inorganic P	mmol/kg	15.1	15.7	18.6
Total solids	%w/w	12.01	13.64	13.30

6.2.2 Surface Composition

Stickiness is a surface phenomenon hence the composition of the particles surface is of interest. Powder surface composition depends largely on the development and composition of the air-water interface of droplets formed in the spray-drying tower (Kim et al. 2003). Surface-active components adsorb preferentially to the particle surface during spray drying due to the air-water interface generated, resulting in an over representation of fat and protein at the outer layer of the particle. The process parameters during the spray-drying were of minor importance to the composition of the powder surface as long as the transport of components to the droplets air water interface was fast (Kim et al. 2003).

6.2.2.1 Electron Spectroscopy for Chemical Analysis

Electron spectroscopy for chemical analysis (ESCA) is a well-established technique for the analysis of solid surfaces. ESCA gives direct information about the powder surface

independent of particle size. It is possible to quantitatively estimate the relative atomic concentration of elements present in the specimen surface. Electrons emitted from the sample originate from near the surface region for most solids (~ 10 nm). By using ESCA the percent coverage of different components such as protein, carbohydrate and fat (represented schematically to simplify milk's many components) on the powder surface is calculated. ESCA measurements are very reliable (Kim et al. 2002), subsequently the surface composition results are also expected to be reliable. Errors associated with this technique are reported to be 3%. ESCA resolution is approximately $^{1}/_{5}^{th}$ of the surface layer affected during 0.05 s exposure in the particle gun at 20 $m.s^{-1}$ based on amorphous lactose diffusivity.

Powders were analysed by ESCA by Prof. Dong Chen (now MONASH University) and his team at Auckland University. The results of the six powders investigated for surface composition are shown in Table 6-3 and 6-4. There was little difference between the surface compositions for powders standardised by either lactose source. A slight difference in %lactose at the surface is seen in WMP between permeate and lactose solution standardised powders. The difference observed between unstandardised and standardised powders was expected due to the addition of lactose by standardisation. These results confirm that fat is over represented at the surface when compared to the bulk, consistent with studies by Kim et al. (2002; 2003; 2005), Faldt and Sjoholm (1996) and Faldt and Bergenstahl (1994). Faldt and Sjoholm (1996) investigated the surface composition of WMP by ESCA and found 55% fat, 30% protein and 15% lactose at the particle surface.

Table 6-3. Surface and bulk composition (%wt) for SMP samples. Surface composition estimated by ESCA.

	Unstandardised		Lactose standardised		Permeate standardised	
	surface	bulk	surface	bulk	surface	bulk
Lactose	24.2*	44.6	28.4*	58.9	29.6	58.8
Protein	53.4	51.9	51.1	36.6	49.3	37.2
Fat	22.4	0.5	20.5	0.5	21.0	0.5

*surface values significantly different at 3% error level

Table 6-4. Surface and bulk composition (%wt) for WMP samples. Surface composition estimated by ESCA.

	Unstandardised		Lactose standardised		Permeate standardised	
	surface	bulk	surface	bulk	surface	bulk
Lactose	3.7*	39.1	7.0*	45.4	5.0*	43.8
Protein	18.2	33.3	17.8	27.2	18.6	33.4
Fat	78.1	25.8	75.3	26.3	76.5	25.9

*surface values significantly different at 3% error level

Faldt and Bergenstahl (1996b) propose that fat is encapsulated by protein, with whey protein having less ability to encapsulate fat than sodium caseinate. Faldt and Bergenstahl (1996b) used model emulsions and provide evidence of surface-active protein present at the air water interface. The release of fat to the particle surface after exposure to humid conditions results in particle agglomeration and loss of structure. Changes in the surface composition, structure and properties resulting from lactose crystallisation are processes occurring in the interior of the particles rather than on the surface (Faldt and Bergenstahl 1996a). However in powders containing no lactose, fat is released but the particle structure remains intact. In contrast Kim et al. (2002; 2003) provide evidence that surface fat in dairy powder is unprotected free fat.

Even though the surface layer (~ 10 nm) contains significantly less %lactose than the bulk, the amorphous lactose mechanism is still observed as the major mechanism for stickiness development. It is unknown how the essentially hydrophobic particle surface can still demonstrate stickiness due to the amorphous lactose mechanism when exposed to short residence time (0.05 s) experienced in the particle gun barrel. The amorphous lactose mechanism is observed even in high fat powders above a critical RH (Zuo 2004). With the particle surface largely covered in hydrophobic fat dairy powders still demonstrate strong hygroscopic properties.

Particle indents provide increased surface area, which may contribute to the amorphous lactose mechanism and powder hygroscopicity observed. Kim et al. (2003) found that SMP surface typically consisted of deep and shallow folds and dents. Mistry et al. (1992)

reports that lactose and protein influence the powder particle surface structure, producing wrinkles on the particles and thereby increasing particle surface area. Previous studies by Buma and Henstra (1971) observed wrinkles caused by uneven shrinkage with no contribution by lactose. Mistry et al. (1992) observed that as the lactose content of SMP was reduced, and protein content increased, wrinkles from the particle surface gradually disappeared. Their findings suggest that milk proteins and lactose alone may not have a direct influence on the surface structure, but the interaction between protein and lactose at a lactose content of more than 33% coupled with uneven shrinking during drying may be responsible for surface wrinkles. It is possible that changes in the particle microstructure due to increased lactose content and powder composition have a combined effect in altering a powders stickiness property.

6.2.2.2 Confocal Laser Scanning Microscopy

Using confocal laser scanning microscopy (CLSM) it is possible to stain fat and protein with fluorescent dyes and observe the distribution throughout a particle (Hermansson et al. 2000). Foster (2002) used this technique to observe fat bridges and pooling in milk powders. Baechler et al. (2005) reports that in spray dried WMP, amorphous lactose forms a continuous matrix in which proteins, fat and air are dispersed. Using CLSM (Figures 6-1 to 6-3) we see that the fat is indeed small particles distributed throughout the particle bulk, and that the particles are porous with an uneven surface.

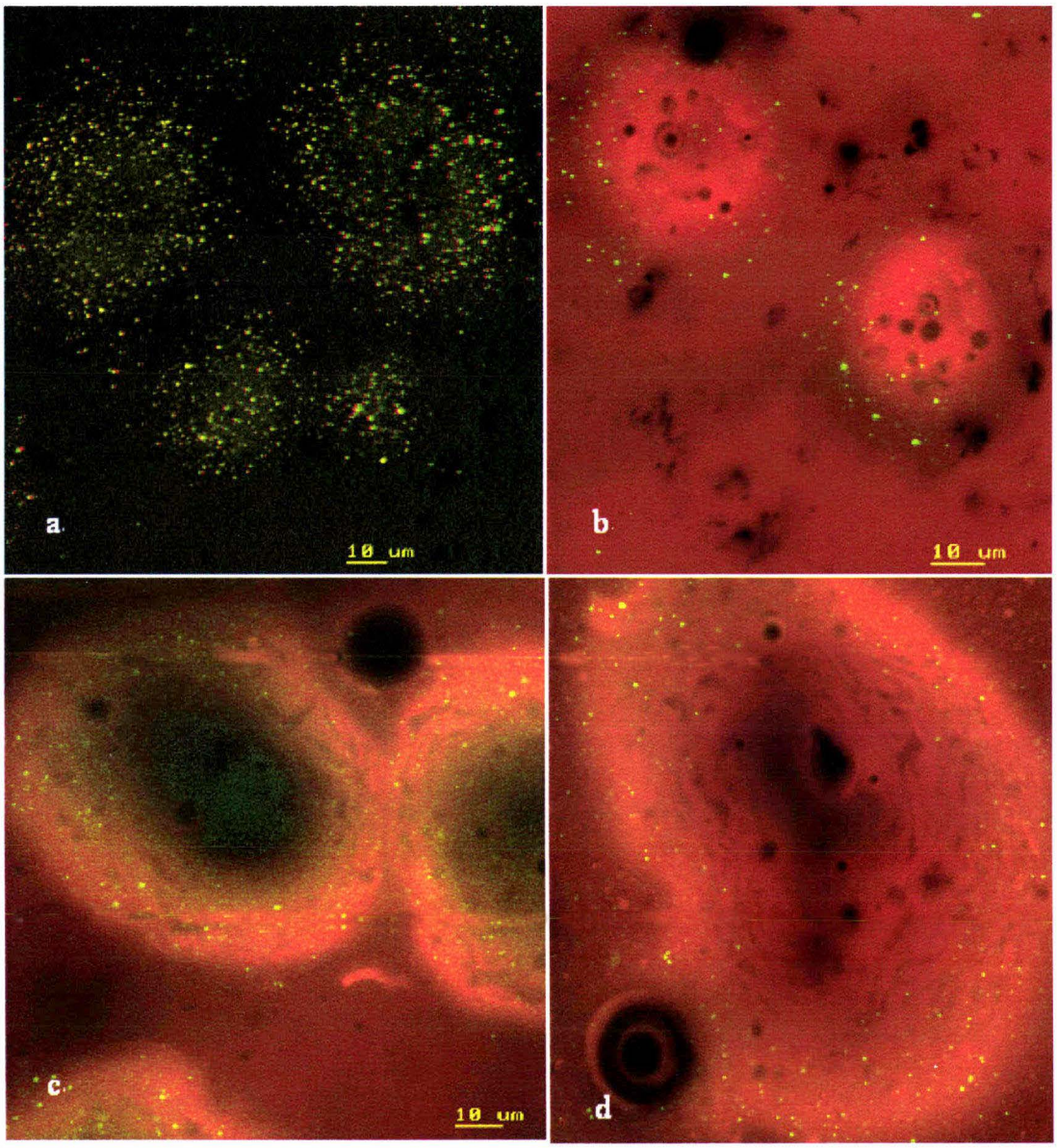

Figure 6-1. SMP stains: a) lactose standardised 3D fat image, b) lactose standardised dual fat and protein stain, c) unstandardised dual fat and protein stain, d) permeate standardised dual fat and protein stain.

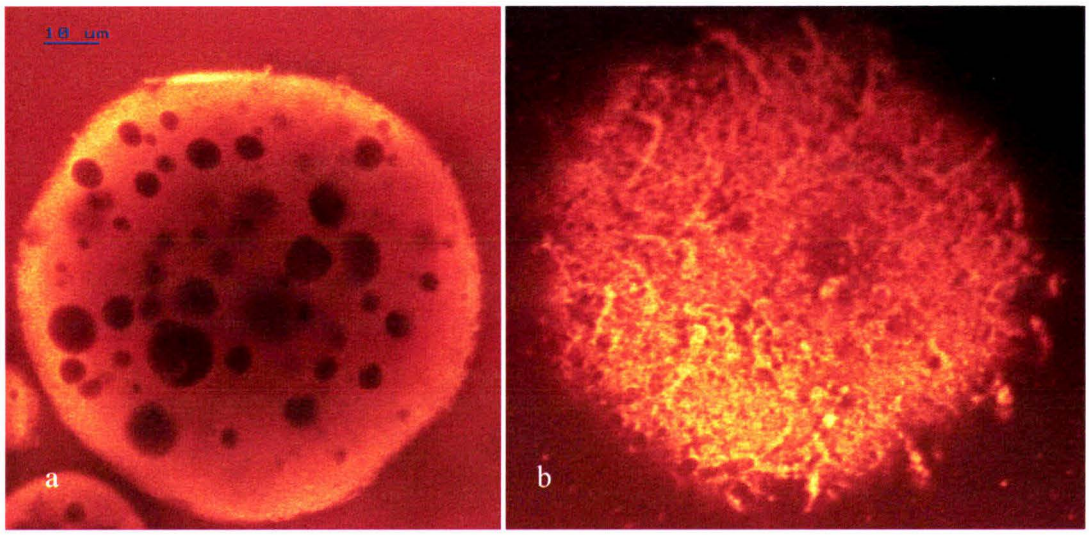

Figure 6-2. Permeate standardised SMP protein stains: a) cross section showing particle porosity, b) surface showing surface indentations.

Citifluor glycerol/PBS mounting solution containing antifadent AF1 was used to dissolve powdered dye at concentrations of 0.3 and 0.15%. Nile blue dye is non-fluorescent at wavelengths used in confocal microscopy and was used to stain fat. Nile blue contains a small amount of Nile red that diffuses into the fat droplets enabling imaging. Nile blue fluoresced green under the set up used in this work; brighter intensity in fluorescence represents greater concentrations of fat. Nile blue does not stain fat crystals. Fast green was used to stain protein; however problems were encountered with background fluorescence due to the gradual dissolution of protein into the mounting media, resulting in indistinct particle edges. Fast green fluoresces red-yellow under the microscope set up used, with brighter red-yellow representing greater concentrations of protein. Depth slices through the particle appear darker towards the centre due to the particle density and limited ability of the laser to penetrate into the centre of the particle.

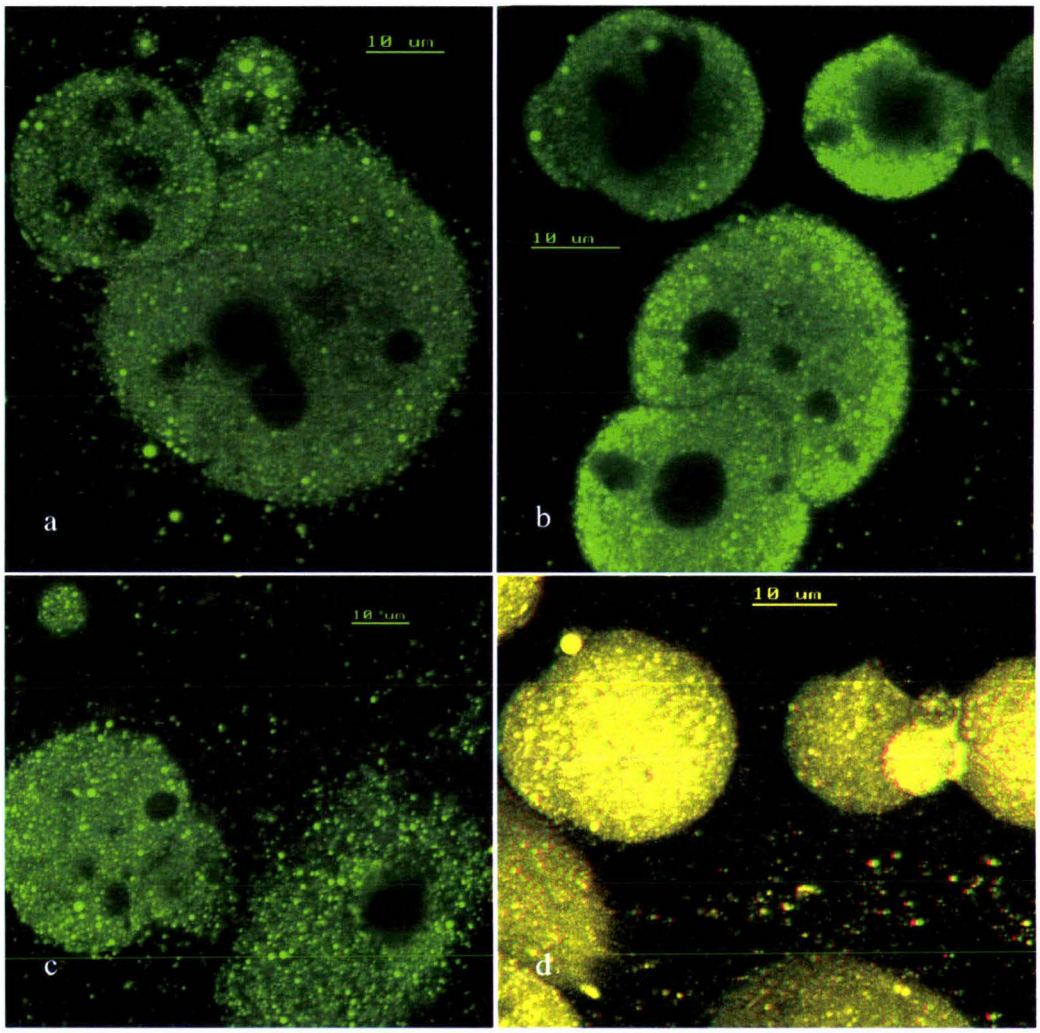

Figure 6-3. WMP fat stains: a) lactose standardised, b) unstandardised, c) permeate standardised, d) WMP unstandardised 3D fat image. Note presence of solidified fat bridging in top right hand corner.

Dual staining was achieved by mixing the two 0.3% dye solutions together at a 1:1 ratio but was not entirely successful due to background protein fluorescence. Glycerol is reported to cause some gradual dissolution of milk powder and give background fluorescence in the presence of Nile blue dye (McKenna 1997). This problem was not able to be overcome in the timeframe available and could be due to surface protein detaching from the particles. Alternative mounting media and protein stains need to be investigated for further CLSM imaging. Auty et al. (2001) and McKenna (1997) report the use of glycerol, polyethylene glycol, propanediol and other commercial mounting

solutions. Commercial solutions resulted in the best images, glycerol resulted in gradual dissolution of the powder and background fluorescence, while propylene glycol was less viscous resulting in powder streaming but gave slow dissolution. McKenna (1997) suggests that for examining detailed protein-protein and protein-fat interactions in SMP/WMP only transmission electron microscopy (TEM) will suffice.

CLSM was investigated with the idea of identifying differences between powders standardised with different lactose sources. By dual imaging of protein and fat the remaining unstained particle must be amorphous lactose and air bubbles, based on elimination. The powders investigated showed no distinct differences between the images obtained, and the dissolution of protein observed made it very difficult to draw a clear boundary around a particular particle and determine which parts would be amorphous lactose. CLSM imaging for SMP and WMP does confirm that the particles are porous with fairly evenly dispersed fat and protein droplets throughout the bulk. CLSM allows imaging up to 0.2 – 1 μm resolution, which does not enable differences at a surface level to be identified in a way that ESCA does. By eye at this resolution there was no evidence of a high fat concentration at the surface, implying that the ESCA measurements are of a very thin fat layer.

CLSM images obtained under the same magnification and laser intensity for cross section slices through various particles can be further analysed by intensity profiling using the appropriate software. This analysis gives the different concentrations of either protein or fat across the particle slice and could be used to investigate differences between similar powders. Russ (2005) provides various techniques for image analysis.

6.2.2.3 Surface Composition Effect on $(T-T_g)_{critical}$

The relationship between bulk composition and $(T-Tg)_{critical}$ has been investigated by Zuo (2004), illustrating that increasing bulk lactose composition decreases $(T-Tg)_{critical}$. Figure 6-4 shows that increasing bulk lactose expressed as %TS using the results presented in this chapter combined with results from Zuo (2004) decreases $(T-Tg)_{critical}$. Using the data from known surface analysis and estimated values (Appendix 6), the same

results are plotted in Figure 6-5. For SMP and whey protein concentrate (WPC) a negative linear relationship between surface lactose and $(T-Tg)_{critical}$ was observed. However WMP and cream powder (CP), which have a higher proportion of fat both in the particle bulk and at the surface, do not show a trend similar to SMP. Powders with higher fat components are likely to have less lactose at the surface due to the hydrophobic fat competing for the air-water interface during spray drying.

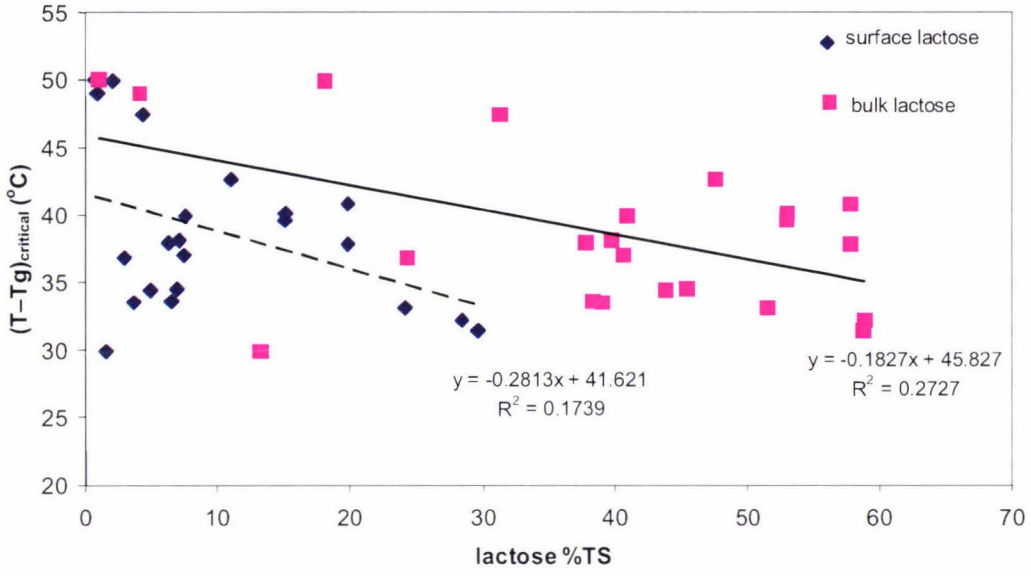

Figure 6-4. Bulk and surface (10 nm) lactose (%TS) affect on $(T-Tg)_{critical}$ for various powders tested by the particle gun technique.

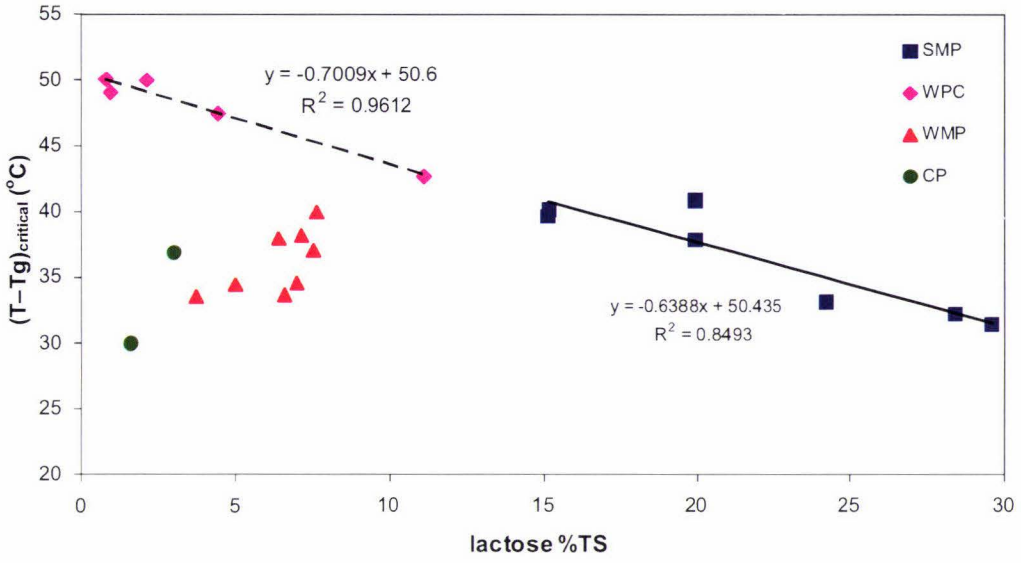

Figure 6-5. Surface lactose (%TS) affect on $(T-Tg)_{critical}$ of various powders tested by the particle gun technique.

6.3 SMP RESULTS

No significant difference between $(T-Tg)_{critical}$ or the rate of stickiness development was obtained between powders standardised to similar protein levels with either form of standardisation (Table 6-5). There is no evidence by either surface composition, bulk composition, stickiness measured by the fluid bed or the particle gun to suggest that different lactose sources used for milk standardisation have any effect on the stickiness of the resulting powder. These results provide evidence that the claims by various operators regarding different standardisation methods are unsubstantiated. Problems with powder stickiness are likely to be due to other process parameters rather than composition.

Table 6-5. SMP stickiness results from particle gun and fluid bed methods.

SMP	Powder a_w	Particle gun		Fluid bed
		$(T-Tg)_{critical}$ (± 0.8 °C)	Slope (± 0.45 %deposition/°C)	T–Tg (± 2 °C)
unstandardised[1] (45% protein)	0.23	33.6	3.10	34
permeate standardised[1] (34% protein)	0.17	31.5	4.1	23
lactose standardised[1] (34% protein)	0.19	32.5	4.03	19
permeate standardised[2] (32-33% protein)	0.18	32.7	3.76	22
Lactose standardised[2] (32-33% protein)	0.18	32.6	3.4	24
Lactose standardised[2] (32-33% protein)	0.18	35.6	4.15	23
permeate standardised[2] (32-33% protein)	0.19	35.0	3.10	25
permeate standardised[2] (32-33% protein)	0.20	35.1	3.14	21
permeate standardised[3] (32-33% protein)	0.09	32.3	2.15	13
Lactose standardised[3] (32-33% protein)	0.07	32.3	2.35	11
permeate standardised[3] (34-35% protein)	0.08	30.4	1.15	13
Lactose standardised[3] (34-35% protein)	0.06	30.9	1.44	10

[1] Fonterra Research Centre (Appendix 2) [2] naturally agglomerated SMP from Te Rapa (Appendix 3)

[3] not agglomerated SMP obtained from Waitoa (Appendix 3)

There is a difference noted between samples obtained from Waitoa compared to Te Rapa (Stork wide body dryer) due to natural agglomeration of the powder particles in the Stork wide body dryer design. The agglomerated powders were less cohesive resulting in significantly higher T–Tg values obtained by the fluid bed method. This is consistent

with work done in relation to particle size using the fluid bed apparatus by D. L. Pearce, N. T. Russell and A. G. Foskett (2004, personal communication). Differences between the Waitoa samples standardised to 32 – 33% protein compared to 34 – 35% protein are insignificant due to the inherent error of the test methods. The rate of stickiness was higher in powders containing higher levels of amorphous lactose (32 – 33% compared to 34 – 35% protein at ~ 0.08 a_w). Zuo (2004) and D. L. Pearce, N. T. Russell and A. G. Foskett (2004, personal communication) report that increasing amorphous lactose decreases the sticky point making the powder harder to handle.

The rate of stickiness development was not significantly different for any standardised SMP tested at a_w values between 0.17 – 0.23. These samples included two methods of permeate processing, refer to Appendix 3 for sample codes. The lower rates of stickiness development obtained for the four powders obtained from Waitoa (0.06 – 0.09 a_w) are due to the effect a_w has on the slope of the T–Tg plot (Chapter 4, section 4.4.3); that is increasing stickiness rates with increasing powder a_w.

6.4 WMP RESULTS

Ozkan et al. (2002) report that SMP caked at higher temperatures than WMP. A similar effect is seen for the results shown here, with SMP fluid bed results being slightly higher than the WMP results. However the fluid bed results of T. Llewellyn (2005, personal communication) suggest that T–Tg values are slightly higher for WMP than SMP results.

The results from the WMP samples tested reflect the trends observed with the SMP samples (Table 6-6). There was no significant difference between the rate of stickiness development or sticky point by either method between the different powders. The $(T–Tg)_{critical}$ values obtained for WMP are slightly higher than SMP with slower rates of stickiness development which is consistent with Zuo (2004).

Table 6-6. WMP stickiness results from particle gun and fluid bed methods.

		Particle gun		Fluid bed
WMP	Powder a_w	$(T-Tg)_{critical}$ (± 0.8 °C)	Slope (± 0.45 %deposition/°C)	T–Tg (± 2 °C)
unstandardised[1] (45% protein)	0.10	33.6	1.59	20
permeate standardised[1] (34% protein)	0.15	34.5	2.32	22
lactose standardised[1] (34% protein)	0.14	34.6	2.02	17

[1] Fonterra Research Centre (Appendix 2)

6.5 CONCLUSIONS

There was no significant difference between the stickiness behaviour observed between powders standardised by either pure lactose solution or milk permeate. There was no significant difference between either the bulk or surface composition for powders made by either method of standardisation, with the exception of surface %lactose in WMP. Therefore the additional minerals present in permeate standardised powders are well below the level required to have a significant impact on stickiness behaviour. These results provide evidence that the claims by operators regarding additional stickiness problems due to standardisation by permeate are unsubstantiated. Difficulties in stickiness experienced must be due to additional process parameters.

The myth that permeate standardised powders are more difficult to handle persists in industry. It is recommended that thorough records of plant cyclone blockage data including standardisation method, permeate concentration, lactose content, permeate composition and permeate treatment be recorded. Until such hard evidence exists the myth continues.

No significant differences in $(T-Tg)_{critical}$ were found between protein standardisation to 32 – 33% and 34 – 35%. However the rate of stickiness development was higher in 32 – 33% protein powders due to the increased amorphous lactose content. A recommended

extension of this work is to investigate what effect, if any, permeate treatment methods and permeate concentration due to seasonal protein variations has on the stickiness characteristics.

Examination of the distribution of fat and protein in milk powders was possible by CLSM, however the resolution of this method was not great enough to enable visualisation of differences at a surface level. CLSM is however suitable for 3D and cross-section images of powders containing protein and fat. ESCA measures a very thin layer of fat (~ 10 nm compared to 0.5 μm effected in particle gun) and perhaps this layer of fat is too small to have any significant effect on the stickiness behaviour. The results of this chapter suggest this is the case. The CLSM figures also support the thought that ESCA is measuring a too small a fat layer, which at the 0.2 – 1 μm level of resolution demonstrates that any fat layer present must be less than 0.2 – 1 μm thick. Hence if a layer of fat is present as suggested by ESCA, it is very thin. The results presented here plus those of Zuo (2004) and Chatterjee (2004) show that there is no significant fat effect observed on $(T-Tg)_{critical}$ for powders below a certain fat content. The fat at the particle surface needs to get to a level of 0.235 g fat/g powder or 1.95 $g.m^{-2}$ (related to a total fat content greater than or equal to 42%) to start to have an observable effect (Foster 2002). Therefore the ESCA measurement is irrelevant to the $(T-Tg)_{critical}$ value as it does not measure deep enough into the powder particle.

It is still unknown how high fat powders including WMP, where the particle surface is largely covered in fat, still exhibit lactose stickiness mechanisms. It remains a mystery as to how the lactose covered by non polar fat can react to RH changes in the short time a particle spends in the particle gun. This mechanism can only be hypothesised and it is recommended further work be carried out with respect to surface composition and T-Tg.

CHAPTER 7 - INDUSTRIAL APPLICATION OF STICKINESS WORK

7.1 INTRODUCTION

Investigations into powder stickiness are of interest to the diary industry in order to predict and thus avoid powder blockages to reduce downtime within Fonterra factories. Various projects have been carried out in relation to powder stickiness (Bronlund 1997; Brooks 2000; Chatterjee 2004; Foster 2002; McLeod 2002; O'Donnell et al. 2002; Zuo 2004) followed by the development and implementation of models for optimising spray-drying conditions.

Typically spray drying involves a residence time of ~ 20 s for atomised particles in the drying chamber (Masters 1991). The critical parameter in spray drying is the outlet air temperature. In sticking and caking the T–Tg value is important in determining the conditions under which sticking problems begin. Under different dryer configurations different outlet conditions of temperature and RH are achieved however similar absolute humidity values are obtained. The absolute humidity is of importance when applying findings to different dryer configurations. Stickiness problems most frequently arise in fluid bed and cyclone regions of dryer configurations.

7.2 INDUSTRIAL SITUATION

SMP manufactured at Fonterra Te Rapa uses a Stork wide body dryer (D5) operating at ~ 23 tonne powder.hr^{-1}, fed from two of three evaporators running at ~ 10 tonne solids.hr^{-1}. Six Stork cyclones run off the dryer, resulting in typical SMP moisture contents of 5 – 7% in the fluid bed and 3 – 4% in the final product. Stickiness difficulties in industrial dryers such as those encountered at Te Rapa typically occur in the dryer cyclones (Figure 7-1 and 7-2).

Figure 7-1. Dryer 5 cyclone riser tube after SMP blockage.

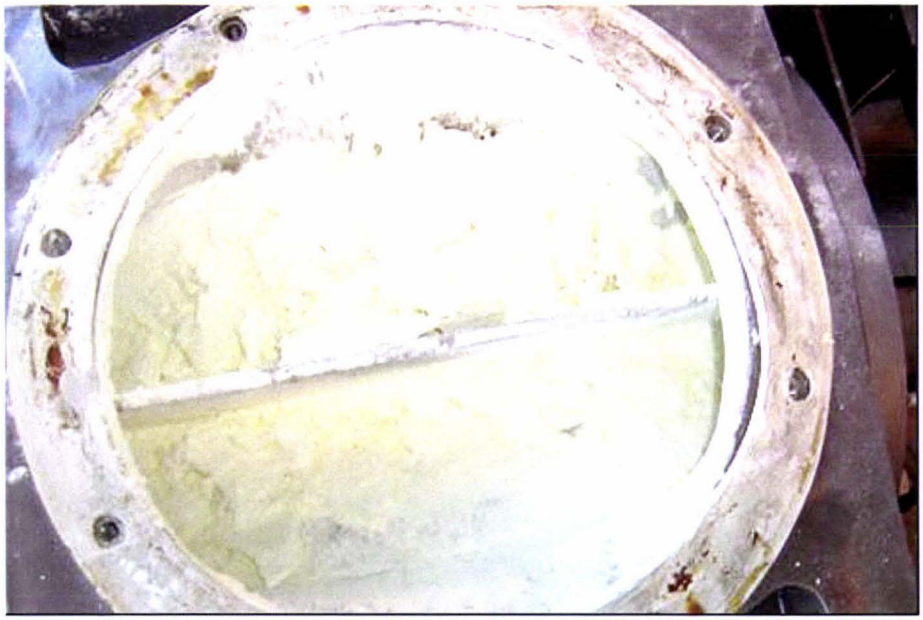

Figure 7-2. Dryer 5 cyclone 4 rotary valve after SMP blockage.

7.2.1 Implementation of Sticky Curves

Implementation of the current knowledge of stickiness in milk powder spray drying continues to improve. N. T. Russell (2005, personal communication) has created models based on the stickiness data obtained prior to and including work by Zuo (2004). This

model (Figure 7-3) lies between the particle gun and fluid bed predictions and has been implemented for plant control with the addition of a dryer specific component.

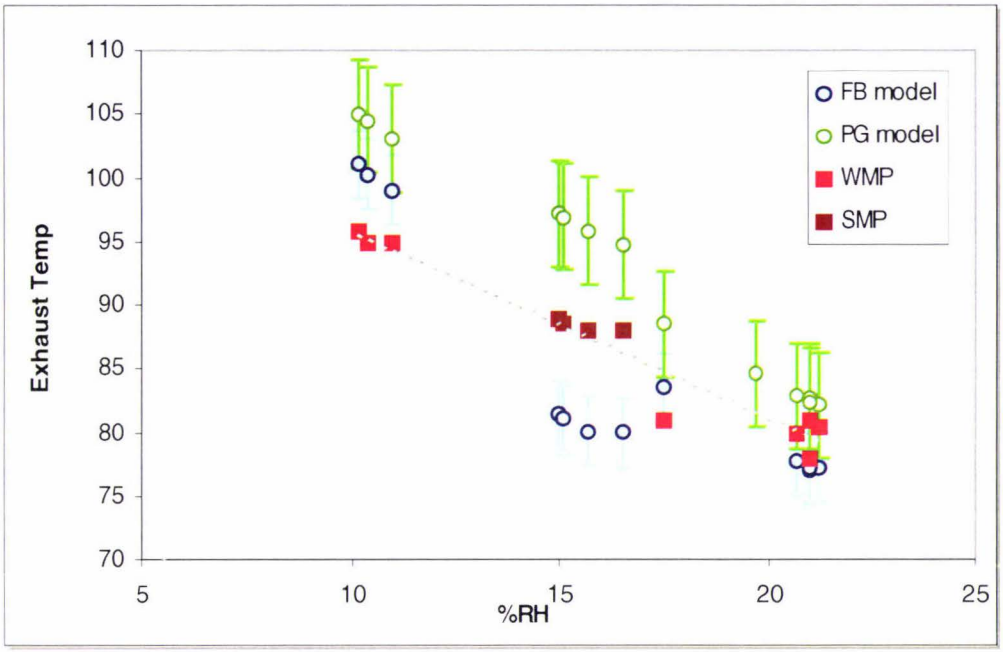

Figure 7-3. Current model compared to WMP and SMP blockage data prior to 2004/05 season, N. T. Russell (2005, personal communication).

The current set up allows dryer operators to view a line on the operating screen representing the division between the sticky and non-sticky conditions for powder processing (Figure 7-4). Such a line provides a visual guide for operators to view how far they can push the dryer towards the critical point where stickiness begins to become a problem. Currently this line is obtained by comparing the laboratory determined sticky curve for a particular powder to current data for conditions under which blockage problems were experienced. The operating curve is created based on the dryer outlet conditions. The estimate for the sticky curve of a particular powder includes a dryer specific bias. A first approximation of the sticky curve is taken as -1.3°C/RH based on the Tg curve for lactose over the temperature range of interest. The bias is experienced based for a particular dryer/cyclone configuration. For different compositional powders the slope remains constant and the intercept is varied accordingly. If the plant is running well outside the predicted sticky curve, then the bias plus a small safety margin is

changed to reflect this (D. L. Pearce, N. T. Russell and A. G. Foskett, 2004, personal communication). It is the operator's role to run the dryer as close to the sticky curve as possible.

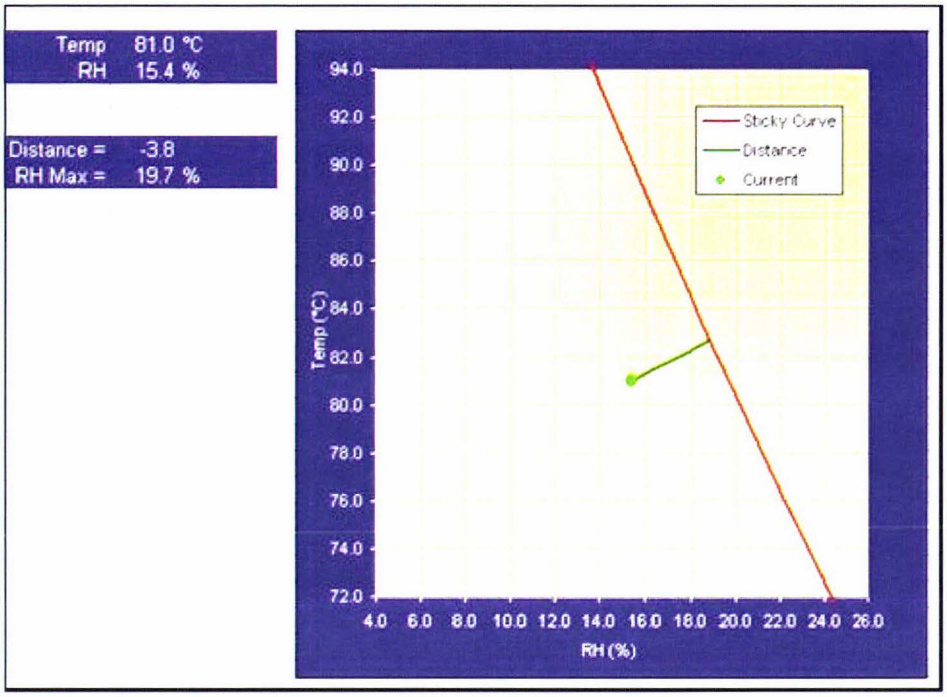

Figure 7-4. Example of a sticky curve used to guide dryer operators, N. T. Russell (2005, personal communication).

7.2.2 Te Rapa Blockage Data

Blockage data prior to the 2004/05 season does not differentiate between blockages due to stickiness mechanics and blockages due to other factors such as air ingress or air hold up due to poor valve maintenance. Data were obtained for nine D5 blocks between September and October 2005. Prior to this data set a major upgrade of rotary valves was completed, therefore the data should not be biased towards blockages due to valve malfunction. Rotary valves are known to have severe limitations regarding sticky and hygroscopic products (Perry and Green 1997). Any product hanging in the rotor sections of the valve will not fall away quickly, leaving the valve inoperable. Hammering above the valve can assist products with a tendency to stick to clear the valve; alternatively the rotor clearance can be adjusted. The downfall with adjusting the valve clearance is that

air can leak back up into the dryer, causing condensation and instant blocking. Improved designs of tapped rotors are available.

The operating point data obtained at the time of blockage for cyclones connected with D5 at Te Rapa are shown in Figure 7-5. All data obtained was for SMP, mostly standardised with milk permeate. The cubic Tg line for amorphous lactose was fitted to the temperature and RH conditions of the air exiting the dryer chamber at the time of blocking. The resultant sticky point was Tg + 27°C, i.e. a $(T-Tg)_{critical}$ value of 27°C. This result is lower than the initiation of stickiness value obtained by the particle gun method for SMP (30 – 35°C), and higher than results obtained by the fluid bed (19 – 25°C), Chapter 5, Table 5-1. This mid-range T–Tg value is consistent with Russell's model.

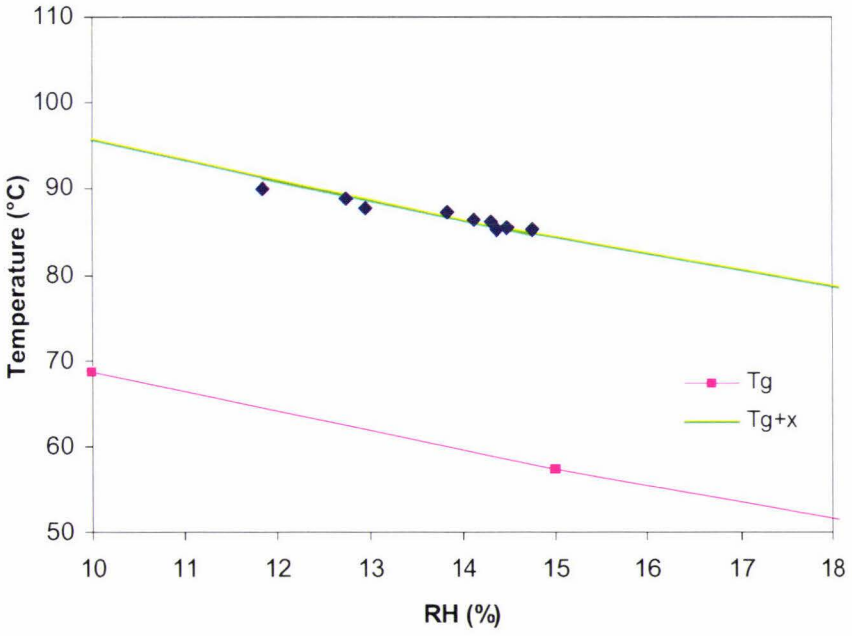

Figure 7-5. Operating point data at the time of blockage for D5 processing SMP, 2005 season.

7.3 Possible Reasons for Plant Blockages

Blockages in cyclones occur for various reasons. Operators at Te Rapa have observed that powder bridges at the base of the cyclone, just above the rotary valve (Figures 7-1 and 7-2), but it is unknown whether the initial powder deposits form higher up and then

fall down or whether the build up is occurring above the rotary value. Photos obtained of cyclone blockages in D5 show powder build up around the RH probe at the base of the cone suggesting that the build up begins at the lower levels of the cyclone. Powder build up at the base of cyclones has been reported by J. Abrahamson (2005, personal communication). There were no indications that the blocks are related to changing ambient conditions within the factory, and no data relating to this has been recorded.

Blockages in powder transport lines and in cyclones are principally caused by cohesion, initiated by adhesion (Bhandari and Howes 2005). Although powders may not stick on brief contact, large surface liquid bridges develop when the particles come in close contact (such as in a narrow duct or cyclone neck) and the temperature of the powder tends to approach the surrounding air temperature. A solid glass (amorphous solid) will have low surface energy and will not stick to any other low energy solid surfaces. Due to the transition from glass to rubbery (or liquid) state, the surface energy of the material increases and the molecules start interacting with the solid surface (Bhandari and Howes 2005). If the particles remain in a high-energy sticky state, they will stick upon contact to any high-energy solid surface. The severity of the stickiness problem will depend on the property of the powder material at a particular temperature, and the surface energies of the contact surfaces (Bhandari and Howes 2005). Masters (1991) suggests that wide ducts can reduce particle build up and friction.

F. Lin (2005, personal communication) has put forward the suggestion that feed back control for changing the dryer inlet conditions results in time delays that are too great to avoid potential blockages. Industrially the outlet RH and temperature are measured and the information linked back to the inlet feed rate and temperature to enable appropriate adjustments. However in practice this situation results in hourly product readings and can cause delays in operators making adjustments from 20 minutes up to an hour, by which time it is too late to avoid blockages via feed rate adjustments. Such delays provide ample time for adhesion to initiate between the particles and the cyclone surfaces, resulting in blockages.

7.3.1 Cyclone Air Flow Patterns

Flow through the cyclone is essentially a double spiral, with the presence of the upward spiral forming a central core. The central core diameter has been related to the exit cyclone duct diameter (Masters 1991). Particles enter the cyclone tangentially and are thrown out to the wall by the centrifugal force. The particles then move down the cyclone walls where there is a greater concentration of particles to gas (Abrahamson et al. 2002; Saruchera 1999). The centre vortex is known to be transient and rotates around the base of the cyclone cone (where the axial velocity tends to zero) acting as a vacuum cleaner and entraining particles (J. Abrahamson, 2005, personal communication; Derksen and Van den Akker 2000; Solero and Coghe 2002). Many other authors provide evidence towards the existence of a vortex core precession (Derksen 2003; Derksen and Van den Akker 2000; Shalaby et al. 2005; Solero and Coghe 2002; Zhao and Abrahamson 1999). Evidence of fluid dynamic instabilities such as vortex breakdown and precessing vortex core has been reported by Solero and Coghe (2002). Particle flow in Stairmand high efficiency cyclones has been well described by an axially dispersed plug flow model (Saruchera and Abrahamson 2002).

It has been observed that a line of solids often accumulates at the base of the cyclone cone, approximately half an outlet diameter (do) above the outlet (J. Abrahamson, 2005, personal communication). J. Abrahamson (2005, personal communication) observed a demarcation line of solids around the bottom of the cyclone cone at a level of approximately half do, created by the particles rotating around. Below this line build up occurs because the vertical gas velocity tends towards zero at that point. Cone choking is commonly found for small cyclones (Abrahamson et al. 2002).

The velocity of the particles at the cyclone wall is actually much lower than the inlet gas velocity and particles exist at a higher particle concentration. It was demonstrated in Chapter 5 that reducing particle velocity decreased $(T-Tg)_{critical}$. The most likely explanation is that at specific points in the cyclone system where the particle velocity is reduced, sticking is likely to commence at a lower $(T-Tg)_{critical}$ value than that predicted by the particle gun at 20 $m.s^{-1}$.

7.3.2 Cyclone Pressure Drop

A pressure drop exists between the inlet and outlet of a gas cyclone due to frictional and kinetic energy losses. The increase in air velocity at the cone apex where the air turns before spiralling upwards towards the exit can also induce a change in pressure, influencing the temperature and RH of the air. It was speculated that this change in air conditions due to the increased air velocity may be a factor contributing towards powder blockages. This factor will only be influential provided that the deviation in air conditions was large enough to alter the Tg of the powder.

Zhao and Abrahamson (1999) carried out FLUENT[9] simulations predicting tangential and axial velocity profiles for a gas cyclone, indicating a central isolated core along the vertical axis where the axial gas flow is in reverse direction to the outflow. Their predictions compare reasonably well with the analytical values given. Both axial and tangential velocities appear to peak at the edge of this central core. The circumferential and tangential gas velocities are seen to slowly decrease towards the chamber wall (Solero and Coghe 2002; Zhao and Abrahamson 1999). Cyclone predictions by Shalaby et al. (2005) and Solero and Coghe (2002) suggest that the central region in the cyclone rotates like a solid body where the tangential velocity is increasing with increasing radius. Past a particular radius the tangential velocity starts to decrease reaching zero velocity at the wall. The maximum gas velocity experienced in the centre vortex is in the range of 2 – 3 times the inlet velocity, depending on the cyclone geometry (J. Abrahamson, 2005, personal communication). This is consistent with experimental data for gas cyclones reported by Solero and Coghe (2002) who suggest the highest velocity in the cylindrical body is approximately 1.7 times the inlet mean velocity, and Shalaby et al. (2005) who predict a maximum tangential velocity of approximately 1.24 times the inlet velocity, reached at a radius approximately 25% from the centre of the cyclone.

The pressure drop in a cyclone due to the velocity profile experienced was calculated for a typical industrial cyclone (Appendix 5C). Polytropic expressions for compression were

[9] The simulations were carried out with FLUENT 3.03, using 3-dimensional non-symmetric flow, and algebraic stress model in polar coordinates

used for the reversible adiabatic process (no heat exchange with the surroundings) taken from (Sinnott 1985). There was indeed a small pressure drop due to the increased gas velocity in the centre vortex of the cyclone, resulting in a slight temperature drop and RH increase. However this had an insignificant effect on altering the particle Tg with only a slight drop in Tg and T–Tg observed (T–Tg dropped from 19.53°C to 19.34°C at an inlet velocity of 15 $m.s^{-1}$). At inlet velocities of 15 – 25 $m.s^{-1}$ it is unlikely that the small drop in RH will be a contributing factor of any blockage. A significant drop in air RH is only observed at air velocities greater than 100 $m.s^{-1}$ (J. Abrahamson, 2005, personal communication). It is more likely that the blockages in the cyclone are due to other factors such as airflow, particle loading, particle residence times and variations in gas temperature and moisture.

7.3.3 Cyclone Temperature Investigation D5 Te Rapa

Temperatures were recorded for a single D5 cyclone manufacturing SMP. Wall temperatures at four points of interest were recorded (Figure 7-6). The aim of this temperature log trial was to obtain an estimate of the boundary layer temperatures just inside the cyclone wall where particles are directed down the walls at a greater concentration and lower velocity than in the bulk of the cyclone. Duplicate probes were placed at sample point 2 and 3 with one insulated from the outside ambient air and one not insulated. The non-insulated probe gave an estimation of the wall temperature with natural heat loss to the environment, while the insulated probe gave a temperature reading unaffected by the heat loss to the environment.

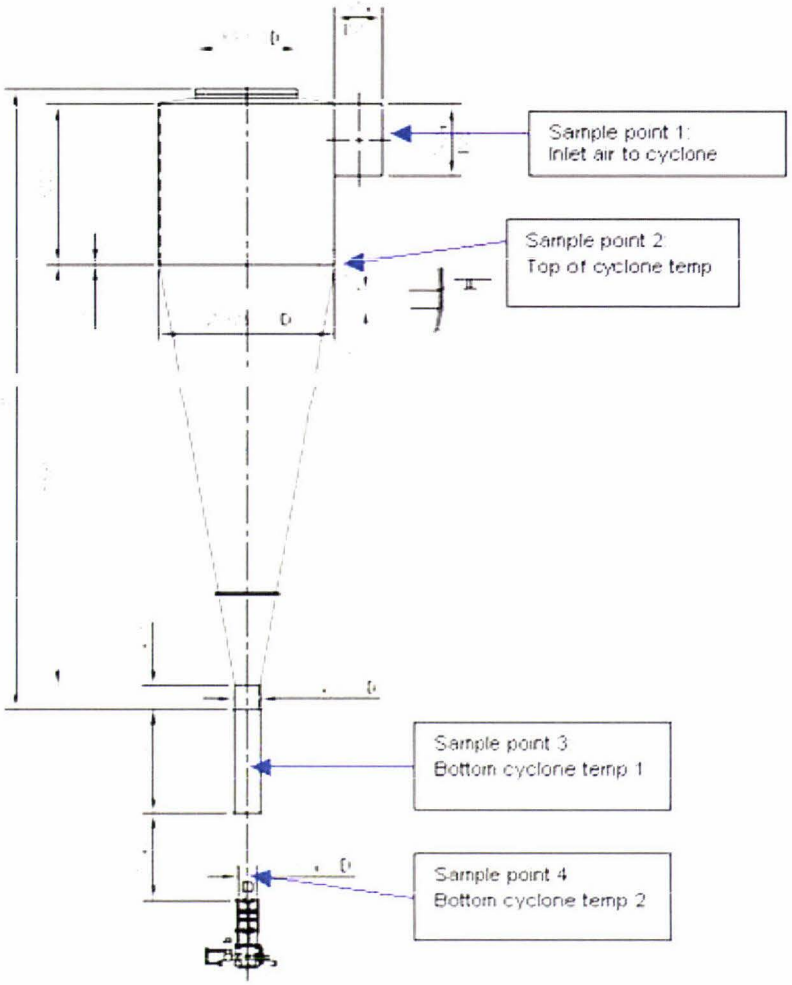

Figure 7-6. Sample 1: Inlet - 2 probes un-insulated, Sample 2: Top of cyclone - 1 probe insulated, 1 probe un-insulated, Sample 3: Bottom of cyclone - 1 probe insulated, 1 probe un-insulated, Sample 4: Above rotary valve - 2 probes un-insulated.

The temperature data (Figure 7-7) obtained for the probes at the four sites described in Figure 7-6 shows fairly large temperature jumps. The inlet cyclone air temperature was recorded as 78°C with a RH of 18%. The temperature jumps are due to the eye button probes used which round measurements to ± 0.5°C and were set to log at 30 minute intervals. The temperature probes at the rotary valve and top of dropper tube (sample point 3 and 4) gave lower readings than the other probes. Corresponding RH and T–Tg values were calculated for the average temperature at each sample point (Appendix 5D). T–Tg and RH values increased dramatically below the base of the cyclone apex, where

the wall temperature was significantly cooler (Figure 7-7). This is due to the different powder concentration and flow behaviour once the powder leaves the main cyclone chamber. An extended data set for the second trial running from start up to shut down of a D5 cyclone is given in Appendix 7.

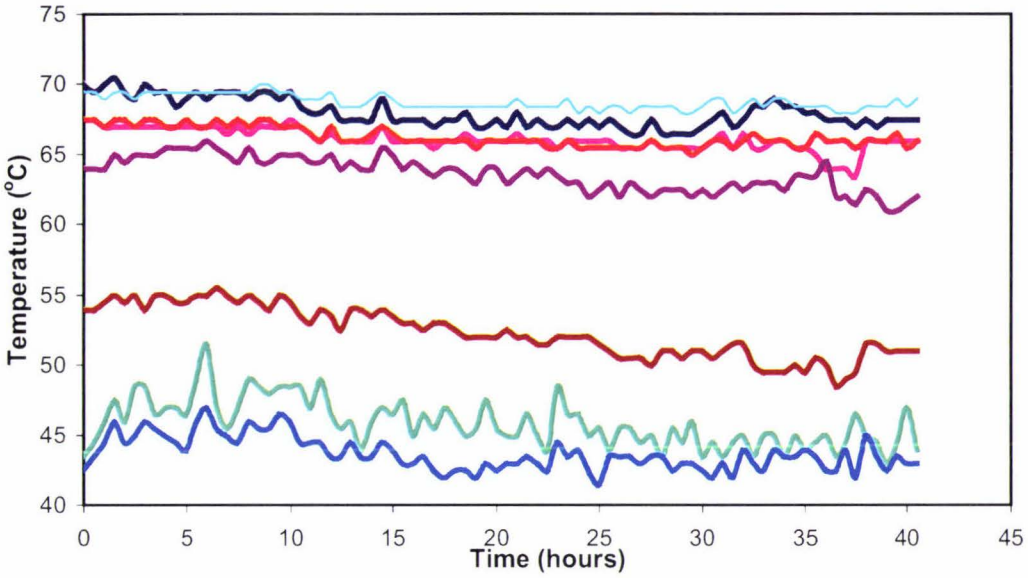

Figure 7-7. Temperature readings for D5 cyclone operating with SMP. – cone top insulated (68°C) – cone top un-insulated (66°C), – cyclone inlet (66°C) – cyclone inlet (69°C) – cone bottom insulated (64°C) – cone bottom un-insulated (52°C) – rotary valve (46°C) – rotary valve (44°C).

Two phenomena are occurring in the cyclone and associated ducting. In the top part of the cyclone before the dropper tube, particles are suspended in the bulk air with turbulent gas flows. Air conditions dominate the temperature of the particle surface and the wall temperature. In the dropper tube and rotary valve positions, the particle concentration is increased and the particles flow as a dense mass with a fraction of air associated. In this situation the particles have the dominating influence on the air properties and wall temperature. Because the particles are the dominating fraction, they will influence the air RH by adsorbing/desorbing moisture.

The operating point resulted in a T–Tg value of 28°C, one degree above the T–Tg value predicted from blockage data (72.2, Figure 7-5.). Data for the blockages were all at

operating temperatures of 80°C and above, while standard operating data has 80°C as the upper limit. The T–Tg value obtained for the main cyclone chamber wall temperature (65°C) was 33°C, equivalent to the T–Tg value predicted by the particle gun. This suggests that drying was operating right on the upper limit of stickiness development where blockages occur. The temperature of the cyclone wall where particles are moving at slower velocities and at higher concentrations may provide conditions which sufficiently exceed $(T\text{-}Tg)_{critical}$ and initiate blockages. The wall temperature may be the limiting factor rather than the inlet air temperature. An alternative interpretation is that there are additional factors that trigger the cyclone blockage.

Using heat transfer equations (Appendix 5E) the inside wall temperature of the cyclone was estimated. There was little temperature difference across the cyclone wall, indicating that the outside wall temperature is a reasonable estimate of the inside wall temperature. However calculated predictions for the outside wall temperature were considerably lower than those obtained experimentally (39 compared to 65°C), indicating an over estimation of the heat loss and the heat transfer coefficient for the outer wall. It has been suggested that the temperature of the air leaving the cyclone is generally 4°C lower than the inlet gas temperature, which is in agreement with the 3.5°C temperature drop calculated.

7.3.4 Particle Residence Times

Investigations into particle residence times in gas cyclones has been performed by (Kemp et al. 1998; Saruchera 1999; Saruchera and Abrahamson 1997; Saruchera and Abrahamson 2002). These studies measured the particle residence time using a pulse of coloured particles. Such studies have shown that the particle residence time is much longer than the gas residence time. Particle axial velocity determines residence time, and in turn slip velocity between the solids and gas influences the axial velocity (Saruchera and Abrahamson 2002). Both the particle mean residence time and back-mixing increased strongly with cone angle (Saruchera and Abrahamson 2002), while decreasing cone height had a smaller effect in increasing particle residence time. Blunt cone angles resulted in larger residence times than steeper angles. There appeared to be no dependence of residence time on gas velocity or on solids-gas loading (Kemp et al.

1998). The velocity of particle flows along the wall becomes important under high particle loadings and is also dependent on cyclone geometry.

Residence times ranged from about 0.55 to 1.2 s for the particle size range (210 – 700 μm) with a solids-gas loading of 0.05 to 0.12 $kg.s^{-1}$ (Saruchera and Abrahamson 2002). Saruchera and Abrahamson (1997) report a mean particle residence time of 1.12 s with 95% of the particles having a residence time between 0.6 and 1.6 s. Increasing particle density roughly doubled the residence time, with the most likely explanation being that particles are clustered closer to the wall and wall friction effects are therefore comparatively greater. Larger particles experienced larger residence times, whereas with smaller particles the drag forces are larger compared to the centrifugal force. Small particles travel more suspended in the gas phase with less interaction with the wall, resulting in lower slip velocities between gas and solids (Saruchera 1999).

Increasing the solid content of the solution entering the dryer decreases the fines due to increased viscosity and lower pressure through the lance resulting in forming a larger droplet. Less fines result in less powder passing through the cyclones. Fines from the cyclones generally have a higher moisture content than the finished product. In addition cyclone particles are much more cohesive than the main fraction (Rennie et al. 1999) because particle size has a marked effect on cohesion (Buma 1971). Faldt and Sjoholm (1996) report that powder from the cyclones is generally inferior to the bulk powder exiting the dryer and fluid bed.

Experiments on drying occurring within the cyclone by Kemp et al. (1998) indicate increasing the gas flow without increasing solids flow rate increases the gas temperature and drying. This would result in the particles experiencing a greater T–Tg, possibly above the non-sticky conditions. A similar effect is shown by Zuo (2004), where increasing throughput increases T–Tg as a function of both the inlet and outlet temperature. Kemp et al. (1998) goes on to suggest that if the solids-gas loading is increased, there is a significant fall in drying in the cyclone as the gas temperature falls. This means that particles exiting the cyclone would be moister, and approach their sticky

point due to the depression of Tg at higher moisture levels. Therefore increasing solids throughput requires a corresponding increase in gas mass flow rate to maintain the heat balance (Kemp et al. 1998). Increasing the gas inlet temperature would increase the drying rate but could push the particles above the $(T-Tg)_{critical}$, leading to sticking and blocking. Increasing particle density is expected to increase residence time and thus increase drying (Kemp et al. 1998).

7.4 CONCLUSIONS

The current practice of recording blockage data and matching the updated models to each dryer configuration appears to be working. The blockage data for SMP in terms of T–Tg values (27°C) for exit air conditions lies between the particle gun (30 – 35°C) and fluid bed results (19 – 25°C). Calculations and measurements show that conditions in the cyclone base where blockages occur have lower velocities and higher mass concentrations than the conditions used by the particle gun. This suggests that the $(T-Tg)_{critical}$ point will be lower than that measured by the particle gun, as has been shown here. The T–Tg obtained experimentally by the particle gun technique should be adjusted due to the particle velocity and contact time variations in various parts of the dryer configuration. D5 appears to be operating on or close to the sticky point for SMP obtained from D5 blockage data (T–Tg of 28°C).

It is recommended that the influence of altering the gas and solid flow rates through the cyclone be monitored to avoid exceeding the particle's $(T-Tg)_{critical}$ conditions resulting in sticking and blockage problems. Sticking can be initiated by lowering the particles Tg via either a higher moisture content, exposure to a higher air temperature or a combination of moisture and temperature leading to blockage problems at the cyclone outlet. This effect will be compounded due to lower particle velocities and higher particle concentrations at the cyclone base and rotary valve.

The current trend to eliminate problems with amorphous powders and cyclone blockages is to implement bag houses. However bag houses present their own complex problems as

they are washable; although in practice they are not easily washed and frequently cause problems.

CHAPTER 8 - CONCLUSIONS & RECOMMENDATIONS

The particle gun measures the initiation of stickiness point for dairy powders as $(T-Tg)_{critical}$. In addition the particle gun also provides information on the rate of stickiness development with increasing humidity. These stickiness characteristics were found to be a function of the particle gun air velocity, angle of impact, powder a_w and ambient air conditions.

Increasing powder a_w increased the rate of stickiness development, however $(T-Tg)_{critical}$ remained constant indicating that the initiation of stickiness is indeed a surface phenomenon. Increasing the ambient room RH lowered $(T-Tg)_{critical}$, making the powder appear stickier than when tested at low ambient air RH conditions. It is therefore important to maintain constant testing conditions when comparing various powders tested on different days. Under standard testing conditions (powder feed rate of 0.3 $g.s^{-1}$, particle gun air velocity of 20 $m.s^{-1}$, ambient air at < 50 %RH, room temperature ~ 20°C and constant powder a_w) $(T-Tg)_{critical}$ was reproducible within ± 0.8°C for SMP while the rate of stickiness development was reproducible within ± 0.45 %deposition/°C. The addition of the vibratory feeder and controlled ambient air surroundings significantly improved the reproducibility achieved by Zuo (2004).

Increasing air velocity through the particle gun increased $(T-Tg)_{critical}$ but had little effect on the rate of stickiness development. This can be explained by the increased impact force and decreased time of impact for particles travelling at higher velocities requiring greater adhesion forces to stick to the collection plate. The increased velocity also resulted in less time for the particle surface to equilibrate with the air in the particle gun therefore less of the particle surface would have been affected. Decreasing the angle of impact that the particles strike the collection plate decreased the rate of powder build up but had no significant effect on $(T-Tg)_{critical}$. Air velocities below 10 $m.s^{-1}$ could be trialed in the particle gun in future work and $(T-Tg)_{critical}$ values correlated to dryer specific air velocity profiles.

The results obtained from the particle gun rig are consistently higher than those obtained by the fluid bed test method. These findings imply that the experimental value of $(T-Tg)_{critical}$ may need to be adjusted when implemented in industrial cyclones to compensate for changes in particle velocity and angle of impact. At angles of impact below 90°, the maximum T–Tg tolerable before significant powder deposition occurs would be higher than the $(T-Tg)_{critical}$ predicted at 90°. This is due to the reduced rate of powder deposition observed at impact angles less than 90°.

Protein down standardisation of milk powder via the addition of milk permeate compared to lactose solution had no detectable effect on the stickiness characteristics of SMP or WMP as measured by the particle gun and the fluid bed rig. Little difference was seen between either the bulk or the surface composition of the two milk powders, however permeate standardised milk contained higher levels of milk salts and ash than lactose standardised milk. This provides evidence which dispels speculation by operators that permeate standardisation produces a more difficult to handle powder. It is recommended that thorough documentation of plant cyclone blockages be compiled, in particular noting of the standardisation details.

Increasing the amorphous lactose content of the powder had a small effect of decreasing the sticky point. A negative linear relationship was observed between surface lactose (%TS) and $(T-Tg)_{critical}$ for SMP and WPC based on actual and approximated surface composition data. Increasing amorphous lactose at the particle surface of SMP and WPC decreased the sticky point obtained similar to the relationship for bulk composition reported by Zuo (2004). Further work is required to investigate the relationship between powder surface composition and its stickiness characteristics.

Industry blockage data indicates that the $(T-Tg)_{critical}$ where blockages occur in the cyclones was 27°C for SMP. Currently Te Rapa D5 is running satisfactorily for SMP at a T–Tg value of 28°C. The T–Tg value obtained using blockage data lies between the fluid bed and particle gun predictions. This is in agreement with the model created by N. T.

Russell (2005, personal communication). Outside wall temperatures were used to obtain an estimate of the inner wall temperature of a D5 cyclone. Particles move at a slower velocity down the cyclone wall with increased particle concentrations and have a greater tendency for particle-particle interactions. Under standard SMP operation the cyclone wall temperature corresponded to a T–Tg value of 33°C, the same $(T-Tg)_{critical}$ value predicted by the particle gun for standardised SMP. This implies that the cyclone was operating correctly at the maximum T–Tg value before particles become sticky enough to cause blockage problems. An alternative interpretation is that the dryer and cyclones are able to operate above the $(T-Tg)_{critical}$ predicted by the particle gun, with additional factors causing the cyclone to block.

The particle gun provides a useful method to investigate a powder's stickiness properties. This method gives reproducible results when used under standard testing conditions and allows the isolation of factors influencing stickiness behaviour such as velocity and angle. Particle gun results can successfully be used to predict blockages in industrial scale cyclones with the inclusion of a dryer specific correction factor.

NOMENCLATURE

a_w	water activity	
a	particle diameter	m
A	area	m^2 or ft^2 [10]
B	WLF constant for SMP	
c	BET constant	
c	constant related to the energy of bonding (2.81)	
C	WLF constant for SMP	
CRC	critical relative humidity	%RH
Cp	specific heat capacity	$J.m^{-3}.^oC$ or $BTU/lb_m.R$ [10]
d_{50}	mean diameter of particles	µm
do	particle gun outlet diameter	m
D	amorphous lactose diffusivity	$m^2.s$
D_i	inside diameter of cyclone	ft [10]
D_o	outside diameter of cyclone	ft [10]
e	coefficient of restitution	
E_1	Young's modulus for impacting particle	Pa
E_2	Young's modulus for surface	Pa
f	constant which corrects the properties of the multi layer with respect to the bulk liquid (1.01)	
F_A	fraction of spherical particle affected	%
Fo	Fourier number (dimensionless)	
F	force	N
F_t	applied force	N
g_c	Universal constant – 1 in SI units	
G	mass velocity	$lb.hr^{-1}.ft^2$ [10]
h_a	heat transfer coefficient air side	$BTU/hr.ft^2.^oF$ [10]
h_c	heat transfer coefficient – convection	$BTU/hr.ft^2.^oF$ [10]
h_i	heat transfer film coefficient inside	$BTU/hr.ft^2.^oF$ [10]
h_r	heat transfer coefficient – radiation	$BTU/hr.ft^2.^oF$ [10]
H	absolute humidity	kg water/kg air
j_h	factor for heat transfer (dimensionless)	
J	momentum	$kg.ms^{-1}$
k	contribution factor for water component in Gordon Taylor equation	
K	thermal conductivity	$W.m^{-1}.^oC^{-1}$
m	step count	
m	mass flow rate	$kg.s^{-1}$
mp	mass of particle	kg
mfa	mass flow rate of air down particle gun barrel	$kg.s^{-1}$
mfp	mass flow rate of particles down particle gun barrel	$kg.s^{-1}$
M	moisture content	g water/g dry powder
M_a	moisture content of external medium	g water/g air

[10] Imperial units used in heat transfer equations (Appendix 5E) taken from Kern (1950).

M_{av}	average moisture content of particle	g water/g dry powder
M_i	initial moisture content of particle	g water/g dry powder
M_f	moisture content not including residual moisture	g water/g dry powder
M_o	monolayer moisture content (6.27 g/100 g dry powder)	g water/g dry powder
n	number of replicates	
p	water vapour pressure exerted by food	Pa
p_o	vapour pressure of pure water at the food temperature	Pa
P	pressure	kPa or psi [10]
q	volumetric flow rate	$m^3.s^{-1}$
Q	heat flow	$BTU.hr^{-1}$ [10]
r	distance travelled from particle surface to particle centre	m
R	particle radius	m
Re	Reynolds number (dimensionless)	
RH	relative humidity	%RH
t	time	s
T	temperature	°C
Tg	glass transition temperature	°C
T–Tg	temperature between particle temperature and particle Tg	°C
t_n	student's t-distribution	
U_o	overall heat transfer coefficient	$BTU/hr.ft^2.°F$ [10]
V	velocity	$m.s^{-1}$
v_1	Poisson ratio for impacting particle	
v_2	Poisson ratio for surface	
w	mass fraction for Gordon Taylor equation	
x	inter particle bridge radius	m
x	wall thickness	m
x_i	mass fraction of multi component powder	
X	diameter of viscous bridge required for sticking	m
Y	fraction of change achieved	
Y_{av}	average fraction of change achieved in particle	
Y_c	fraction of change achieved at particle centre	
z	wall thickness	ft

α	Hertzian constant	
γ	surface tension	$N.m^{-1}$
ε	emissivity	
η_g	viscosity at the glass transition temperature	Pa s
θ	angle of impact	°
θ	temperature	°C
θ_a	external medium temperature	°C
θ_i	initial particle temperature	°C
λ	thermal conductivity	$W.m^{-1}.°C$ or $BTU/hr.ft^2.°F$ [10]
μ	viscosity	Pa s
μ_g	viscosity at the glass transition temperature	Pa s
μ_w	viscosity at the wall temperature	Pa s

π	pi	
ρ	density	$kg.m^{-3}$
σ	surface tension	$N.m^{-1}$

REFERENCES

Abrahamson, J., Jones, R., Lau, A., and Reveley, S. (2002). "Influence of entry duct bends on the performance of return-flow cyclone dust collectors." *Powder Technology*, 123, 126-137.

Adhikari, B., Howes, T., Bhandari, B. R., and Truong, V. (2003a). "In situ characterisation of stickiness of sugar-rich foods using a linear actuator driven stickiness testing device." *Journal of Food Engineering*, 58, 11-22.

Adhikari, B., Howes, T., Bhandari, B. R., and Truong, V. (2003b). "Surface stickiness of drops of carbohydrate and organic acid solutions during convective drying: Experiments and modelling." *Drying Technology*, 21(5), 839-873.

Adhikari, B., Howes, T., Lecomte, D., and Bhandari, B. R. (2005). "A glass transition temperature approach for the prediction of the surface stickiness of a drying droplet during spray drying." *Powder Technology*, 149, 168-179.

Aguilera, J. M., de Valle, J. M., and Karel, M. (1995). "Caking phenomena in amorphous food powders." *Trends in Food Science & Technology*, 6(May), 149-155.

Auty, M. A. E., Twomey, M., Guinee, T. P., and Mulvihill, D. M. (2001). "Development and application of confocal scanning laser microscopy methods for studying the distribution of fat and protein in selected diary products." *Journal of Dairy Research*, 68, 417-427.

Baechler, R., Clerc, M.-F., Ulrich, S., and Benet, S. (2005). "Physical changes in heat-treated whole milk powder." *Lait*, 85, 305-314.

Bhandari, B., and Howes, T. (2005). "Relating the stickiness property of foods undergoing drying and dried products to their surface energetics." *Drying Technology*, 23, 781-797.

Bhandari, B. R., Datta, N., and Howes, T. (1997). "Problems associated with spray drying of sugar-rich foods." *Drying Technology*, 15(2), 671-684.

Bhandari, B. R., and Howes, T. (1999). "Implication of glass transition for the drying and stability of dried foods." *Journal of Food Engineering*, 40, 71-79.

Bloore, C. G. (1981). "A quality control system for the manufacture of spray dried milk powder," Doctor of Philosophy in Technology, Massey University, Palmerston North.

Boonyai, P., Bhandari, B., and Howes, T. (2004). "Stickiness measurement techniques for food powders: a review." *Powder Technology*, 145, 34-46.

Boonyai, P., Bhandari, B., and Howes, T. (2005). "Measurement of glass-rubber transition temperature of skim milk powder by static mechanical test." *Drying Technology*, 23, 1499-1514.

Bronlund, J. E. (1997). "The modelling of caking in bulk lactose," Doctor of Philosophy in Process and Environmental Technology, Massey University, Palmerston North.

Brooks, G. E. (2000). "The sticking and crystallisation of amorphous lactose," Master of Technology in Chemical Technology, Massey University, Palmerston North.

Buma, T. J. (1970). "Determination of crystalline lactose in spray-dried milk products." *Netherland Milk Dairy Journal*, 24, 129-132.

Buma, T. J. (1971). "Free fat in spray-dried whole milk. 5. Cohesion; determination, influence of particle size, moisture content and free-fat content." *Netherland Milk Dairy Journal*, 25, 107-122.

Buma, T. J., and Henstra, S. (1971). "Particle structure of spray-dried milk products as observed by a scanning electron microscope." *Netherland Milk Dairy Journal*, 25, 75-80.

Buma, T. J., and van der Veen, H. K. C. (1974). "Accurate specific optical rotations of lactose, and their dependence on temperature." *Netherland Milk Dairy Journal*, 28, 175-185.

Chatterjee, R. (2004). "Characterising stickiness of dairy powders," Master of Technology in Bioprocess Engineering, Massey University, Palmerston North.

Chen, X. D., Rennie, P. R., and Mackereth, A. R. (2004). "Combined influences of humidity and temperature upon the inter-particle stickiness of a whole milk powder." *International Journal of Food Properties*, 7(3), 499-509.

Chuy, L. E., and Labuza, T. P. (1994). "Caking and stickiness of dairy-based food powders as related to glass transition." *Journal of Food Science*, 59(1), 43-46.

CODEX. (1999). "Milk powders and cream powder." Codex Alimentarius Commission, Rome.

Crofskey, C. M. (2000). "Investigation into the caking problems associated with spray dried cream powders 55 and 77." Massey University, Palmerston North, NZ.

Department of Material Science and Engineering Cornell University. (2006). *Cornell University* [online]. Available from: http://www.mse.cornell.edu/courses/engril11/modulus.htm. [Accessed 15 January 2006].

Derksen, J. J. (2003). "Separation performance predictions of a stairmand high-efficiency cyclone." *AIChE Journal*, 49(6), 1359-1371.

Derksen, J. J., and Van den Akker, H. E. A. (2000). "Simulation of vortex core precession in a reverse-flow cyclone." *AIChE Journal*, 46(7), 1317-1331.

Downton, G. E., Flores-Luna, J. L., and King, C. J. (1982). "Mechanism of stickiness in hygroscopic, amorphous powders." *Industrial and Engineering Chemistry Fundamentals*, 21, 447-451.

Early, R. (1998). "The technology of dairy products." Blackie Academic & Professional, London, UK, 436.

Engineering Statistics Handbook. (2005). *NIST SE MATECH* [online]. Available from: http:// www.itl.nist.gov/div898/handbook/eda/section3/eda3672.htm. [Accessed 15 January 2006].

Faldt, P., and Bergenstahl, B. (1994). "The surface composition of spray-dried protein-lactose powders." *Colloids and Surfaces A: Biointerfaces*, 90, 183-190.

Faldt, P., and Bergenstahl, B. (1996a). "Changes in surface composition of spray-dried food powders due to lactose crystallisation." *Lebensmittel-Wissenschaft und - Technologie*, 29, 438-446.

Faldt, P., and Bergenstahl, B. (1996b). "Spray-dried whey protein/lactose/soybean oil emulsions. 1. Surface composition and particle structure." *Food Hydrocolloids*, 10(4), 421-429.

Faldt, P., and Bergenstahl, B. (1996c). "Spray-dried whey protein/lactose/soybean oil emulsions. 2. Redispersability, wettability and particle structure." *Food Hydrocolloids*, 10(4), 431-439.

Faldt, P., and Sjoholm, I. (1996). "Characterisation of spray-dried whole milk." *Milchwissenschaft*, 51(2), 88-92.

Fitzpatrick, J. J., Iqbal, T., Delaney, C., Twomey, T., and Keogh, M. K. (2004). "Effect of powder properties and storage conditions on the flowability of milk powders with different fat contents." *Journal of Food Engineering*, 64, 435-444.

Foster, K. D. (2002). "The prediction of sticking in dairy powders," Doctor of Philosophy in Bioprocess Engineering, Massey University, Palmerston North.

Foster, K. D., Bronlund, J. E., and Paterson, A. H. J. (2005). "The contribution of milk fat towards the caking of dairy powders." *International Dairy Journal*, 15, 85-91.

Fox, P. F. (1995). "Heat-induced changes in milk." International Dairy Federation, Brussells, Belgium, 447.

Fox, P. F. (1997). "Advanced dairy chemistry." Chapman & Hall, London, UK, 519.

Fox, P. F., and McSweeney, P. L. H. (1998). *Dairy chemistry and biochemistry*, Thomson Science, London, UK.

Fox, P. F., and McSweeney, P. L. H. (2003). "Advanced dairy chemistry." Kluwer Academic / Plenum Publishers, New York, USA, 605-1318.

Hancock, B. C., and Dalton, C. R. (1999). "The effect of temperature on water vapour sorption by some amorphous pharmaceutical sugars." *Pharmaceutical Development and Technology*, 4(1), 125-131.

Hardham, J. F. (1998). "Effect of protein standardisation of milk by addition of UF milk permeate of the composition and storage stability of UHT processed milk." *The Australian Journal of Dairy Technology*, 53, 22-27.

Harper, W. J. (1992). "Lactose and lactose derivatives." Whey and lactose processing, J. G. Zadow, ed., Elsevier Science Publishers Ltd, New York, USA, 317-360.

Hennigs, C., Kockel, T. K., and Langrish, T. A. G. (2001). "New measurements of the sticky behaviour of skim milk powder." *Drying Technology*, 19(3&4), 471-484.

Hermansson, A.-M., Langton, M., and Loren, N. (2000). "New approaches to characterising food microstructures." *MRS bulletin*(December).

Hoppmann, W. H. (1995). "Effect of impact on structures." Shock and Vibration Handbook, C. M. Harris, ed., McGraw-Hill, USA, 9.3-9.13.

Johnson, K. L. (1985). *Contact Mechanics*, Cambridge University Press, Cambridge, Great Britain.

Jouppila, K., and Roos, Y. H. (1994a). "Water sorption and time-dependent phenomena of milk powders." *Journal of Dairy Science*, 77, 1798-1808.

Jouppila, K., and Roos, Y. H. (1994b). "Glass transitions and crystallization in milk powders." *Journal of Dairy Science*, 77, 2907-2915.

Kachrimanis, K., and Malamataris, S. (2004). ""Apparent" Young's elastic modulus and radial recovery for some tableted pharmaceutical excipients." *European Journal of Pharmaceutical Sciences*, 21, 197-207.

Kantak, A. A., and Davis, R. H. (2005). "Collisions of spheres with wet and dry porous layers on a solid wall." *Chemical Engineering Science*, 61, 417-427.

Kemp, I. C., Frankum, D. P., Abrahamson, J., and Saruchera, T. "Solids residence time and drying in cyclones." *11th International Drying Symposium*, Halkidiki, Greece, 581-588.

Kern, D. Q. (1950). *Process Heat Transfer*, McGraw-Hill Book Company, Inc., New York.

Kieviet, F. G., van Raaij, J., de Moor, P. P. E. A., and Kerkhof, P. J. A. M. (1997). "Measurement and modelling of the air flow pattern in a pilot-plant spray dryer." *Chemical Engineering Research and Design*, 75(A3), 321-328.

Kim, E. H.-J., Chen, X. D., and Pearce, D. (2002). "Surface characterization of four industrial spray-dried dairy powders in relation to chemical composition, structure and wetting property." *Colloids and Surfaces B: Biointerfaces*, 26, 197-212.

Kim, E. H.-J., Chen, X. D., and Pearce, D. (2003). "On the mechanisms of surface formation and the surface compositions of industrial milk powders." *Drying Technology*, 21(2), 265-278.

Kim, E. H.-J., Chen, X. D., and Pearce, D. (2005). "Melting characteristics of fat present on the surface of industrial spray-dried dairy powders." *Colloids and Surfaces B: Biointerfaces*, 42, 1-8.

Lazar, M. E., Brown, A. H., Smith, G. S., Wong, F. F., and Lindquist, F. E. (1956). "Experimental production of tomato powder by spray drying." *Food Technology*, 10, 129-137.

Leclercq-Perlat, M.-N., and Lalande, M. (1994). "Cleanability in relation to surface chemical composition and surface finishing of some materials commonly used in food industries." *Journal of Food Engineering*, 23, 501-517.

Lockemann, C. A. (1999). "A new laboratory method to characterise the sticking properties of free-flowing solids." *Chemical Engineering and Processing*, 38, 301-306.

Masters, K. (1991). *Spray drying handbook*, Longman Scientific & Technical, Singapore.

Matweb Team. (2006). *Matweb Team* [online]. Accessed from: http://www.matweb.com/search/specificmaterial.asp?bassnum=ms0001&n=1. [Accessed 15 January 2006].

McKenna. (1997). "Examination of whole milk powder by confocal laser scanning microscopy." *Journal of Dairy Research*, 64, 423-432.

McLeod, J. (2002). "Lactose smearing in transport lines," Masters in Process Engineering, Massey University, Palmerston North.

Michalski, M., Desobry, S., and Hardy, J. (1997). "Food materials adhesion: a review." *Critical Reviews in Food Science and Nutrition*, 37(7), 591-619.

Mistry, V. V., Hassan, H. N., and Robison, D. J. (1992). "Effect of lactose and protein on the microstructure of dried milk." *Food Structure*, 11, 73-82.

Morr, C. V. (1992). "Whey utilization." Whey and lactose processing, J. G. Zadow, ed., Elsevier Science Publishers Ltd, New York, USA, 133-156.

Newstead, D. F., Woodhams, D. J., Cook, W. R., and Conaghan, E. F. (1977). "The use of permeate from the ultrafiltration of whey for standardizing the protein concentration of recombined evaporated milk." *New Zealand Journal of Dairy Science and Technology*, 12, 146-151.

Nezbed, R. L. (1974). "Method of treating lactose." Kraftco Corporation, New York, USA.

O'Donnell, A. M., Bronlund, J. E., Brooks, G. F., and Paterson, A. H. J. (2002). "A constant humidity air supply system for pilot scale applications." *International Journal of Food Science and Technology*, 37, 369-374.

Ozkan, N., Walisinghe, N., and Chen, X. D. (2002). "Characterization of stickiness and cake formation in whole and skim milk powders." *Journal of Food Engineering*, 55, 293-303.

Ozmen, L., and Langrish, T. A. G. (2002). "Comparison of glass transition temperature and sticky point temperature for skim milk powder." *Drying Technology*, 20(6), 1177-1192.

Ozmen, L., and Langrish, T. A. G. (2003). "An experimental investigation of the wall deposition of milk powder in a pilot-scale spray dryer." *Drying Technology*, 21(7), 1253-1272.

Palsey, H., Haloulos, P., and Ledig, S. (1995). "Stickiness - a comparison of test methods and characterisation parameters." *Drying Technology*, 13(5-7), 1587-1601.

Palzer, S. (2005). "The effect of glass transition on the desired and undesired agglomeration of amorphous food powders." *Chemical Engineering Science*, 60, 3959-3968.

Papadakis, S. E., and Bahu, R. E. (1992). "The sticky issues of drying." *Drying Technology*, 10(4), 817-837.

Paterson, A. H., Bronlund, J. E., Zuo, J. Y., and Chatterjee, R. (2006). "Analysis of particle gun derived dairy powder stickiness curves." *International Dairy Journal*, as submitted.

Paterson, A. H. J., Brooks, G. E., and Bronlund, J. E. "The blow test for measuring the stickiness of powders." *Conference of Food Engineering, AICHE Conference*, Reno, Nevada, USA.

Paterson, A. H. J., Brooks, G. F., Bronlund, J. E., and Foster, K. D. (2005). "Development of stickiness in amorphous lactose at constant T-T_g levels." *International Dairy Journal*, 15(5), 513-519.

Peleg, M. (1993). "Glass transitions and the physical stability of food powders." The glassy state in foods, J. M. V. Blanshard and P. J. Lillford, eds., Nottingham University Press, Nottingham, 435-453.

Perry, R. H., and Green, D. W. (1997). *Perry's Chemical Engineers' Handbook*, McGraw-Hill, USA.

Pocius, A. V. (2002). *Adhesion and Adhesives Technology*, Hanser Gardner Publications, Cincinnati, OH.

Ramakrishna, B. L. (2006). *The INVSEE Project* [online]. Available from: http://www.invsee.eas.asu.edu/nmodules/engmod/propym.html. [Accessed 15 January 2006].

Rennie, P. R., Chen, X. D., Hargreaves, J. B., and Mackereth, A. R. (1999). "A study of the cohesion of dairy powders." *Journal of Food Engineering*, 39, 277-284.

Roginski, H., Fuquay, J., and Fox, P. (2003). "Encyclopaedia of dairy sciences." Academic Press, Amsterdam, New York, 2500.

Roos, Y., and Karel, M. (1991b). "Phase transitions of mixtures of amorphous polysaccharides and sugars." *Biotechnology Progress*, 7, 49-53.

Roos, Y., and Karel, M. (1991c). "Plasticising effect of water on thermal behaviour and crystallisation of amorphous food models." *Journal of Food Science*, 56(1), 38-43.

Roos, Y., and Karel, M. (1993). "Effects of glass transitions on dynamic phenomena in sugar containing food systems." The glassy state in foods, J. M. V. Blanshard and P. J. Lillford, eds., Nottingham University Press, Nottingham, 207-223.

Roos, Y., Karel, M., and Kokini, J. L. (1996). "Glass transitions in low moisture and frozen foods: effects on shelf life and quality." *Food Technology*, 50(11), 95-108.

Russ, J. C. (2005). *Image analysis of food microstructure*, CRC Press, Florida, USA.

Sanderson. (1991). "Opportunities for whey and permeate powders." *Food Research Quarterly*, 51(1&2), 29-31.

Saruchera, T. (1999). "Measurement and modelling of particle residence time in a return flow cyclone," Doctor of Philosophy in Chemical Engineering, University of Canterbury, Christchurch.

Saruchera, T., and Abrahamson, J. "Residence time of granular particles through a cyclone - analysis using moments, laplace transform and least squares methods." *Chemeca*, Rotorua, New Zealand, 201-213.

Saruchera, T., and Abrahamson, J. "Granular particle flows in a cyclone-measurement of rope velocities and residence times." *9th APCChE Congress*, Christchurch, New Zealand.

Schuck, P., Blanchard, E., Dolivet, A., Mejean, S., Onillon, E., and Jeantet, R. (2005). "Water activity and glass transition in dairy ingredients." *Lait*, 85, 295-304.

Shalaby, H., Pachler, K., Wozniak, K., and Wozniak, G. (2005). "Comparative study of the continuous phase flow in a cyclone separator using different turbulence models." *International Journal for Numerical Methods in Fluids*, 48, 1175-1197.

Siegel, R. (2006). *Bionicsurfaces* [online]. Available from: http://www.bionicsurfaces.de/properties.htm. [Accessed 15 January 2006].

Sienkiewicz, T., and Riedel, C. (1990). "Whey and whey utilization." Possibilities for utilisation in agriculture and foodstuffs production, Berlag Th. Mann, Germany, 379.

Sinnott, R. K. (1985). *Chemical Engineering*, Pergamon Press, Oxford, New York.

Solero, G., and Coghe, A. (2002). "Experimental fluid dynamic characterisation of a cyclone chamber." *Experimental Thermal and Fluid Science*, 27, 87-96.

Teunou, E., and Fitzpatrick, J. J. (1999). "Effect of relative humidity and temperature on food powder flowability." *Journal of Food Engineering*, 42, 109-116.

Teunou, E., Fitzpatrick, J. J., and Synnott, E. C. (1999). "Characterisation of food powder flowability." *Journal of Food Engineering*, 39, 31-37.

Wikipedia. (2006). *Wikimedia Foundation Inc* [online]. Available from: http://en.wikipedia.org/wiki/mild_steel. [Accessed 15 January 2006].

Winter, M. (2005). *Web elements* [online]. Available from: http://www.webelements.com [Accessed 15 January 2006].

Xu, C., and Zhu, J. (2005). "Experimental and theoretical study on the agglomeration arising from fluidisation of cohesive particles - effects of mechanical vibration." *Chemical Engineering Science*, 60, 6529-6541.

Zall, R. R. (1992). "Sources and composition of whey and permeate." Whey and lactose processing, J. G. Zadow, ed., Elsevier Science Publishers Ltd, New York, USA, 1-72.

Zhao, J. Q., and Abrahamson, J. (1999) "The flow in conical cyclones." *Second International Conference on CFD in the Minerals and Process Industries*, Melbourne, Australia, 497-502.

Zuo, J. Y. (2004). "The stickiness curves of dairy powder." Master of Technology in Bioprocess Engineering, Massey University, Palmerston North.

Zuo, J. Y., Paterson, A. H., Bronlund, J. E., and Chatterjee, R. (2006). "Using the particle gun technique to measure instantaneous stickiness of dairy powders." *International Dairy Journal*, in press.

APPENDIX 1 - RH PROBE CALIBRATION CURVES

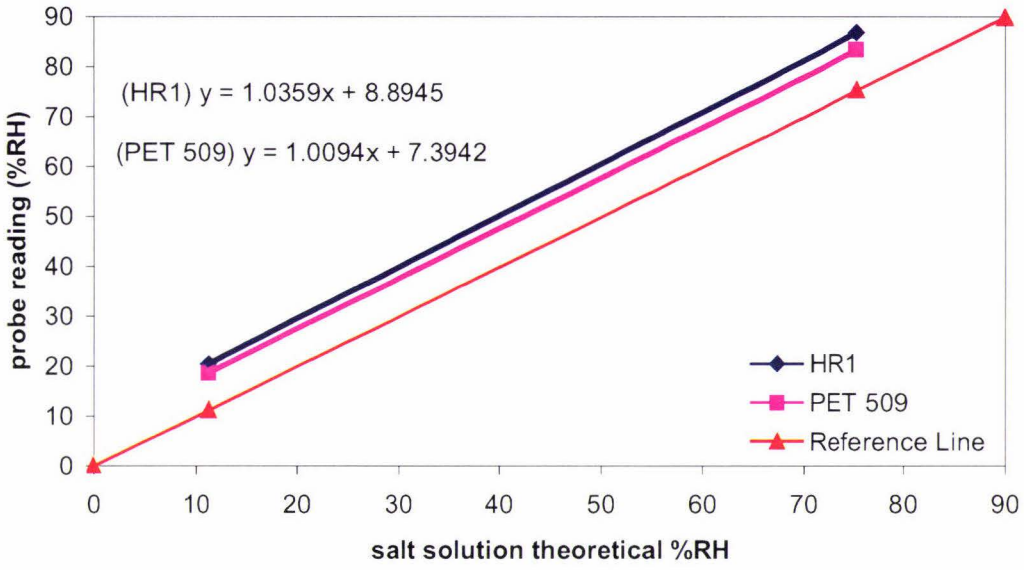

Figure A1-1. HR1 and PET 509 probe calibrations using salt solutions LiCl (11.3%RH) and NaCl (75.4%RH) April 2005.

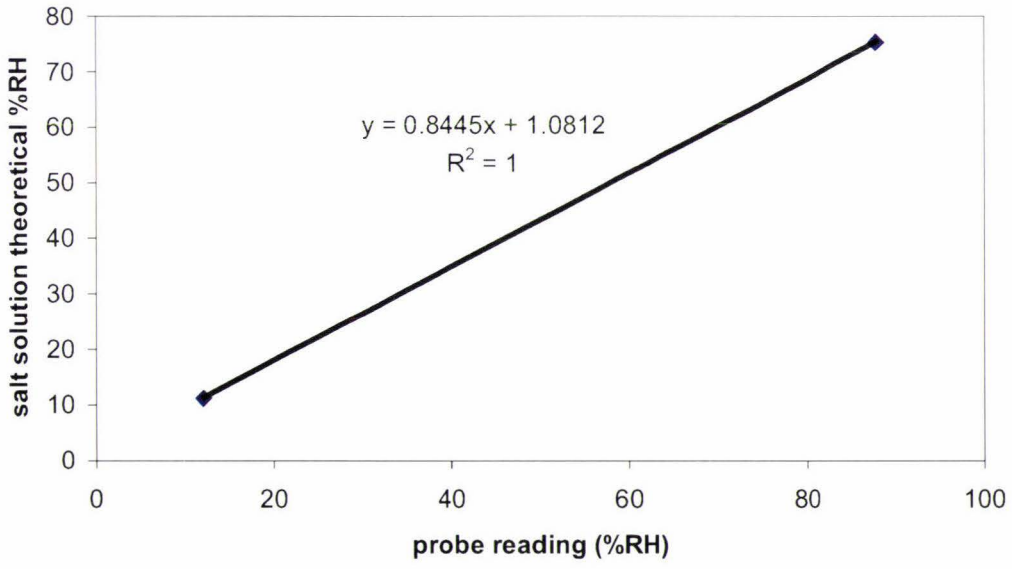

Figure A1-2. HR1 recalibration August 2005 using salt solutions LiCl (11.3%RH) and NaCl (75.4%RH).

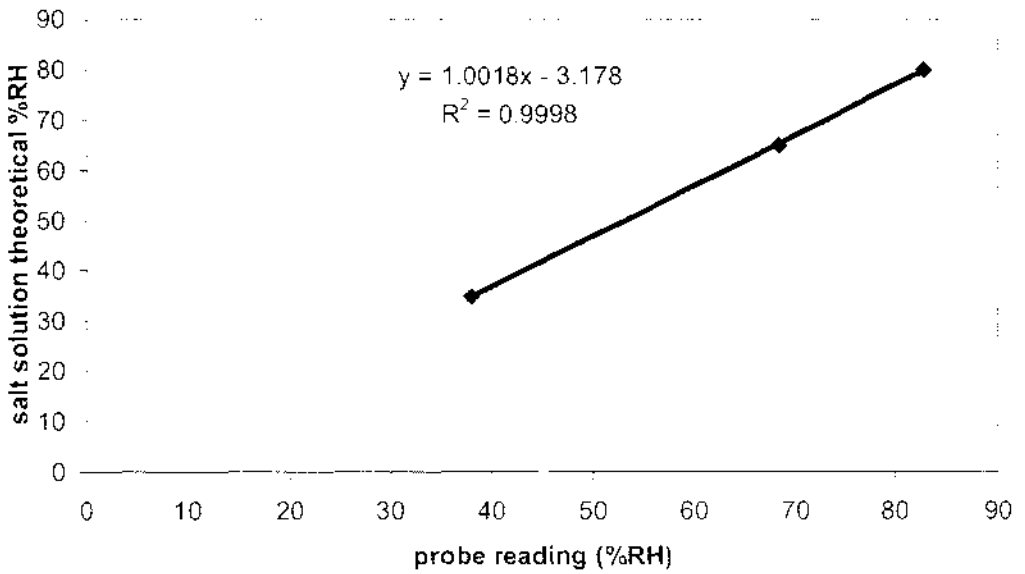

Figure A1-3. Hygrocal RH probe calibrations using Rotronic Ag chemical standards 35%, 65% and 80%, May 2005.

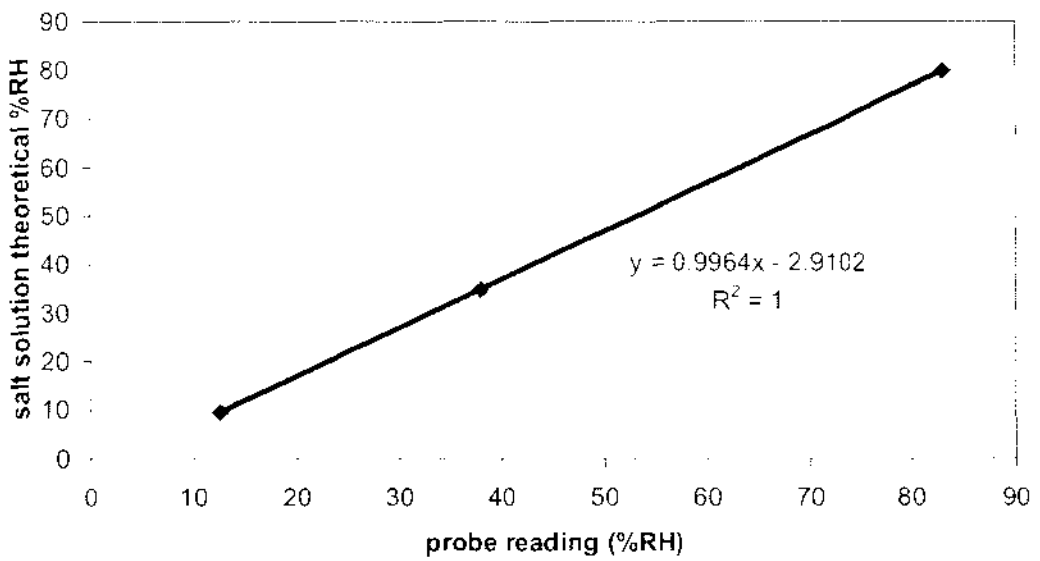

Figure A1-4. Fluid bed RH probe calibrations using Rotronic Ag chemical standards 80%, 65% and 10%, June 2005.

APPENDIX 2 - SKIM & WHOLE MILK POWDERS

Table A2-1. SMP production conditions

Protein (%wt)	Standardisation	*Spray drying conditions*	
		main chamber exhaust air temperature (°C)	SFB inlet temperature (°C)
37	Lactose solution	92	85
37	Milk permeate	92	85
52	NA	89	86

Table A2-2. WMP production conditions

Protein (%wt)	Standardisation	*Spray drying conditions*	
		main chamber exhaust air temperature (°C)	SFB inlet temperature (°C)
27	Lactose solution	76	70
33	Milk permeate	76	70
33	NA	79	70

Table A2-3. Bulk composition for SMP standardised by lactose solution and milk permeate.

	Relative bulk mass (%wt)		
	Unstandardised	Lactose standardised	Permeate standardised
Lactose	51.5	58.9	58.8
Protein	44.6	36.6	37.2
Fat	0.5	0.5	0.5
Minerals	3.9	4.5	4.0

Table A2-4. Bulk composition for WMP standardised by lactose solution and milk permeate.

	Relative bulk mass (%wt)		
	Unstandardised	Lactose standardised	Permeate standardised
Lactose	39.1	45.4	43.8
Protein	33.3	27.2	33.4
Fat	25.8	26.3	25.9
Minerals	1.8	1.1	0

APPENDIX 3 - COMMERCIAL POWDERS

Table A3-1. Additional SMP obtained from Fonterra Te Rapa, Hamilton.

Powder	Protein level	Standardisation	Spec	Code
SMP	32-33%	permeate	20-0157	FP24, unit L4800-L4850
SMP	32-33%	lactose	20-0157	FP24, unit L4870-L4930
SMP	32-33%	permeate	20-0157	GP25, unit L8120-L8150
SMP	32-33%	permeate	20-0157	GP25, unit L8165-L8190
SMP	32-33%	lactose	20-0157	GP25, unit L8210-L8270

Table A3-2. Additional SMP obtained from Waitoa, Hamilton.

Powder	Protein level	Standardisation	Spec	Code
SMP	32-33%	permeate	20-0160	GP15, unit D8457
SMP	32-33%	lactose	20-0160	GP15, unit D8456
SMP	34-35%	permeate	20-0160	GP14, unit D8455
SMP	34-35%	lactose	20-0160	GP14, unit D8454

APPENDIX 4 - ADDITIONAL PARTICLE GUN RESULTS

A. Factorial results

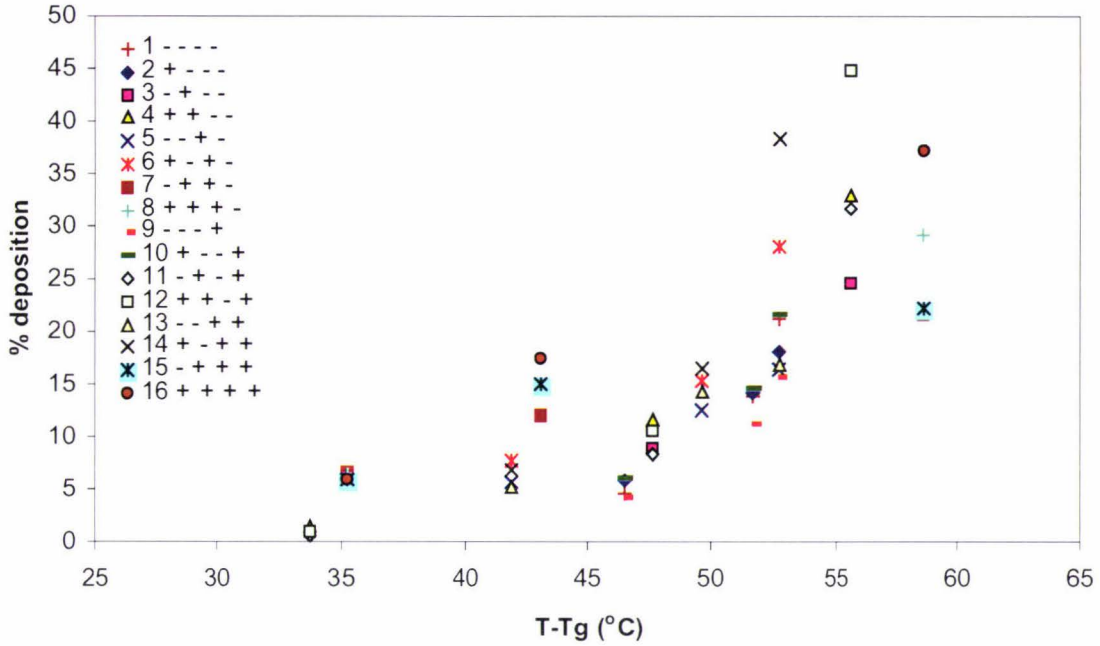

Figure A4-1. 2^4 factorial results using unstandardised SMP. Factors listed in order of A, B, C, D. A refers to initial powder a_w, B to ambient temperature, C to ambient air RH and D to powder feed rate.

B. Particle gun powder feed rate results

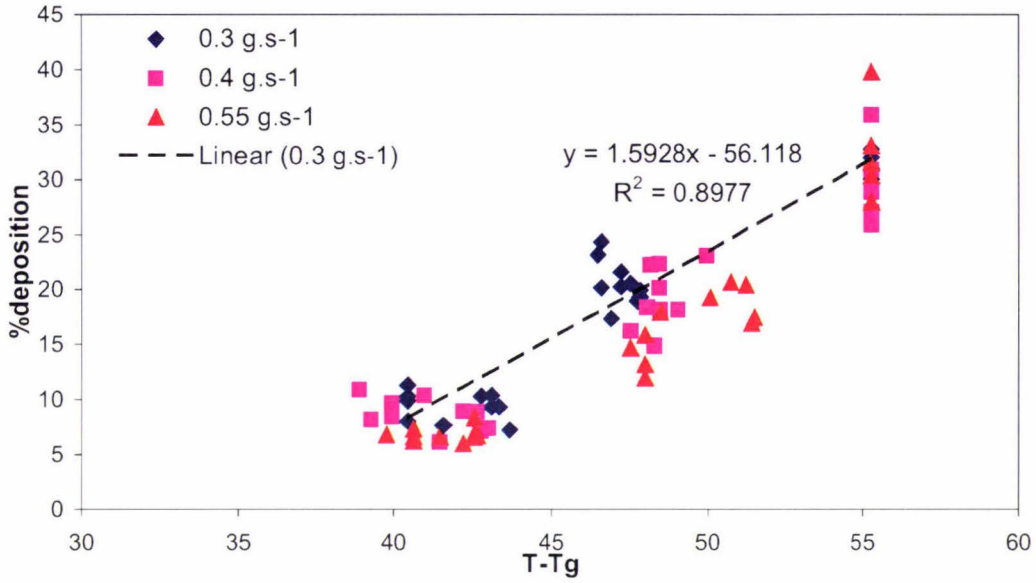

Figure A4-2. Effect of SMP feed rate on T–Tg results from the particle gun rig.

Table A4-1. Results from SMP feed rate trials on the particle gun.

Feed rate $g.s^{-1}$	T-Tg °C	%deposition %	Stdev	%error	Average Stdev
0.30	40.69	9.52	1.54	16.15	1.47
	47.53	19.51	1.54	7.90	
	46.91	21.77	1.91	8.77	
	43.21	9.38	1.27	13.55	
	55.31	31.37	1.10	3.50	
0.40	39.82	9.59	1.17	12.23	1.98
	48.34	16.52	1.66	10.04	
	48.63	21.32	1.92	8.99	
	42.42	7.77	1.22	15.66	
	55.31	29.75	3.94	13.24	
0.55	40.64	6.76	0.40	5.85	1.95
	48.01	14.74	2.35	15.95	
	51.03	18.99	1.69	8.91	
	42.49	6.93	0.87	12.52	
	55.31	32.56	4.46	13.69	

C. Particle gun plate height results

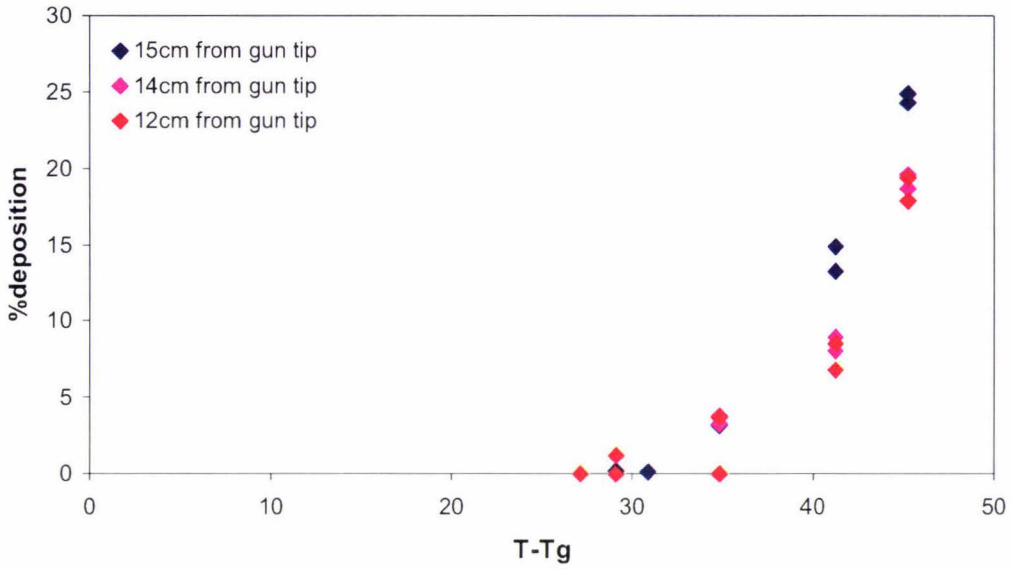

Figure A4-3. Effect of particle gun plate height on T–Tg at 20 m.s^{-1}, 90° angle of impact, unstandardised SMP.

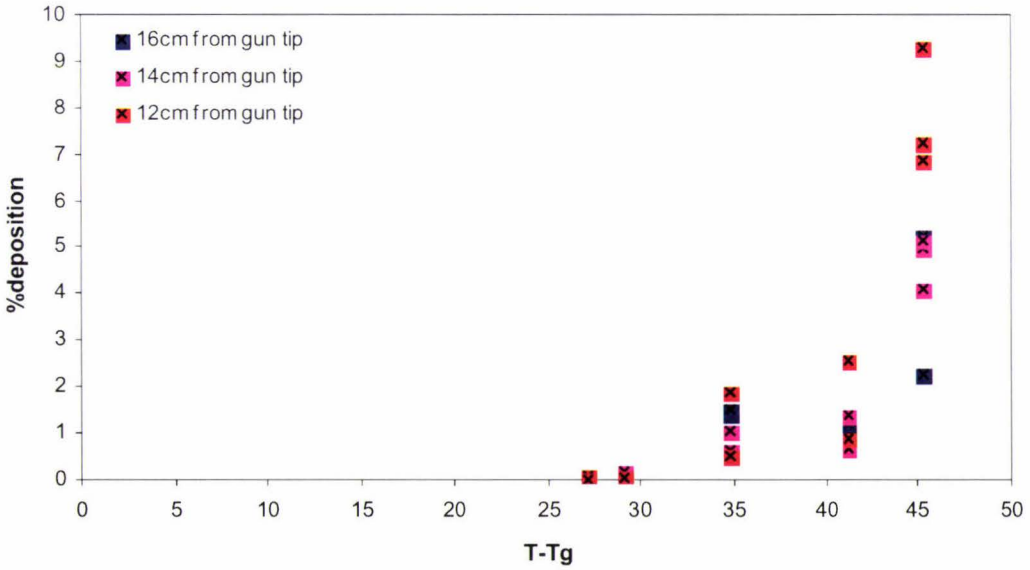

Figure A4-4. Effect of particle gun plate height on T–Tg at 20 m.s^{-1}, 29° angle of impact, unstandardised SMP.

D. Particle gun results from ambient air condition and initial powder water activity trials.

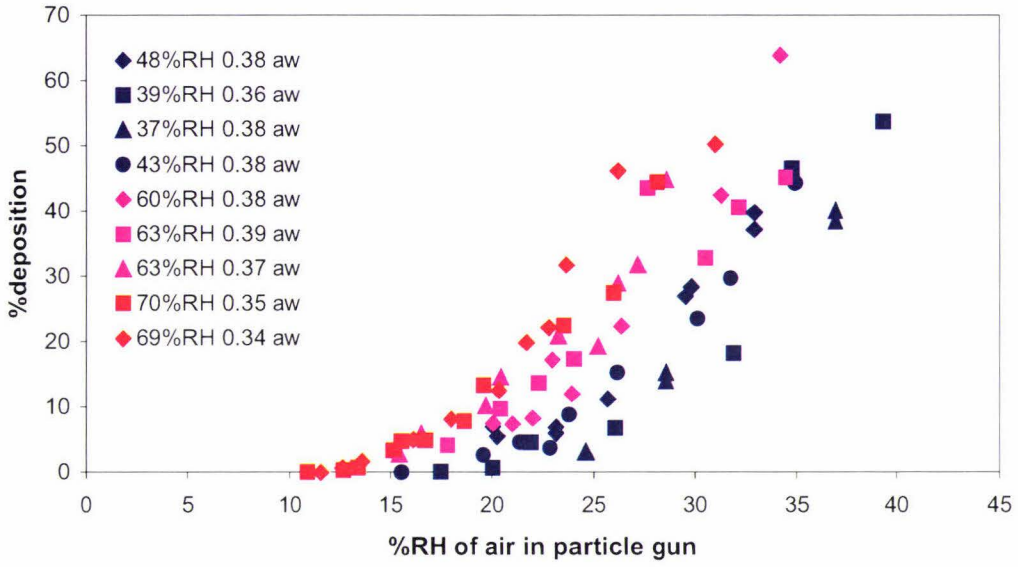

Figure A4-5. Particle gun results showing the effect of initial powder water activity and ambient air conditions using unstandardised SMP at 20 $m.s^{-1}$.

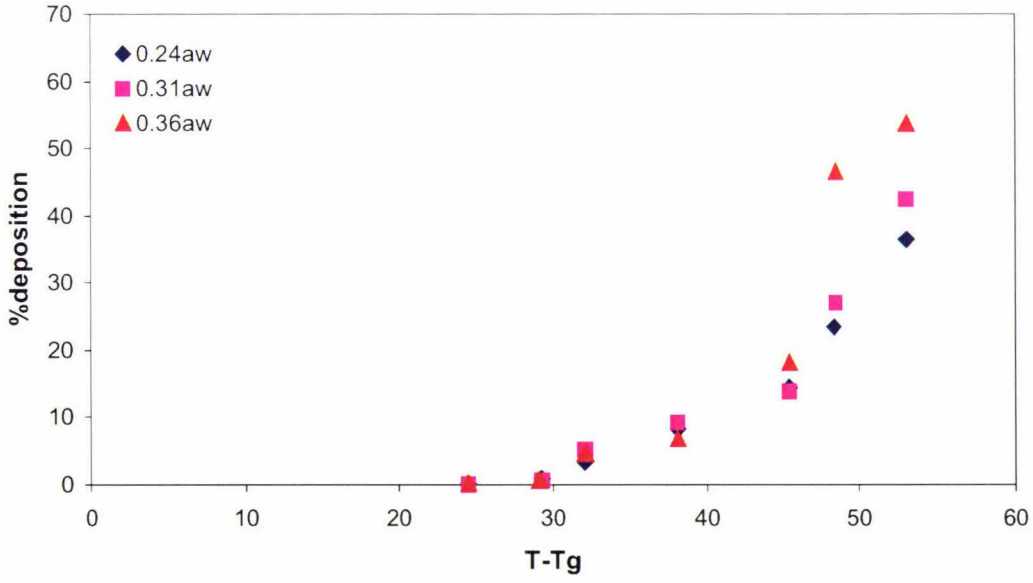

Figure A4-6. Particle gun results showing the effect of initial powder water activity at ambient air 39 ± 3%RH and 24°C on T–Tg using unstandardised SMP at 20 $m.s^{-1}$.

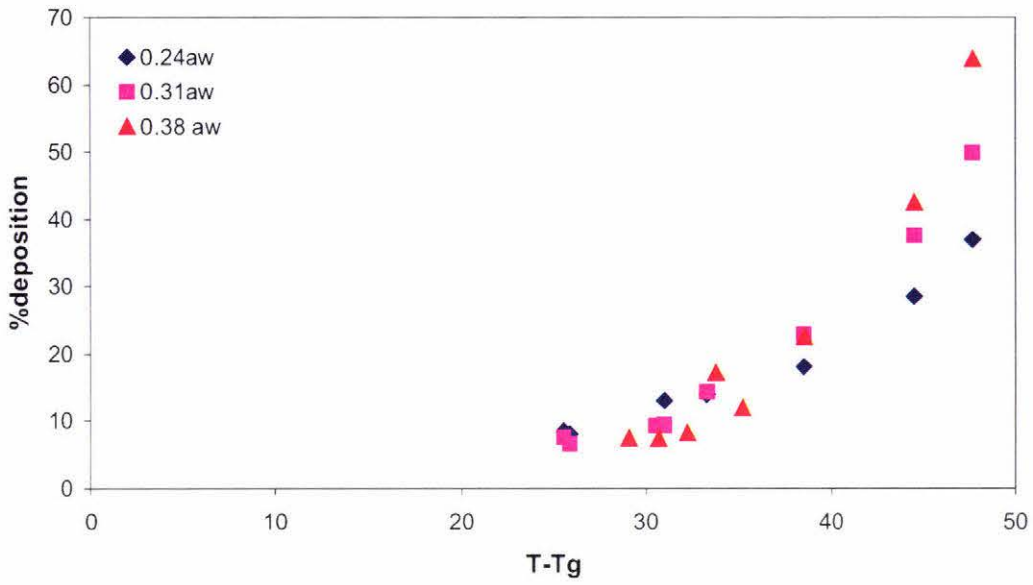

Figure A4-7. Particle gun results showing the effect of initial powder water activity at ambient air 60 ± 2%RH and 15.5°C on T–Tg using unstandardised SMP at 20 m.s^{-1}.

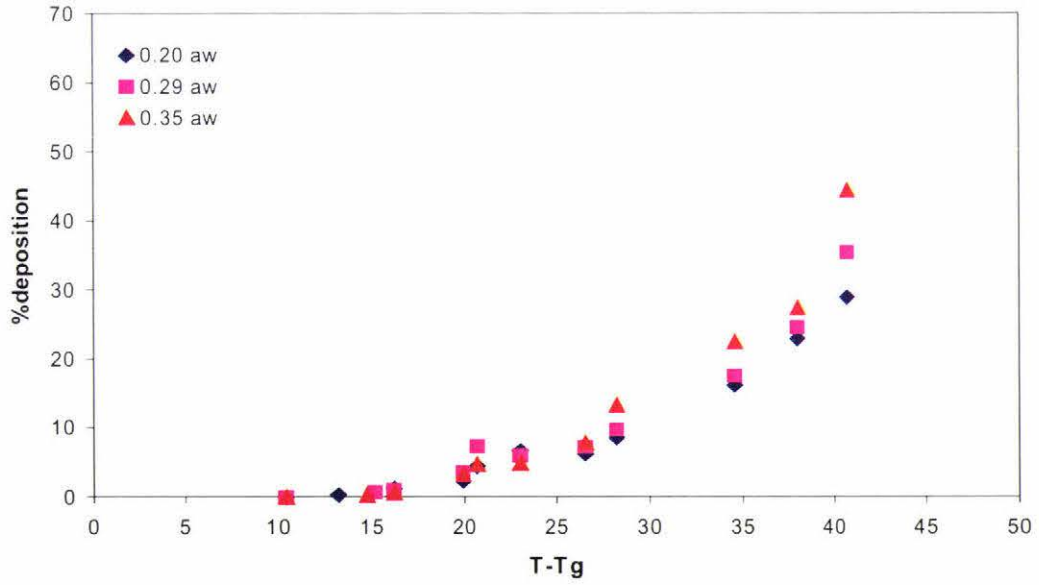

Figure A4-8. Particle gun results showing the effect of initial powder water activity at ambient air 70 ± 2%RH and 20°C on T–Tg using unstandardised SMP at 20 m.s^{-1}.

E. Effect of impact force on particle gun results

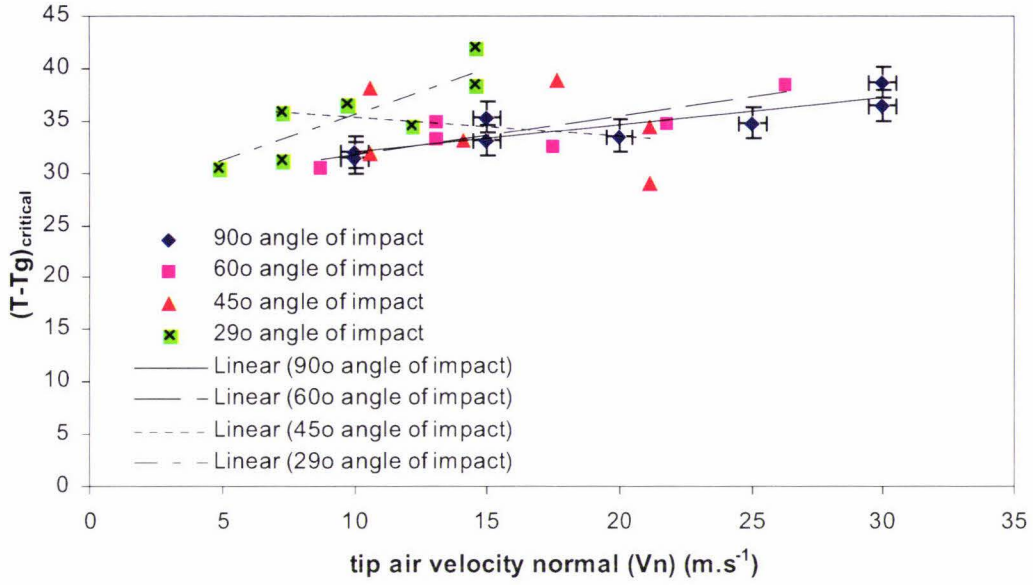

Figure A4-9. Angle of impact and air velocity converted to normal force versus $(T-Tg)_{critical}$.

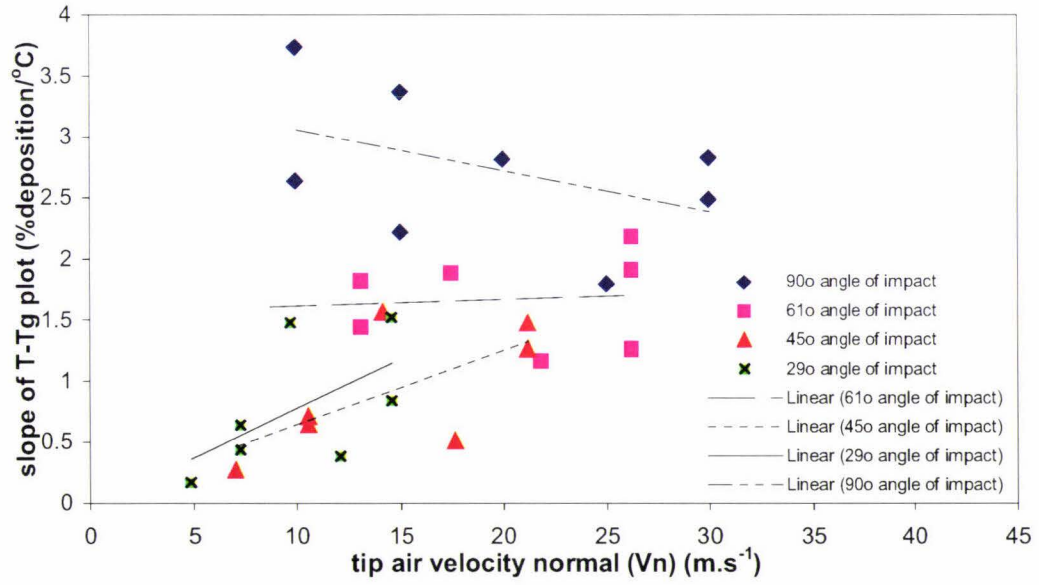

Figure A4-10. Angle of impact and air velocity converted to normal force versus rate of powder deposition.

APPENDIX 5 - CALCULATIONS

A. Air drawn into particle gun barrel due to venturi effects

Subscript 1 refers to air travelling into the particle gun barrel from the humidification column and the inline air heater. Subscript 2 refers to the ambient conditions in the room and the air being drawn into the top of the particle gun through the powder feeding funnel. Subscript 3 refers to the conditions at the particle gun barrel outlet.

a. Calculations

```
m1*cp1*T1+m2*cp2*T2=m3*cp3*T3+HL
HL=m1*cp1*T1-m3closed*cp3closed*T3closed

T1=88
T2=25
T3=78
T3closed=80
RH1=RELHUM(AirH2O,T=T1,P=Pr,w=w3closed)

RH2=0.44
RH3=0.17
RH3closed=0.165
Pr=110
Pr2=101.3
Pr3=101.3

r2=0.003
r3=0.0065
V3=21
V3closed=20
m3closed=p3closed*V3closed*pi*r3^2
m3=p3*V3*pi*r3^2
m2=p2*V2*pi*r2^2
V2=m2/pi/r2^2/p2

cp1=CP(AirH2O,T=T1,P=Pr,R=RH1)
cp2=CP(AirH2O,T=T2,P=Pr2,R=RH2)
cp3=CP(AirH2O,T=T3,P=Pr3,R=RH3)
cp3closed=CP(AirH2O,T=T3closed, P=Pr3,R=RH3closed)

p2=DENSITY(AirH2O,T=T2,P=Pr2,w=w2)
p3=DENSITY(AirH2O,T=T3,P=Pr3,w=w3)
p3closed=DENSITY(AirH2O,T=T3closed,P=Pr3,w=w3closed)

w2=HUMRAT(AirH2O,T=T2,P=Pr2,R=RH2)
w3=HUMRAT(AirH2O,T=T3,P=Pr3,R=RH3)
w3closed=HUMRAT(AirH2O,T=T3closed,P=Pr3,R=RH3closed)

percentairthrufunnelmassflow=m2/m3*100
percentairthrufunnelvelocity=V2/V3*100
```

b. Solutions

cp1=1094 [J/kg-K]
cp2=1023 [J/kg-K]
cp3=1091 [J/kg-K]
cp3closed=1096 [J/kg-K]
HL=8.721E+09 [J/s]
m1=90579 [kg/s]
m2=0.000006962 [kg/s]
m3=0.002595 [kg/s]
m3closed=0.002447 [kg/s]
p2=1.167 [kg/m^3]
p3=0.9311 [kg/m^3]
p3closed=0.9219 [kg/m^3]
percentairthrufunnelmassflow=0.2682 [-]
percentairthrufunnelvelocity=1.004 [-]
Pr=110 [kPa]
Pr2=101.3 [kPa]
Pr3=101.3 [kPa]
r2=0.003 [m]
r3=0.0065 [m]
RH1=0.1306 [-]
RH2=0.44
RH3=0.17
RH3closed=0.165
T1=88 [C]
T2=25 [C]
T3=78 [C]
T3closed=80 [C]
V2=0.2109 [m/s]
V3=21 [m/s]
V3closed=20 [m/s]
w2=0.008716 [-]
w3=0.04939 [-]
w3closed=0.05223 [-]

B. RH change in particle gun barrel due to powder particle flow

Initial powder a_w taken as 0.2 a_w. Initial air humidity entering particle gun barrel taken as 30%RH.

a. Calculations

mfp=0.3/1000	mass flow of particles
mfa=20*area*densitya	mass flow of air through particle gun barrel
densitya=0.995	density of air at 78°C
area=3.1416*daim^2/4	cross sectional area of particle gun barrel
daim=8*10^(-3)	inside diameter of particle gun barrel
c1=mfp/mfa	ratio of mass flow rates
mp=4*pi*(4.14*1e-5)^3/3/densityp	mass of particle
densityp=1.14e3 [kg/m^3]	density of particle
ap=mp/c1	air with particle
waterinair=Hi*mp/c1	water in air entering barrel
Hi=0.094	absolute humidity of air entering barrel
wa=(M_e-M_i)*mp*0.036	water in air associated with particle
M_i=0.0529	moisture content of particle initially
M_e=0.061	moisture content of particle exiting barrel

waterairout=waterinair-wa water in air exiting barrel
wmax=Hi/0.3*ap maximum water in air
RHout=waterairout/wmax*100 RH of air exiting barrel

b. **Solutions**

ap=8.693E-16 [-]
area=0.00005027 [m^2]
c1=0.2999 [-]
daim=0.008 [m]
densitya=0.995 [kg/m^3]
densityp=1140 [kg/m^3]
Hi=0.094
M_e=0.061
M_i=0.0529
mfa=0.001 [-]
mfp=0.0003
mp=2.607E-16
RHout=29.97 [%RH] insignificant change from 30%RH air
wa=7.697E-20 [kg/kg]
waterairout=8.164E-17 [kg/kg]
waterinair=8.172E-17 [kg/kg]
wmax=2.724E-16 [-]

C. Temperature, pressure and RH changes in cyclone air in response to centre vortex

a. Equations

RH=RELHUM(AirH2O,T=T1,P=P1,w=w1) RH of air entering cyclone
T1=85 temperature of air entering (T1)
P1=102 pressure of air entering
w1=0.043 humidity ratio
RH2=RELHUM(AirH2O,T=T2,P=P2,w=w1) RH of air in centre vortex
P2=100 pressure in centre vortex
T2+273.15=(T1+273.15)*(P2/P1)^0.228 temperature in centre vortex (T2)
Tg1=-530.66*RH^3+652.06*RH^2-366.33*RH+99.458
Tg2=-530.66*RH2^3+652.06*RH2^2-366.33*RH2+99.458
(T-Tg)1=T1-Tg1 T-Tg at inlet conditions
(T-Tg)2=T2-Tg2 T-Tg at centre vortex conditions

b. Solutions

(T-Tg)1=19.53 [C]
(T-Tg)2=19.12 [C]
P1=102 [kPa]
P2=100 [kPa]
RH=0.1136 [%RH]
RH2=0.1187 [%RH]
T1=85 [C]
T2=83.39 [C]
Tg1=65.47 [C]
Tg2=64.27 [C]
w1=0.043 [kg/kg]

D. RH and T–Tg calculations from D5 cyclone wall temperature

All temperatures are wall temperatures measured with eye button temperature probes ± 0.5°C.

a. Equations

T1=66.3 Sample point 1, cyclone inlet air (probe 1, un-insulated)
T2=68.8 Sample point 1, cyclone inlet air (probe 2, un-insulated)
T3=68.0 Sample point 2, top of cyclone (probe 3, insulated)
T4=66.1 Sample point 2, top of cyclone (probe 4, un-insulated)
T5=63.6 Sample point 3, bottom of cyclone (probe 5, insulated)
T6=52.3 Sample point 3, bottom of cyclone (probe 6, un-insulated)
T7=45.9 Sample point 4, bottom of cyclone (probe 7, un-insulated)
T8=43.7 Sample point 4, bottom of cyclone (probe 8, un-insulated)
Tc=78.6 temperature of air entering cyclone
RH=18.4/100 RH of air entering cyclone
P1=101 system pressure

h=HUMRAT(AirH2O,T=Tc,P=P1,R=RH) absolute humidity ratio for air entering
RH1=RELHUM(AirH2O,T=T1,P=P1,w=h)
RH2=RELHUM(AirH2O,T=T2,P=P1,w=h)
RH3=RELHUM(AirH2O,T=T3,P=P1,w=h)
RH4=RELHUM(AirH2O,T=T4,P=P1,w=h)
RH5=RELHUM(AirH2O,T=T5,P=P1,w=h)
RH6=RELHUM(AirH2O,T=T6,P=P1,w=h)
RH7=RELHUM(AirH2O,T=T7,P=P1,w=h)
RH8=RELHUM(AirH2O,T=T8,P=P1,w=h)

(T-Tg)1=T1-((-530.66*(RH1^3))+(652.06*(RH1^2))-(366.33*RH1)+99.458)
(T-Tg)2=T2-((-530.66*(RH2^3))+(652.06*(RH2^2))-(366.33*RH2)+99.458)
(T-Tg)3=T3-((-530.66*(RH3^3))+(652.06*(RH3^2))-(366.33*RH3)+99.458)
(T-Tg)4=T4-((-530.66*(RH4^3))+(652.06*(RH4^2))-(366.33*RH4)+99.458)
(T-Tg)5=T5-((-530.66*(RH5^3))+(652.06*(RH5^2))-(366.33*RH5)+99.458)
(T-Tg)6=T6-((-530.66*(RH6^3))+(652.06*(RH6^2))-(366.33*RH6)+99.458)
(T-Tg)7=T7-((-530.66*(RH7^3))+(652.06*(RH7^2))-(366.33*RH7)+99.458)
(T-Tg)8=T8-((-530.66*(RH8^3))+(652.06*(RH8^2))-(366.33*RH8)+99.458)

b. Solutions

h=0.05545 [kg/kg]
P1=101
RH=0.184
RH1=0.3106 [RH]
RH2=0.2782 [RH]
RH3=0.2881 [RH]
RH4=0.3133 [RH]
RH5=0.3504 [RH]
RH6=0.5957 [RH]
RH7=0.8199 [RH]
RH8=0.9183 [RH]
T1=66.3 [C]
T2=68.8 [C]
T3=68 [C]
T4=66.1 [C]
T5=63.6 [C]
T6=52.3 [C]

T7=45.9 [C]
T8=43.7 [C]
Tc=78.6 [C]
(T-Tg)1=33.62 [C] T-Tg of air at the wall temperature of the inlet to cyclone
(T-Tg)2=32.22 [C] T- Tg of air at the wall temperature of the inlet to cyclone
(T-Tg)3=32.65 [C] T-Tg of air at the wall temperature top of cyclone (insulated)
(T-Tg)4=33.73 [C] T-Tg of air at the wall temperature at top of cyclone
(T-Tg)5=35.28 [C] T-Tg of air at the wall temperature at bottom of cyclone (insulated)
(T-Tg)6=51.84 [C] T-Tg of air at the wall temperature bottom of cyclone
(T-Tg)7=101 [C] T-Tg of air at the wall temperature above rotary valve
(T-Tg)8=141.7 [C] T-Tg of air at the wall temperature above rotary valve

E. Heat transfer calculations for inside wall temperature estimations

Equations taken from Kern (1950), calculated in imperial units.

a. Equations

ha=(hr+hc) air heat transfer coefficient on the outside wall
Tamb=35*1.8+32 ambient room temperature outside dryer
Ts=Tamb+dT outside surface wall temperature
c1=0.173
hc=0.4*((dT)/do)^0.25 heat transfer coefficient estimate for long vertical pipe
T1=(460)+Ts
T2=(460)+Tamb
hr=c1*ε*(((T1/100)^4)-(T2/100)^4)/(T1-T2) heat transfer coefficient - radiation
Tsmeasured=65*1.8+32 temperature of wall top measured sample point 2
ε=0.8 assumed emissivity

Do=3266/25.4 /12 outside diameter of cyclone
Q/A=ha*(Ts-Tamb) Q/A, Ts=temperature of wall outer surface, Tamb=room temperature
Q/A=hi*(Tin-Tm) Q/A, Tin=temperature of air entering cyclone Tm=temperature of wall inner surface
Q/A=(λ/x)*(Tm-Ts) Q/A, Tm=temperature of wall inner surface, Ts=temperature of wall outer surface

jh=hi*Di/z*((Cp* μ /K)^(-1/3))*((μ /μw)^(-0.14)) estimate for hi based on long tube
Di=(3266/(25.4*12))-(2*z) inside diameter of cyclone
jh= 80 from (Kern 1950)
Re=Di*G/μ Reynolds number

sqft=pi*(Di/2)^2 cross sectional area of cyclone
G=m/sqft mass velocity
μ=VISCOSITY(AirH2O,T=Tin,P=P1,w=w1)
μw=u viscosity at the wall temperature
K=CONDUCTIVITY(AirH2O,T=Tin,P=P1,w=w1) thermal conductivity
z=3/25.4/12 wall thickness
λ=26
Tin=78.58*1.8+32 temperature of air entering cyclone
w1=HUMRAT(AirH2O,T=Tin,P=P1,R=RH1)
{back calculation check}
Q1=m*Cp*(Tin-Tout)
Qlosses=Q1 heat loss
Q1=Uo*A*deltaTtop

```
m=kgs*(1/0.4535924)*(60*60)
kgs=19.4*1000/(60*60)
Cp=CP(AirH2O,T=Tin,P=P1,R=RH1)
P1=29/2
RH1=0.184
Q/A=Q1/A                                heat flow/area
A=m2/0.092903                           surface area of cyclone ft^2
m2=m21+m22+m23+m24+m25+m26surface area of cyclone in m^2
surface area of cyclone calculated as a series of cylinders and truncated cones
m21=2*pi*1.899/2*(12365/1000-8396/1000-3200/1000-15/1000-473/1000)
m22=pi*(((3266/2/1000)*(1.633^2+(0.281*1.633/(1.633-0.9495))^2)^0.5)-
((1899/2/1000)*(0.9495^2+(0.281*1.633/(1.633-0.9495)-0.281)^2)^0.5))
m23=2*pi*3266/2000*3215/1000
m24=pi*(((3266/2/1000)*(1.633^2+(8.396*1.633/(1.633-0.228))^2)^0.5)-
((0.228)*(0.228^2+(8.396*1.633/(1.633-0.228)-8.396)^2)^0.5))
m25=2*pi*(456/2000)*(473+2072/1000)
m26=pi*(((0.228)*(0.228^2+(1.740*0.228/(0.228-0.152))^2)^0.5)-
((0.152)*(0.152^2+(1.740*0.228/(0.228-0.152)-1.740)^2)^0.5))

deltaTtop=(Tin-Tamb)        temperature difference at top of cyclone
Tsc=(Ts-32)/1.8             temperature of outside wall in °C
Tsmc=65                     temperature of outside wall measured °C
Tfluidchange=(Tin-Tout)/1.8 temperature change between air into/out of cyclone
                            °C
```

b.Solution

```
A=8321 [ft^2]
c1=0.173 [BTU/hr-ft^2-F]
cp=0.2632 [Btu/lb_m-R]
D=10.7 [ft]
deltaTtop=78.44 [F]
do=10.72 [ft]
dT=6.451 [F]
emi=0.8 [dimensionless]
G=476 [lb_m/(hr-ft^2)]
ha=1.315 [BTU/hr-ft^2-F]
hc=0.3523 [BTU/hr-ft^2-F]
hi=0.1179 [BTU/hr-ft^2-F]
hr=0.963 [BTU/hr-ft^2-F]
jh=80 [-]
k=0.01719 [Btu/hr-ft-R]
kgs=5.389 [kg-s]
lamda=26 [BTU/hr-ft-F]
m=42770 [lb_m/hr]
m2=773.1 [m^2]
m21=1.676 [m^2]
m22=5.996 [m^2]
m23=32.99 [m^2]
m24=49.77 [m^2]
m25=680.6 [m^2]
m26=2.079 [m^2]
P1=14.5
Q1=70608 [Btu/hr]
QA=8.485 [BTU/hr-ft^2]
Qlosses=70608 [Btu/hr]
Re=101248 [dimensionless]
```

RH1=0.184
sqft=89.85 [ft^2]
T1=561.5 [R]
T2=555 [R]
Tamb=95 [F]
Tfluidchange=3.484 [C]
Tin=173.4 [F]
Tm=101.5 [F]
Tout=167.2 [F]
Ts=101.5 [F]
Tsc=38.58 [C]
Tsmc=65 [C]
Tsmeasured=149 [F]
u=0.05029 [lb_m/ft-hr]
Uo=0.1082 [BTU/hr-ft^2-F]
u_w=0.05029 [lb_m/ft-hr]
w1=0.05601 [-]
x=0.009843 [ft]

F. Prediction of $(T-Tg)_{critical}$ using equation (5-1), Palzer (2005)

a. Using Hertzian theory equations

μ=1*10^12	viscosity at glass transition, Palzer (2005)
gc=1	universal constant
E1=1250000	Approximation for SMP from pre-gelatinised starch 1-1.5GPa, (Kachrimanis and Malamataris 2004)
E2=220000000	steel, McLeod (2002)
v1=0.5	for plastic material, McLeod (2002)
v2=0.28	for steel, McLeod (2002)
pair=DENSITY(Air,T=T1,P=P1)	
T1=78	typical temperature of dryer outlet
P1=101	atmospheric pressure (kPa)
q=pi*rg^2*V	volumetric air flow rate through particle gun
V=20	particle gun velocity
rg=0.004	radius of particle gun barrel
X/a=0.1	Palzer (2005)
γ=0.062	saturated lactose at 78 degrees Celsius, Bronlund (1997)
m=PD*(4/3*pi*(R^3))	particle mass
R=0.000041418	particle radius
PD=1140	particle density
a=R*2	particle diameter
C=-14.8	WLF constant for SMP, Foster (2002)
B=25.3	WLF constant for SMP, Foster (2002)
ep=0.15	coefficient of restitution for particle, assumed 0-clay, 1-steel

α=((15/16*(V1^2)*m*(((1-V1^2)/E1)+((1-V2^2)/E2)))^(2/5))*rp^(-1/5)
Hertzian constant, Hoppmann (1995)

T-Tg=(log10((t/z))*B)/(C-(log10(t/z)))

F_t=J/t impact force, Hoppmann (1995)

t= α /V time of impact force, Hoppmann (1995)

z=5*(a^2)*pi/(4*surften*a*pi+F_t*2)*mu*X/a*X/a
rearrangement from Palzer (2005) equation

J=m*V*(1+ep) momentum equation, Hoppmann (1995)

b. Using momentum equation for jet impact on a plate

μ=1*10^12 viscosity at glass transition, Palzer (2005)
gc=1 universal constant
E1=1250000 Approximation for SMP from pre-gelatinised starch 1-1.5GPa, (Kachrimanis and Malamataris 2004)
E2=220000000 steel, McLeod (2002)
v1=0.5 for plastic material, McLeod (2002)
v2=0.28 for steel, McLeod (2002)
pair=DENSITY(Air,T=T1,P=P1)
T1=78 typical temperature of dryer outlet
P1=101 kPa
q=pi*rg^2*V volumetric air flow rate through particle gun
V=20 particle gun velocity
rg=0.004 radius of particle gun barrel
X/a=0.1 Palzer (2005)
γ=0.062 saturated lactose at 78 degrees Celsius, Bronlund (1997)
m=PD*(4/3*pi*(R^3)) particle mass
R=0.000041418 particle radius
PD=1140 particle density
a=R*2 particle diameter
C=-14.8 WLF constant for SMP, Foster (2002)
B=25.3 WLF constant for SMP, Foster (2002)
ep=0.15 coefficient of restitution for particle, assumed 0-clay, 1-steel

α=((15/16*(v1^2)*m*(((1-v1^2)/E1)+((1-v2^2)/E2)))^(2/5))*R^(-1/5)
Hertzian constant
T-Tg=(log10((t/z))*B)/(C-(log10(t/z)))
F_t=pair*q*V/sin(θ)*gc impact force
t= /V time of impact force
z=5*(a^2)*pi/(4*γ*a*pi+F_t*2)*μ*X/a*X/a rearrangement from Palzer (2005)

Vroots=sqrt(Value) for momentum rearrangement of Palzer (2005) & F_t=pqV/sin(θ)
Value=α *4*γ *a*pi/(2*pair*(q/V)/(sin(θ)*α))
θ=90

Table A5-1. Prediction of $(T-Tg)_{critical}$ for the fluid bed rig using Hertzian theory equations for two contacting spheres. Note the equations used for force and the inclusion of collision theory calculations (Xu and Zhu 2005).

	Fluid bed (1)	*Fluid bed (2)*	
	Palzer (2005) universal C & B constants	Foster (2002) C & B constants for lactose	
t	Predicted $(T-Tg)_{critical}$		
1.09E-05	117.7	112.8	
0.1	45.3	31.6	
0.1	45.3	**30.9**	$F=mv^2.a^{-1}$
0.1	46.2	31.6	$F=kg.m.s^{-1}$
0.1		**31.6**	Xu and Zhu (2005)
Air Velocity	0.23 $m.s^{-1}$		

Table A5-2. Hertzian equations for force and time for a particle impacting against steel.

	Particle gun (1)	*Particle gun (2)*	
	Palzer (2005) universal C & B constants	Foster (2002) C & B constants for lactose	
t	Predicted $(T-Tg)_{critical}$		
9.51E-08	**99.3**	**86.5**	$F=pqV/g_c\sin\theta$
1.12E-07	85.2	69.2	$F=J.t^{-1}$
1.12E-07	86.5	70.7	$F=mv^2.a^{-1}$
Air Velocity 20 $m.s^{-1}$			

G. Algebraic manipulation of equation (5-1), Palzer (2005)

$$t=\left(\frac{5a^2\pi}{4\gamma a\pi+2F_1}\right)\eta_c\left(\frac{X}{a}\right)^2 10^{(\text{illegible})}$$

$$T-T_g=\frac{\log_{10}\left(\frac{t}{\tau}\right)B}{C-\log_{10}\left(\frac{t}{\tau}\right)}$$

$$T-T_g=\frac{B}{\left[\frac{C}{\log_{10}\left(\frac{t}{\tau}\right)}-1\right]}$$

let $\tau=\left(\frac{5a^2\pi}{4\gamma a\pi+2F_1}\right)\eta_c\left(\frac{X}{a}\right)^2$

and $F_1=\rho qV/g_c\sin\vartheta$

where $q=VA$. A=cross sectional area

and $t=\frac{\alpha}{V}$

with $\alpha=\left[\frac{15}{16}v_1^2\left(\frac{1-v_1^2}{E_1}+\frac{1-v_2^2}{E_2}\right)m_p^2\right]^{\frac{1}{5}}R^{-\frac{1}{5}}$

assume $\frac{X}{a}$ is constant with increasing velocity

then $\log_{10}\left(\frac{t}{\tau}\right) = \frac{\alpha/V}{\left(\frac{5a^2\pi}{4\gamma a\pi + 2V^2\rho A/\sin\vartheta}\eta_s\left(\frac{X}{a}\right)^2\right)}$

$$= \frac{\alpha\left(4\gamma a\pi + 2V^2\rho A/\sin\theta\right)}{5a^2\pi V\eta_s\left(\frac{X}{a}\right)^2}$$

$$= \frac{\alpha 4\gamma a\pi}{5a^2\pi V\eta_s\left(\frac{X}{a}\right)^2} + \frac{\alpha 2V^2\rho A/\sin\vartheta}{5a^2\pi V\eta_s\left(\frac{X}{a}\right)^2}$$

$$= \frac{1}{V}K_1 + VK_2$$

if $K_2 >> K_1$ i.e. $2\rho A/\sin\vartheta >> 4\gamma a\pi$ then increasing V increases T-Tg

if $K_1 >> K_2$ i.e. $4\gamma a\pi >> 2\rho A/\sin\vartheta$ then increasing V decreases T-Tg

if $F_i = \frac{mV^2}{a}$ or $F_i = \frac{J}{t} = \frac{mV(1+e)}{t}$ then the same result applies

rearranged in quadratic equation form: $y = VK_2 - V^{-1}K_1$

therefore $\frac{dy}{dV} = K_2 - \frac{1}{V^2}K_1$

when $\frac{dy}{dV} = 0$ a local maximum or minimum exists

therefore $\frac{\alpha 4\gamma a\pi}{V^2} = \frac{2\rho A\alpha}{\sin\vartheta}$

$$V = \pm\sqrt{\frac{4\gamma a\pi}{2\rho(A/\sin\vartheta)}}$$

APPENDIX 6 - ESTIMATION OF SURFACE LACTOSE COMPOSITION

Table A6-1. Compositional data for powders with $(T-Tg)_{critical}$ results used to predict $(T-Tg)_{critical}$ from surface composition.

Powder	Bulk composition (%TS)			Surface composition (%TS)		$(T-Tg)_{critical}$	Reference	
	lactose	*fat*	*protein*	*lactose*	*estimate*			
SMP not stdzd	51.5	0.5	51.9	24.2		33.2	Murti	2006
SMP lactose stdzd	58.9	0.5	36.6	28.4		32.3	Murti	2006
SMP permeate stdzd	58.8	0.5	37.3	29.6		31.5	Murti	2006
Instant SMP 1	57.8	0.6	34.3	19.9*	36	37.9	Zuo	2005
Instant SMP 1 (2)	57.8	0.6	34.3	19.9*	36	40.9	Zuo	2005
Instant SMP 2	53.0	0.8	58.2	15.1*	36	39.7	Zuo	2005
Med heat SMP	53.0	0.8	38.1	15.2*	36	40.2	Zuo	2005
SMP	58	1	41	36			Kim et al	2002
SMP	51	1	36	36			Kim et al	2003
WMP not stdzd	39.1	25.8	33.3	3.7		33.6	Murti	2006
WMP lactose stdzd	45.4	26.3	27.2	7		34.6	Murti	2006
WMP permeate stdzd	43.8	25.9	33.4	5		34.5	Murti	2006
Agglomerated WMP	37.8	31.1	25.9	6.4*	2	38	Zuo	2005
High heat WMP	38.3	27.4	27.1	6.6*	3	33.7	Zuo	2005
Regular WMP	40.7	28.4	24.9	7.5*	4	37.1	Zuo	2005
Instant WMP	39.8	29.8	24.7	7.2*	4	38.2	Zuo	2005
Regular WMP 2	40.9	26.9	25.9	7.6*	4	40	Zuo	2005
WMP	40	29	31	2			Kim et al	2002
WMP	36.6	26.6	27.9	2			Kim et al	2003
CP	13	75	12	1			Kim et al	2002
LFCP55	24.4	55.8	16.2	3.0*		36.9	Zuo	2005
HFCP70	13.3	71.8	12.3	1.6*	1	30	Zuo	2005
WPC	8	6	86	6			Kim et al	2002
Whey Protein	1.1	0.5	96.3	0.8*		50.1	Zuo	2005
MCP 44	47.6	0.8	43.5	11.1*		42.7	Zuo	2005
MCP 56	31.3	1.4	59.4	4.4*		47.5	Zuo	2005
MCP 70	18.2	1.5	72.9	2.1*		50	Zuo	2005
MCP 85	4.2	1.7	88.5	1.0*		49.1	Zuo	2005

* estimated from Figure A6-1.

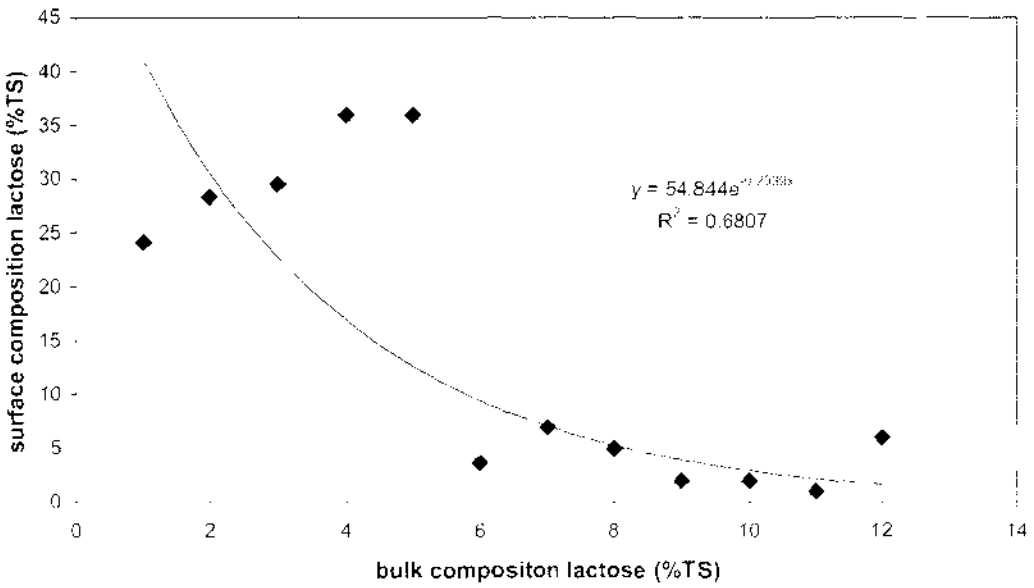

Figure A6-1. Estimation of surface lactose composition from bulk lactose (%TS)

APPENDIX 7 - CYCLONE WALL TEMPERATURE DATA

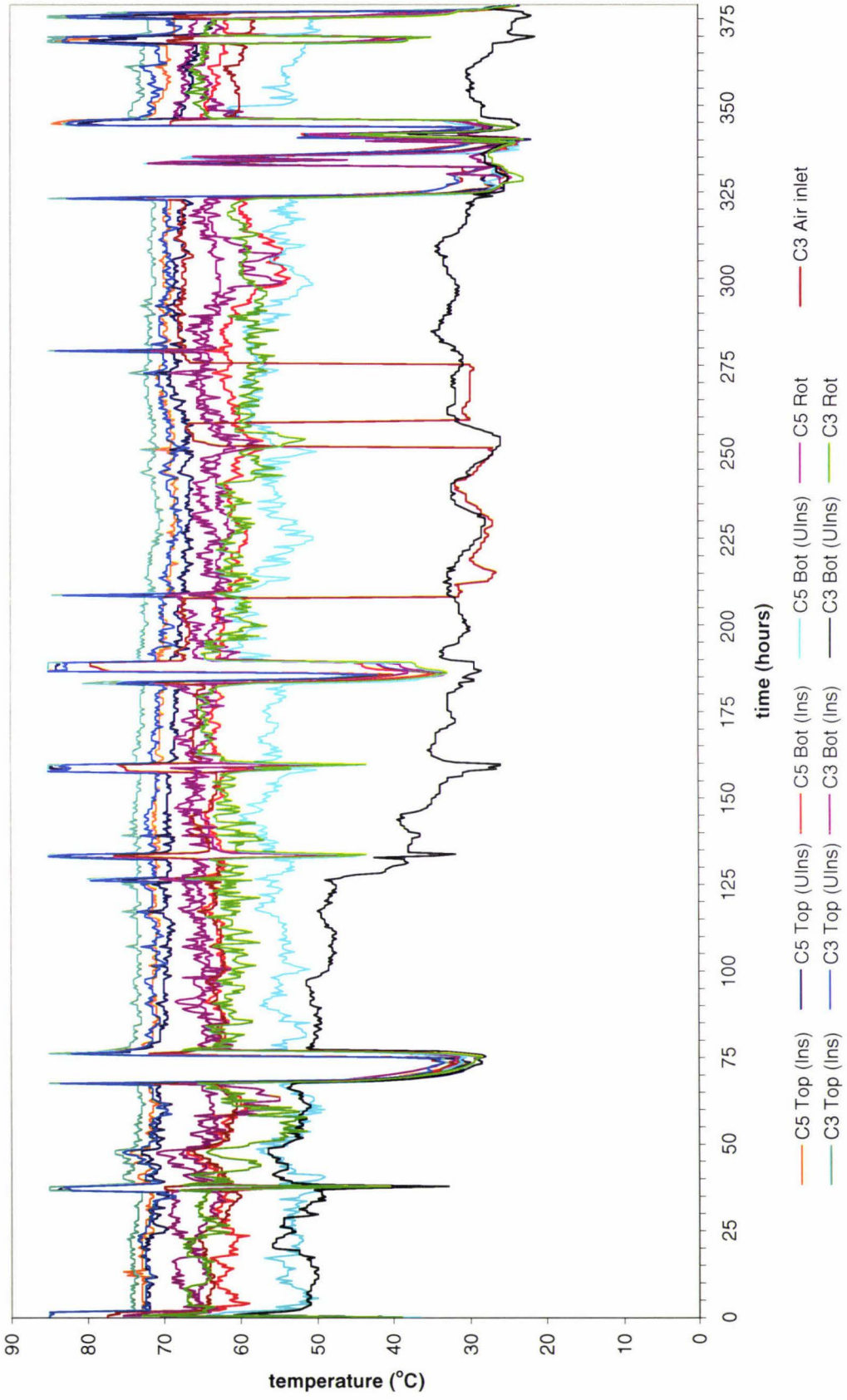

Figure A7-1. Extended temperature data from eye button logger trials on D5 processing SMP from start up to shut down.

Table A7-1. Average cyclone wall temperatures for complete SMP drying cycle. Te Rapa. 22/02/2006 – 10/03/2006.

Position	Average Temperature (°C)
C5 top insulated	68
C5 top un-insulated	67
C5 bottom insulated	59
C5 bottom un-insulated	53
C5 rotary valve	61
C3 air inlet	57
C3 top insulated	71
C3 top un-insulated	69
C3 bottom insulated	61
C3 bottom un-insulated	37
C3 rotary valve	58

Insulated wall temperatures are slightly higher than un-insulated temperatures. C3 bottom un-insulated temperatures appear to be unusually low and dropping in temperature throughout the logging period.